A STUDY AND DESIGN OF PM COLLECTOR USING ELECTROSTATIC PRECIPITATION

PANOD NILPHAI

A THESIS REPORT SUBMITTED IN PARTIAL FULFILLMENT
OF THE REQUIREMENTS FOR THE DEGREE OF
BACHELOR OF MECHANICAL ENGINEERING
SCHOOL OF INTERNATIONAL DISCIPLINARY ENGINEERING
PROGRAMS, SCHOOL OF ENGINEERING
KING MONGKUT'S INSTITUTE OF TECHNOLOGY LADKRABANG
2023

A STUDY AND DESIGN OF PM COLLECTOR USING ELECTROSTATIC PRECIPITATION

PANOD NILPHAI

A THESIS REPORT SUBMITTED IN PARTIAL FULFILLMENT
OF THE REQUIREMENTS FOR THE DEGREE OF
BACHELOR OF MECHANICAL ENGINEERING
SCHOOL OF INTERNATIONAL DISCIPLINARY ENGINEERING
PROGRAMS, SCHOOL OF ENGINEERING
KING MONGKUT'S INSTITUTE OF TECHNOLOGY LADKRABANG
2023

THESIS PROJECT OF YEAR 2023

MECHANICAL ENGINEERING, SCHOOL OF INTERNATIONAL

DISCIPLINARY ENGINEERING PROGRAMS, SCHOOL OF ENGINEERING

KING MONGKUT'S INSTITUTE OF TECHNOLOGY LADKRABANG

Project Title A STUDY AND DESIGN OF PM COLLECTOR USING ELECTROSTATIC PRECIPITATION

Student Name

1. Panod Nilphai Student ID 63011232

MEK SRILOMSAK Advisor

(Asst.Prof.Dr. Mek Srilomsak)

A STUDY AND DESIGN OF PM COLLECTOR USING ELECTROSTATIC PRECIPITATION

Panod Nilphai Student ID 63011232

Advisor Asst.Prof.Dr. Mek Srilomsak

Academic year 2023

ABSTRACT

The purpose of this project is to design and construct an Electrostatic Precipitator (ESP) as a device for the collection of PM particles from the surrounding air. Electrostatic Precipitator is an electro-mechanical system that uses the principles of electrostatic to trap the particulate matter in the air. Its principles are by charging the dust particles in the air using high voltage with charging electrodes where dust particles are charged then the charged PM particles pass through the collector plates that is in high electric field to trap the charged particles. Doing so, the concentration of PM in the air will be lower. This project gives all information about the design and construction of an ESP including all parameters affecting the performance of ESP along with the materials selection. Our focus is that we want to build a device that can collect dry PM from surrounding air for further analysis to find its source with minimal contamination.

Keywords: Electrostatic precipitation, PM, Electric field

ACKNOWLEDGEMENT

Without the contribution of many people, this thesis would not have been existed. It owes the existence to the supports and inspirations from a lot of people.

To my thesis advisor Asst. Prof. Dr. Mek Srilomsak of King Mongkut's Institute of Technology Ladkrabang, I would like to express my deepest gratitude for the encouragement and supervision through all obstacles and challenges since the beginning until the end of my study.

I also want to express my gratitude to all lecturers for your support and guidance to me for the whole two years. Also special thanks to P'Ton who helped advising me from the start to finish of project and special thanks to the initial formula club KMITL students for helping me carry around the equipment and help me secure my equipment throughout the year. Moreover, I also would love to express my gratitude to all respondents who contribute their information and time to this study. And I do believe the study could not have been done without their input.

Finally, I must express my very greatest gratitude to my parents, friends, and all relatives for providing me with unfailing support and continuous motivation throughout my years of study. This accomplishment would not have been possible without them.

Panod Nilphai

TABLE OF CONTENTS

LIST OF TABLES

Table **Page**

LIST OF FIGURES

Figure **Page**

LIST OF FIGURES

(Continued)

Figure **Page**

LIST OF FIGURES

(Continued)

Figure **Page**

LIST OF FIGURES

(Continued)

Figure **Page**

LIST OF FIGURES

(Continued)

Figure **Page**

LIST OF FIGURES

(Continued)

Figure **Page**

LIST OF FIGURES

(Continued)

Figure **Page**

LIST OF SYMBOLS

m_p	Particle's mass
ρ	Density
C_D	Drag coefficient
Re	Reynold number
T	Temperature
μ	Dynamic viscosity
C_C	Cunningham slip factor
δ	Relative gas density
Q	Charge
ε_r	Permittivity of the particle material
η	Collection efficiency

LIST OF DEFINITIONS

ESP	Electrostatic Precipitator / Electrostatic Precipitation
PM	Particulate Matter

CHAPTER 1

INTRODUCTION

1.1 Research Background

Air pollution has a significant impact on human health and the environment. There're many types of air pollution such as dust which is particulate matter, also it can be in gaseous form such as ozone, nitrogen oxides, etc. By comparing all types of air pollution, fine particulate matter is one of the most harmful to human health. Particulate matter includes any airborne substances that are not in the gas phase, and it can be liquid or solid. They are classified as the coarse fraction, PM10 refers to 2.5-10 μm diameter and PM2.5 refers to particles with diameter ≤ 2.5 μm. However, PM2.5 is the most concern as it is small enough to penetrate deep into the respiratory system and can affect both the short and long term of human health.

Average PM2.5 concentration is at its peak during winter season which exceeds the safety exposure limit for human health.

The sources of PM2.5 pollution are diverse, as it could be resulted from natural processes and human activities, where it could be from vehicles emission, emissions from industrial processes, any human activities such as burning in an open area, and natural phenomena such as wildfires. Hence, it is not a simple task to determine its sources accurately according to that location. However, the recent PM source characterization is by chemical analysis to find its chemical composition, assumption of the source is then made.

By discussing with my advisor Asst.Prof.Dr.Mek Srilomsak that it would be better if we could introduce another method of PM source characterization. He had a background in nanostructure analysis, especially in automotive field. However, to be

able to use this method for analysis, dry PM must be collected from the ambient air within the time interval of 24 hours as time changes the sources of PM might vary. That being said, was a big challenge as the normal paper filter might not be suitable as it could give off the filter material when collection which may cause contamination. The objective is to build a device that could collect dry PM from the air within 24 hours timeframe.

In the end, we found that an Electrostatic precipitator (ESP) would suit our purpose according to the objective.

An electrostatic precipitator (ESP) is a device used to remove fine particulate matter (PM), effectively at removing dust and smoke. Originally, it is widely used in industrial processes and its size is very big, it is commonly used in coal-fired power plants, cement plant, etc. It operates on the principle of electrostatic attraction, starting by passing through the ESP, the particles become charged, then it is collected at the collector plate under the influence of an electric field.

In this project is to study the principle of electrostatic precipitation to build a compact size ESP (Powered by normal 220V socket, battery powered, and can be carried around), and most importantly, the removable collector plate that we can take it out to the lab when doing an analysis of its sources.

1.2 Objectives

1. To study basic principles of electrostatic precipitation including all design parameters.

2. To design and construct a compact size ESP that user could pull the collector plate out to use for the further analysis of PM. Target is to be able to collect 100 mg of PM in a period of not exceeding than 24 hours.

1.3 Project Scopes

1. Build an ESP that can collect 100 mg of PM within 24 hours period.

2. Design an ESP to have collector plates that is removable.

1.4 Procedures

1. Study about the Electrostatic Precipitation principle.

2. Buy an ESP kit from China for reviewing and testing. Since we don't have any experience with ESP and it widely existed on a big scale, mostly in factories.

3. Study all the parameters according to the devices

4. Use both theoretical and experimental data for the customized design.

5. Design customized ESP

6. Test the device.

CHAPTER 2

LITERATURE REVIEW

2.1 Introduction

The project focuses on building a PM collector device by using electrostatic precipitation techniques. The context starts from the fundamental of particulate matter (PM) including its basic concepts. The electrostatic precipitation technique will be introduced including all its history of usage and design parameters such as the electric field intensity to effectively charge and collect the particles. The complete system requires air pump and ducts to induce an airflow toward the ESP units, where fluid mechanics is used to determine the pump and duct size. All necessary information will be covered in this thesis.

2.2 Particulate Matter (PM)

Particulate Matter refers to a complex mixture of solid and liquid particles of both inorganic and organic constituents that are suspended in the air. It is composed of various compounds, including but not limited to sulfates, nitrates, ammonia, sodium chloride, carbon, mineral dust, and water. It is classified according to aerodynamic diameter, usually distinguished between coarse or PM10 (particles with an aerodynamic diameter smaller than 10 μm) or fine PM2.5 (aerodynamic diameter smaller than 2.5 μm). Smaller particles generally are more dangerous since, when inhaled, they may reach deep into the human respiratory system. It is measured on a dry basis, as a unit of concentration, mass of PM per unit volume of air, **μg/m^3**. These PM particles are aggregates of many molecules, could be from similar molecules, but often from dissimilar molecules. They form and transform in the air by

several processes. Some particles serve as nuclei upon which vapors condense. Some particles react chemically with atmospheric gases or vapors to form different compounds. When two particles collide in the air, they tend to adhere to each other because of attractive surface forces, thereby forming progressively larger and larger particles by **agglomeration**. The larger a particle becomes, the greater its weight and the greater its likelihood of falling to the ground than continuing suspended in the air. The process where the particles fall to the ground is called **sedimentation**.

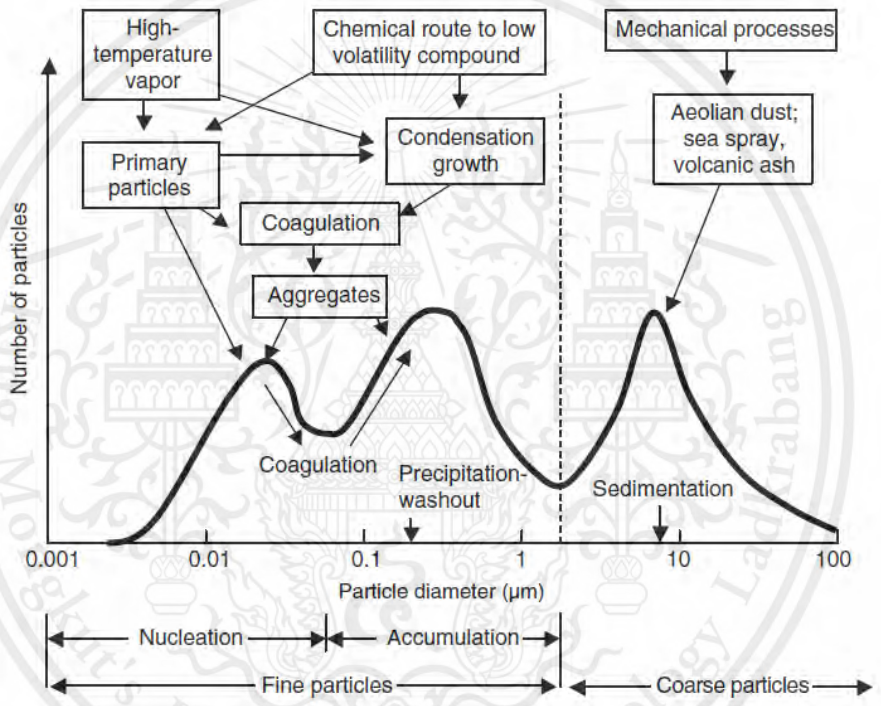

Figure 2.1 Prototypical size distribution of tropospheric particles with selected sources and pathways of how the particles are formed.

Source: Vallero, D. (2014). *Fundamentals of air pollution*. Academic Press.

Terms used to describe the shape and origins of an aerosol includes.

Agglomerate – Refers to a group of particles held together by van de Waals forces or surface tension.

Aggregate - Refers to a heterogeneous (not identical) particle in which the various components are not easily broken up.

Aerosol sources can be classified as **primary or secondary**.

Primary aerosols are those that are emitted directly into the particulate form from sources such as power plants, internal combustion engines, wildfire, open air burning, etc.

Secondary aerosols refer to particles formed within the atmosphere from condensation of vapors, or as a result of chemical reaction species.

Once the particles or aerosol has spread into the atmosphere, their size, number, and chemical compositions are changed by several mechanisms. Processes are described below.

Nucleation mode, (< 0.2 μm diameter). The particles have recently been through condensation processes of hot vapors or freshly formed within the atmosphere by gas to particle conversion.

Accumulation mode, (0.2 - 2 μm diameter). These particles have resulted from the nucleation mode by coagulation or condensation of vapors.

Coarse mode, (> 2 μm) diameter. These particles are mainly formed by mechanical attrition processes. Including soil dust, sea spray and most of industrial dusts

The fine particles are primarily sulfates, nitrates, organics, ammonium, and lead compounds. The coarse particles are introduced to the atmosphere as solids from the surface of the earth and the seas along with the particles from the coagulation-condensation mode which have grown larger. These are primarily silicon, iron, aluminum, sea salt, and plant particles.

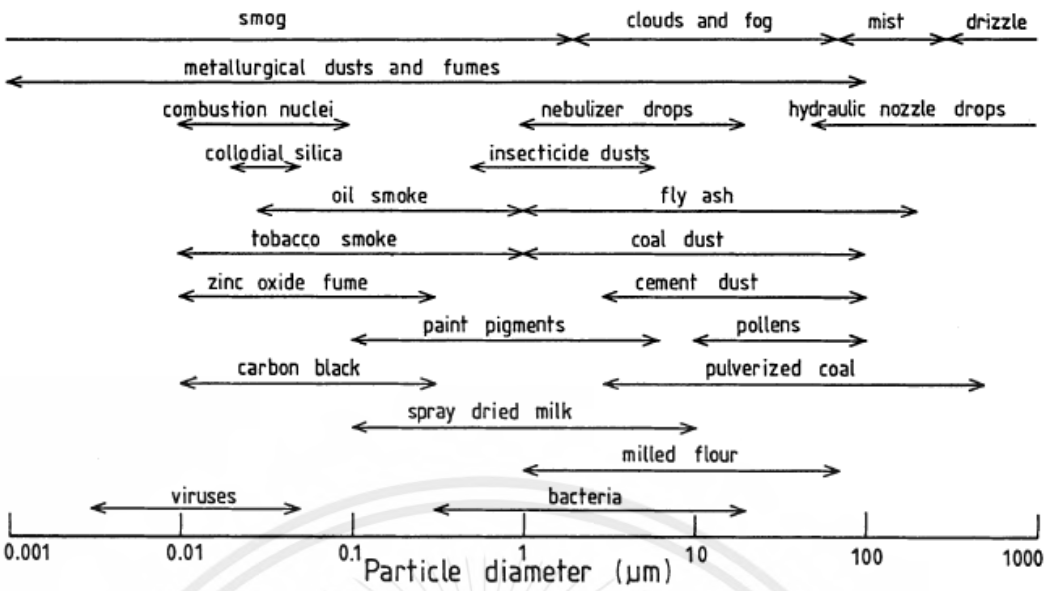

Figure 2.2 Particle size range for aerosol.

Source: Kouimtzis, T., & Samara, C. (2013). *Airborne particulate matter*. Springer.

Dust – It is made of fine particles of solid matter formed by mechanical disintegration of a parent material, such as in crushing, grinding, and blasting.

Fume - Solid particles generated by condensation from the gaseous state, generally after volatilization from melted substance (e.g. welding).

Smoke - Visible aerosol produced by some sort of oxidation process such as burning, or a solid formed by incomplete combustion.

Fog and mist - Liquid particle aerosol produced by the disintegration of liquid or combustion of vapors.

Smog – It is derived from a combination of smoke and fog. It consists of solid and liquid particles created, at least in part, by photochemical reactions.

Hazes - An aerosol that impedes vision and may consist of a combination of water droplets, pollutants, and dust; Particle diameter less than 1 μm.

2.2.1 Source of Particulate Matter (PM)

There are 2 main sources of Particulate Matter (PM) which could be resulted from natural sources or human made. Before human existence, the PM must only come from natural sources where it included all the particulate forms of condensed water vapor which is the condensed and reacted forms of natural organic vapors. Salt particles resulting from the evaporation of water from sea spray. Windborne pollen, fungi, yeasts, rusts, molds, algae, bacteria, and debris come from live and decaying plant and animal life. Some particles come from erosion by the wind from beaches, desert, soil, and rock. However, the actual natural background of PM could never be measured as nowadays there are a mixture of PM from natural and from human made.

Sources of particles are highly variable from different places. They may be emitted directly to the air from stationary sources, such as industries, power plants, open burning, and from moving vehicles (considered as “mobile sources”), by direct emissions from internal combustion engines, where the concentration of PM is at its peak at near-road conditions, e.g., bus stop. Area or nonpoint sources of particles include construction, agricultural activities such as plowing and tilling, mining, and forest fires.

Figures below shows the PM source contribution throughout 3 main regions in Thailand whereas data is retrieved from Ministry of Industry of Thailand. Where it revealed that at different locations, the source of PM is completely different in fraction.

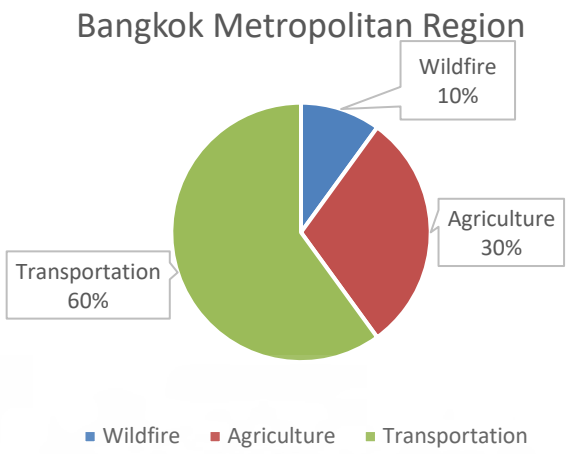

Figure 2.3 PM source at Bangkok Metropolitan Region retrieved from Ministry of Industry

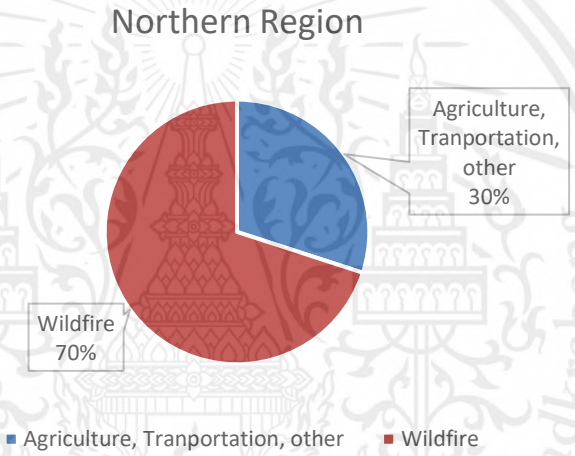

Figure 2.4 PM source at Northern Region retrieved from Ministry of Industry

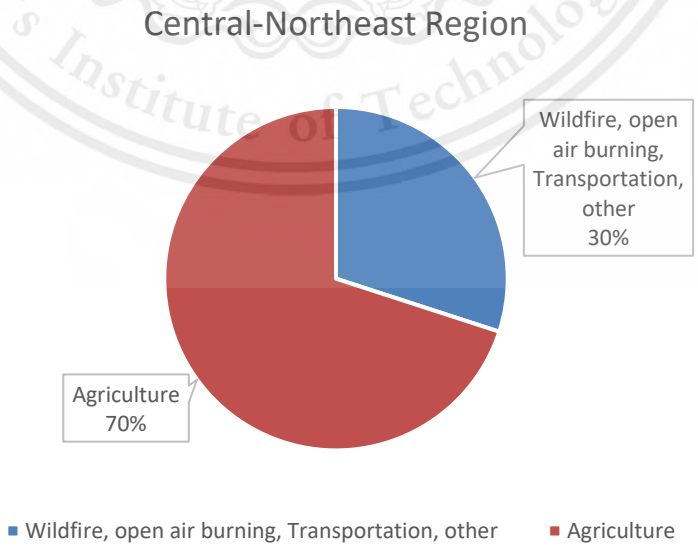

Figure 2.5 PM source at Central-Northeast Region retrieved from Ministry of Industry

2.2.2 Dynamics of Particulate Matter (PM)

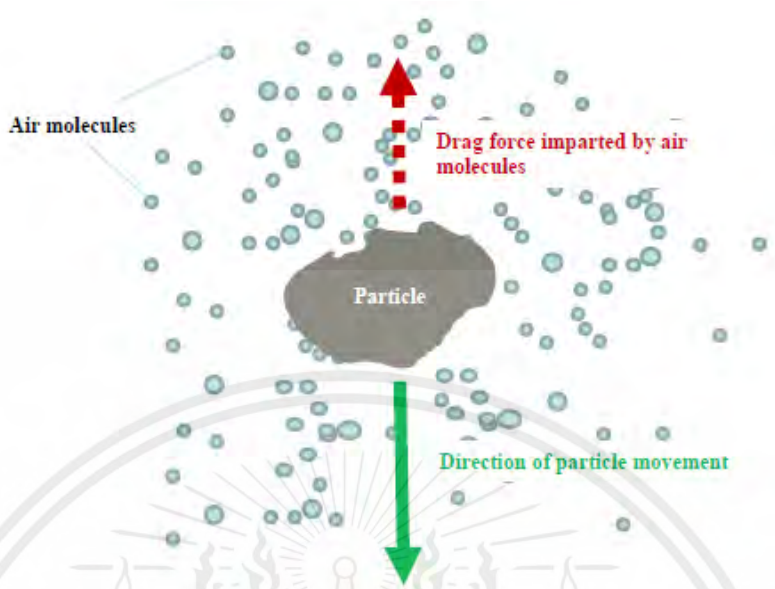

Figure 2.6 Drag force of air imparted onto a particle moving as a result of gravitational force

Source: Vallero, D. (2014). *Fundamentals of air pollution*. Academic Press.

Sum of Force acting on the particle is defined by newton's second law.

$$\sum F = m_p \cdot a_p = m_p \frac{dv_p}{dt} \tag{2.1}$$

Where $\sum F$ = sum of force acting on particle $(g \cdot cm \cdot s^{-2})$

m_p = Particle mass (g)

a_p = Particle acceleration $(cm \cdot s^{-2})$

v_p = Particle velocity $(cm \cdot s^{-1})$

t = Time (s)

2.2.2.1 Gravity

Gravitational Force that causes the PM mass to fall is defined as.

$$F_G = m_p \cdot g = \rho_p \cdot V_p \cdot g \tag{2.2}$$

Where F_G = Gravitational force $(g \cdot cm \cdot s^{-2})$

ρ_p = Particle density $(g \cdot cm^{-3})$

V_p = Particle volume (cm^3)

g = Gravitational acceleration $(980\ cm \cdot s^{-2})$

If the particle is assumed to be spherical, Particle volume (V_p) can be defined as,

$$V_p = \frac{\pi {d_p}^3}{6} \tag{2.3}$$

Where d_p = Physical diameter of the particle (cm)

Substituting the relation (2.3) into equation (2.2) yields.

$$F_G = \frac{\pi {d_p}^3 \rho_p g}{6} \tag{2.4}$$

2.2.2.2 Buoyancy

Buoyancy force acting on the PM mass is defined as,

$$F_B = m_g \cdot g = \rho_g \cdot V_p \cdot g \tag{2.5}$$

Where F_B = Buoyancy force $(g \cdot cm \cdot s^{-2})$

m_g = Mass of displaced gas (g)

ρ_g = Carrier gas density $(g \cdot cm^{-3})$

By assuming the PM particle is perfectly sphere, substitute relation (2.3) into (2.5),

$$F_B = \frac{\pi {d_p}^3 \rho_g g}{6} \tag{2.6}$$

Note that F_B depends on the gas density which is usually air. Despite being a very polluted carrying gas, it is still predominantly air. Which usually density of gas(air) (ρ_g) is lower than density of PM dust (ρ_p) would result in a larger magnitude of gravitational force than the buoyancy force causing the PM dust to fall to the ground.

2.2.2.3 Drag

As the particle begins to move downward due to gravitational force, it encounters a resistive force that increases with increasing downward velocity.

$$F_D = \frac{A_p \cdot \rho_g \cdot V_p^2 \cdot C_D}{2} = \frac{\pi {d_p}^2 \rho_g {v_p}^2 \cdot C_D}{8} \quad (2.7)$$

Where F_D = Drag force $(g \cdot cm \cdot s^{-2})$

A_p = Cross sectional area of the particle (cm)

ρ_g = Carrier gas density $(g \cdot cm^{-3})$

C_D = Drag coefficient

The drag force results from the gas in front of the particle that is being displaced as the particle moves, so it imparts momentum on the gas. Thus, F_D equals the momentum per unit time imparted by the gas on the particle. Some of the particle velocity (v_p) is converted to the gas velocity (v_g). The amount of energy that v_p gives to v_g is related to a factor of friction, which is the drag coefficient (C_D).

The drag coefficient is related to the particle velocity and the flow pattern of the gas around the particle. This flow is determined by Reynold number (Re)

$$Re = \frac{\text{Inertial Forces}}{\text{Viscous Forces}} = \frac{\rho v d_e}{\mu} \quad (2.8)$$

Where d_e = Conduit's equivalent diameter which equivalent to the fluid flow as physical length

μ = Dynamic viscosity $(g \cdot cm^{-1} \cdot s^{-1})$

At very low velocities, the particle moves in discrete layers parallel to one another. The only movement across the fluid layers is molecular motion, which creates viscosity. Which is a laminar flow. Reynolds number can also be expressed in terms of gas viscosity.

$$Re_p = \frac{d_p v_p \rho_g}{\mu_g} \tag{2.9}$$

Where d_p = Particle diameter (cm)

μ_g = Gas viscosity $(g \cdot cm^{-1} \cdot s^{-1})$

There is an existence of laminar, transition, and turbulent flow. For low values of the particle Reynolds number ($Re_p < 1$), the flow is considered laminar. For much greater values of the particle Reynolds number ($Re_p > 1000$), the flow is turbulent. For particle Reynolds numbers between 1 and 1000, the flow is in the transition region, that is the flow can be either laminar or turbulent, depending on the local conditions.

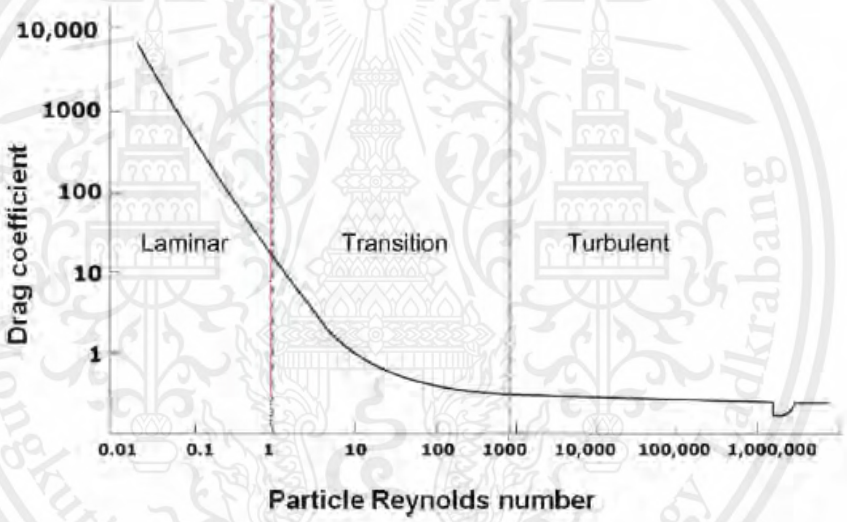

Figure 2.7 Relationship between drag coefficient and particle Reynolds number.

Source: Vallero, D. (2014). *Fundamentals of air pollution*. Academic Press.

Figure 2.7 shows the experimental data relationship between Drag coefficients and particle Reynolds number which drag coefficients are at its peak when the flow is laminar, as opposed to when the flow is turbulent, drag coefficients decreases.

The drag coefficient in the laminar flow region ($Re_p < 1$) is

$$C_D = \frac{24}{Re_p} \tag{2.10}$$

The drag coefficient in the transition flow region ($1 < Re_p < 1000$) is

$$C_D = \frac{18.5}{Re_p^{0.6}} \tag{2.11}$$

The drag coefficient in the laminar flow region ($Re_p > 1000$) is

$$C_D = 0.44 \tag{2.12}$$

These equations apply to particles with diameters > 3 μm, i.e. those where the gas is continuous around the particle. For smaller particles, the gas appears as distinct molecules. Such small-diameter particles can slip between the gas molecules, so they fall faster than relationships above. Ebenezer Cunningham proposed that the drag coefficient should be reduced for small particles. This means that the drag coefficient equation for the laminar region must be modified to include a term called the Cunningham slip correction factor (C_C)

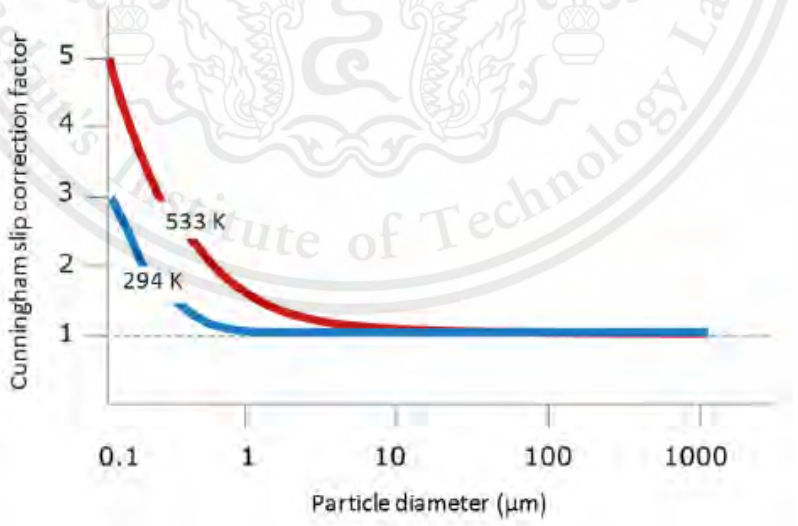

Figure 2.8 Cunningham slip correction factor as a function of temperature and particle diameter.

Source: Vallero, D. (2014). *Fundamentals of air pollution*. Academic Press.

$$C_D = \frac{24}{Re_p \cdot C_C} \tag{2.13}$$

An approximation of the slip correction can be based on the temperature and particle diameter according to the Figure 2.8

$$C_C = 1 + \frac{6.21 \times 10^{-4} T}{d_p} \tag{2.14}$$

Where T = Absolute temperature (K)

d_p = Particle diameter (μm)

By applying the slip corrections and substituting terms allow drag forces to be calculated for each flow region.

The drag force for the laminar region is:

$$F_D = \frac{3\pi\mu_g v_p d_p}{C_C} \tag{2.15}$$

The drag force for the transition region is:

$$F_D = 2.30(d_p \cdot v_p)^{1.4} \cdot {\mu_g}^{0.6} \cdot {\rho_g}^{0.4} \tag{2.16}$$

The drag force for the turbulent region is:

$$F_D = 0.05\pi(d_p \cdot v_p)^2 \cdot \rho_g \tag{2.17}$$

Where μ_g = Gas viscosity ($g \cdot cm^{-1} \cdot s^{-1}$)

d_p = Particle diameter (cm)

ρ_g = Gas density ($g \cdot cm^{-3}$)

v_p = Particle velocity relative to the gas ($cm \cdot s^{-1}$)

C_C = Cunningham slip factor

As observed from the above equation, the two forces dominating particle deposition rate are gravity and drag. Gravity and drag work against one another, either keeping the particle remain suspended or moving it toward settling.

The drag force on the particle also increases with increasing velocity. However, at some point, velocity will become high enough that the drag force will be identical as gravitational force. At this point, the net force will become zero, and the particle will reach a constant velocity which is known as the terminal settling velocity (v_t)

Terminal settling velocity (v_t) for laminar flow is:

$$v_t = \frac{g \cdot C_C \cdot \rho_p \cdot d_p^2}{18\mu_g} \tag{2.18}$$

Terminal settling velocity (v_t) for transition flow is:

$$v_t = \frac{0.153 g^{0.71} \cdot \rho_p^{0.71} \cdot d_p^{1.14}}{\mu_g^{0.43} \cdot \rho_g^{0.29}} \tag{2.19}$$

Terminal settling velocity (v_t) for turbulent flow is:

$$v_t = 1.74 \left(\frac{g \cdot \rho_p \cdot d_p}{\rho_g} \right)^{0.5} \tag{2.20}$$

Particle Size (μm)	Terminal Settling Velocity at 25 °C (cm s^{-1})	Flow Condition
0.1	0.000087	Laminar
1.0	0.0035	Laminar
2.5	0.2	Laminar
10.0	0.304	Laminar
50.0	7.5	Laminar
80.0	19.3	Laminar
100.0	31.2	Transitional
200.0	68.8	Transitional
1000.0	430.7	Transitional
10,000.0	1583	Turbulent
100,000.0	5004	Turbulent

Figure 2.9 Terminal Settling Velocities for Spherical Particles in Air at 25 °C

Source: Vallero, D. (2014). *Fundamentals of air pollution*. Academic Press.

By utilizing the terminal settling velocity equation, Figure 2.9 shows the relationship between particle size and terminal settling velocity.

2.2.3 Particle Morphology

	Shape	Density (ρ_p)and diameter (d)	Aerodynamic diameter (d_p)
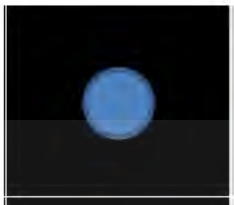	Solid sphere	$\rho_p = 2.0$ g cm^{-3} $d = 1.4$ µm	$d_p = 2.0$ µm
	Hollow sphere	$\rho_p = 0.5$ g cm^{-3} $d = 2.8$ µm	
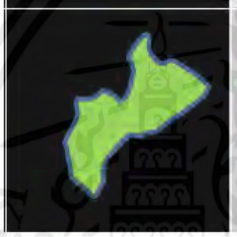	Irregular	$\rho_p = 2.3$ g cm^{-3} $d = 1.3$ µm	

Figure 2.10 Morphology's Effect on Particle Diameter (d) and Density (ρ_p) for Three Particles with the Same Aerodynamic Diameter (d_p)

Source: Vallero, D. (2014). Fundamentals of air pollution. Academic Press

According to the previous part, particles are assumed to be spherical. However, it's not always true in practical cases. Indeed, another particle characteristic that influences removal is the relationship between aerodynamic diameter and shape or morphology. In practical terms, few particles are spheres, so particles that appear to be different in physical size and shape can have the same aerodynamic diameter, as shown in Figure 2.10. Some particles that appear to be similar may have different aerodynamic diameters. Particles can be spheres, hollow spheres, irregular shapes, flakes, fibers, aggregates, and condensation flocs.

2.3 Particulate Matter Control Technologies

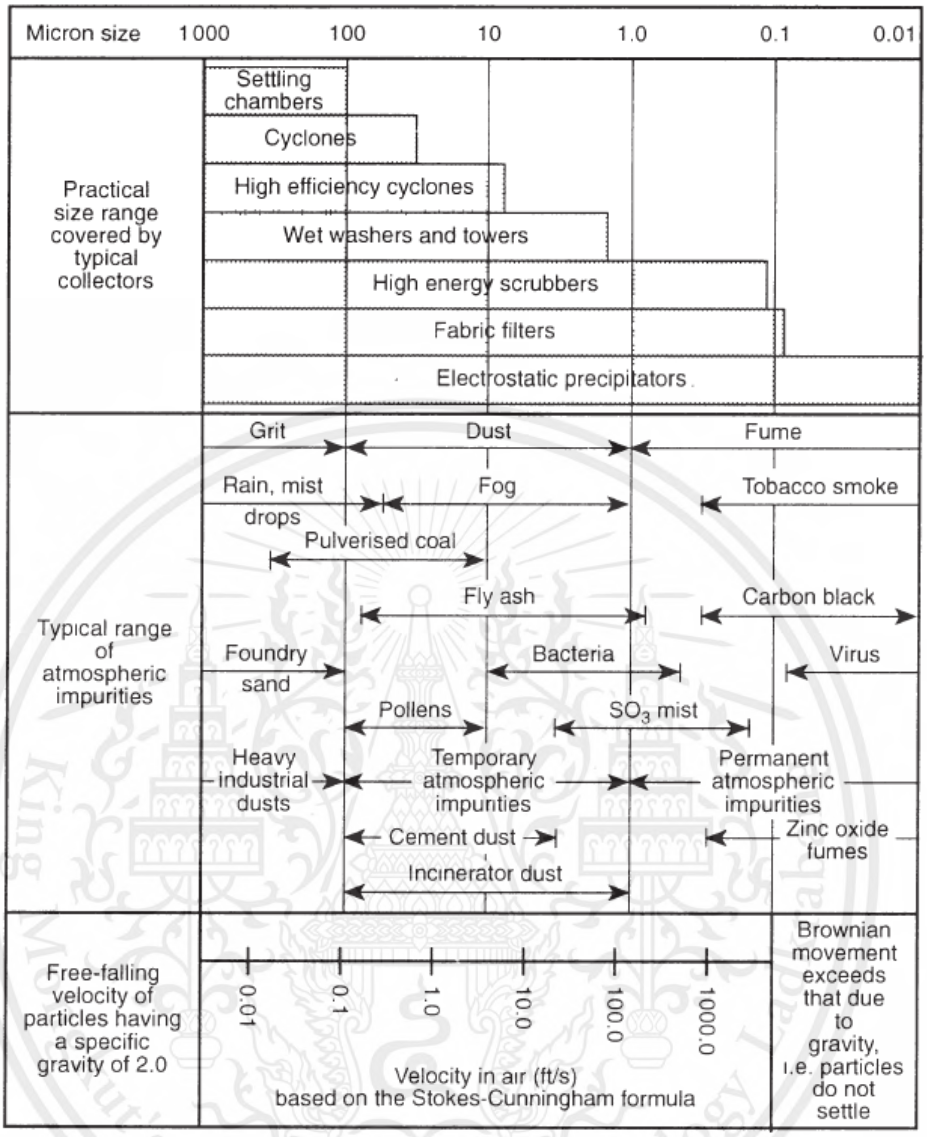

Figure 2.11 Particulate Matter Control Technologies with respect to particle sizes.

Source: Parker, K. (1997). Applied electrostatic precipitation. Springer.

Figure 2.11 shows various particulate matter control technologies along with their particles sizes limitations. Figure 2.9 shows that larger particles tend to settle faster than smaller particles. Technologies such as settling chambers and cyclones are more suitable for larger particles as their settling velocity is higher. Smaller particles often need fabric filters as particles would get trapped easily into the filter material. However, electrostatics technique could also be used to trap particles, especially small particles.

These are the main types of PM control technologies categories according to their collecting method, characteristics, and its efficiency.

2.3.1 Inertial Collectors

Inertial collectors including cyclones, baffles, louvers, and rotating impellers, operate on the principle that the aerosol material in the carrying gas stream has a greater inertia than the gas. Usually, the larger particle sizes with higher settling velocity. Inertial collectors are the most efficient for larger particles. However, smaller particles would not perform well using this technique.

The most common inertial collector is the cyclone, The two basic forms are used: the tangential inlet and the axial inlet (Figure 2.12). In actual industrial practice, the tangential inlet type is usually a large (1-5 m in diameter) single cyclone, while the axial inlet cyclone is relatively small (about 20 cm in diameter and arranged in parallel units for the desired capacity).

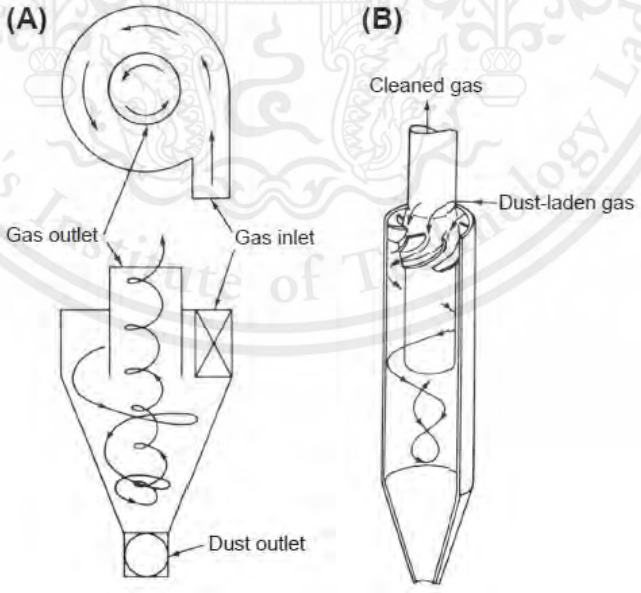

Figure 2.12 Cyclone configurations : (A) tangential inlet and (B) axial inlet.

Source: Vallero, D. (2014). Fundamentals of air pollution. Academic Press

2.3.2 Wet Scrubbers

Scrubbers, or wet collectors, have been used as gas cleaning devices. All wet scrubbers operate by contacting the particles with large quantities of liquid in a fully turbulent area of the device. The particles are allowed to impact or impinge on the liquid droplets, normally water, such that their size and mass increase. As larger water-wetted particles they can be removed from the entraining gas stream in a simple impingement or cyclonic form of separator.

The wet-scrubbing process uses two processes to remove an aerosol from the gas stream. Start by making the particle wet by scrubbing liquid. This process is the same whether the system uses a spray to atomize the scrubbing liquid or a diffuser to break the gas into small bubbles.

The second process employed by wet collectors is to remove the wetted particles on a collecting surface and remove it from the device.

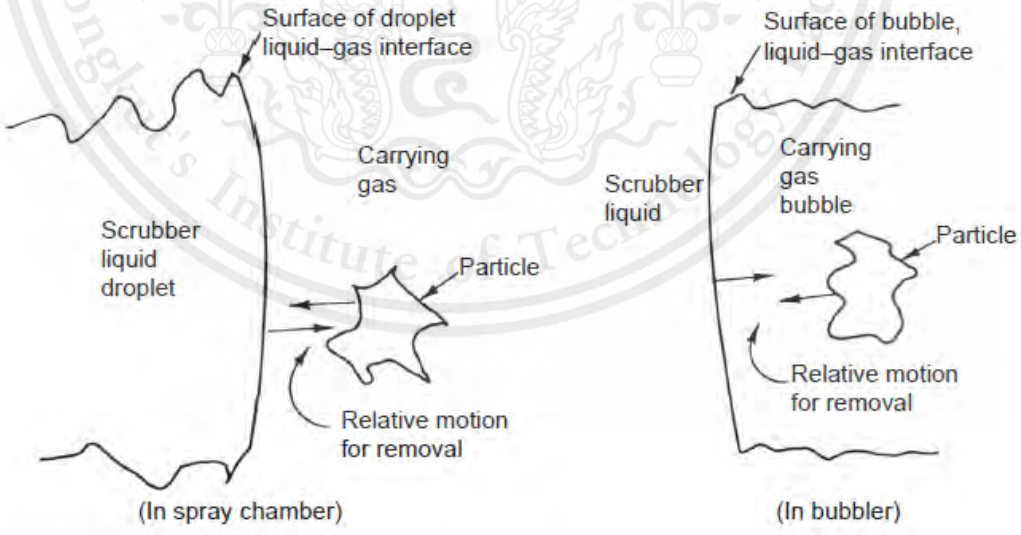

Figure 2.13 Wetting of aerosols in a spray chamber or bubbler

Source: Vallero, D. (2014). Fundamentals of air pollution. Academic Press

2.3.3 Fabric Filter

Fabric Filters have a high ability to eliminate particulate matter (PM) from the gas stream they carry. The process involves PM colliding with and sticking to the filter material, gradually forming a deposit. Over time, this deposit acts as a secondary filtering medium. Eventually, when the deposit becomes too substantial, its efficiency drops and creating a huge pressure drop over a flow, prompting the need for either replacement or cleaning of the filter (If that type of filter can be cleaned).

The filter medium can be fibrous, such as cloth; granular, such as sand; a rigid solid, such as a screen; or a mat, such as a felt pad. It can be in the shape of a tube, sheet, bed, fluidized bed, or any other desired form. The material can be natural or man-made fibers, granules, cloth, felt, paper, metal, ceramic, glass, or plastic. It is not surprising that filters are manufactured in an infinite variety of types, sizes, shapes, and materials.

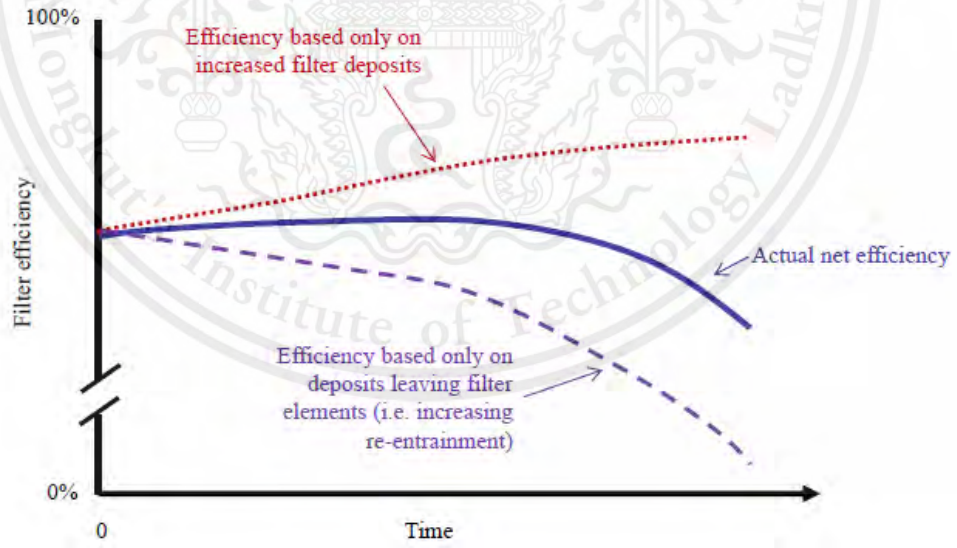

Figure 2.14 Change of filtration efficiency with time.

Source: Vallero, D. (2014). Fundamentals of air pollution. Academic Press

2.3.4 Electrostatic Precipitators (ESP)

Electrostatic precipitator is a device that use the method of electrostatic precipitation to remove impurities from the air either solid or liquid droplets, it is functioning by charging the particles in the first stage then those charged particles move through the collector plates where its trajectory changes to travel into the collector plates as the collector plates is in an electric field, where changed particles are attracted to the oppositely charged plates. It is more effective at collecting smaller particles sizes since it uses electrostatic principles, terminal settling velocity does not have large impact on Electrostatic Precipitator system, since the particle is repelled by electric field strength mostly.

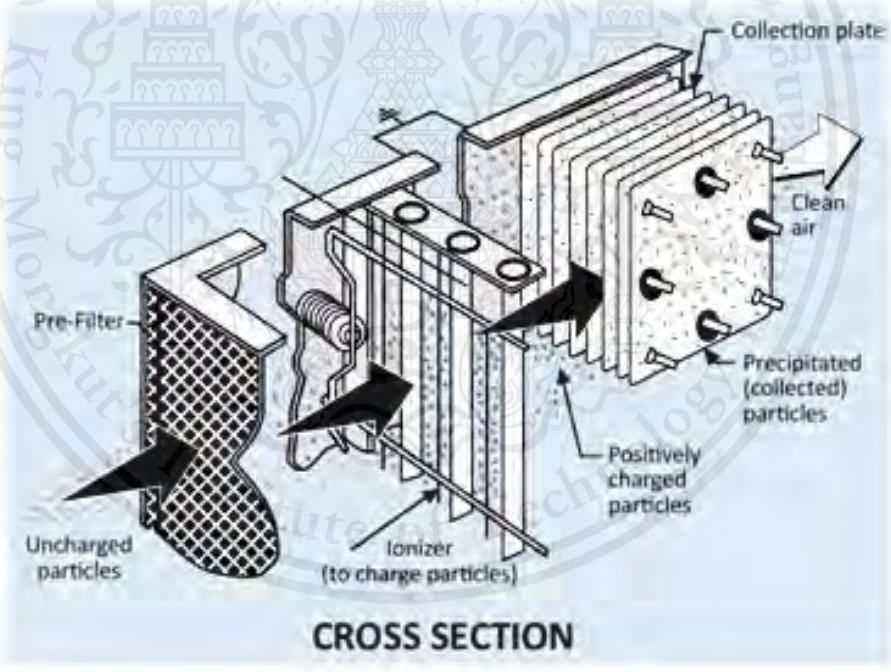

Figure 2.15 Cross section view of ESP

Source: Electrostatic precipitator (ESP). (2023, January 4). Ensavior : High Performance Engineering Solutions. https://ensavior.com/specialized-air-purification-system/electrostatic-precipitator-esp

2.4 Electrostatic Precipitation

2.4.1 History of Electrostatic Precipitators (ESP)

The first significant investigations using electrostatic precipitation were by Professor O. J. Lodge and Mr J. W. Clark, working at Liverpool University in the early 1880s. Lodge was approached and collaborated with Mr. Alfred Walker of Parker, Walker & Co. of Chester, in attempting to remove fumes from gases arising during the smelting of lead at their Works in Deeside.

However, the way they were developing high voltages was by Wimshurst or Voss **electrostatic friction generators**, which stored their charge in Leyden Jar capacitors. (Unlike the high-voltage transformer). Resulted that this method of energization proved **ineffective.** Despite the fact that an electrostatic machine can provide the necessary voltage, it cannot simultaneously deliver the required particle charging current, so the plant failed to live up to expectation.

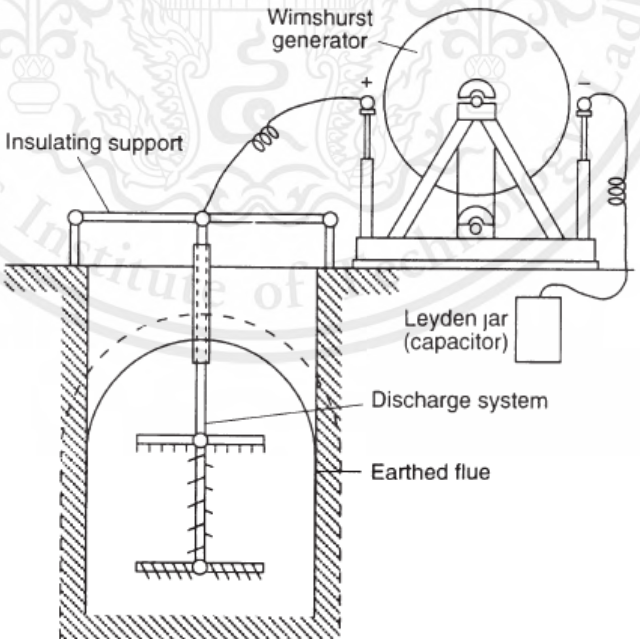

Figure 2.16 Illustration from first US patent on electrostatic precipitation. A.O. Walker, No.342548 (1886).

Source: Parker, K. (1997). Applied electrostatic precipitation. Springer.

The work was being carried out by Dr F. G. Cottrell,a physical chemist, who was studying various ways of controlling air pollution from the Californian Smelters; he made the technological breakthrough for providing high voltage and charging currents simultaneously by using a **high voltage AC transformer** coupled to a synchronous mechanical switch rectifier. This device proved vastly superior to the earlier forms of equipment and led to the successful development of an electrostatic precipitator for the collection of sulphuric acid mist. Cottrell also recognized that negative corona had advantages over positive because of higher electric field strength.

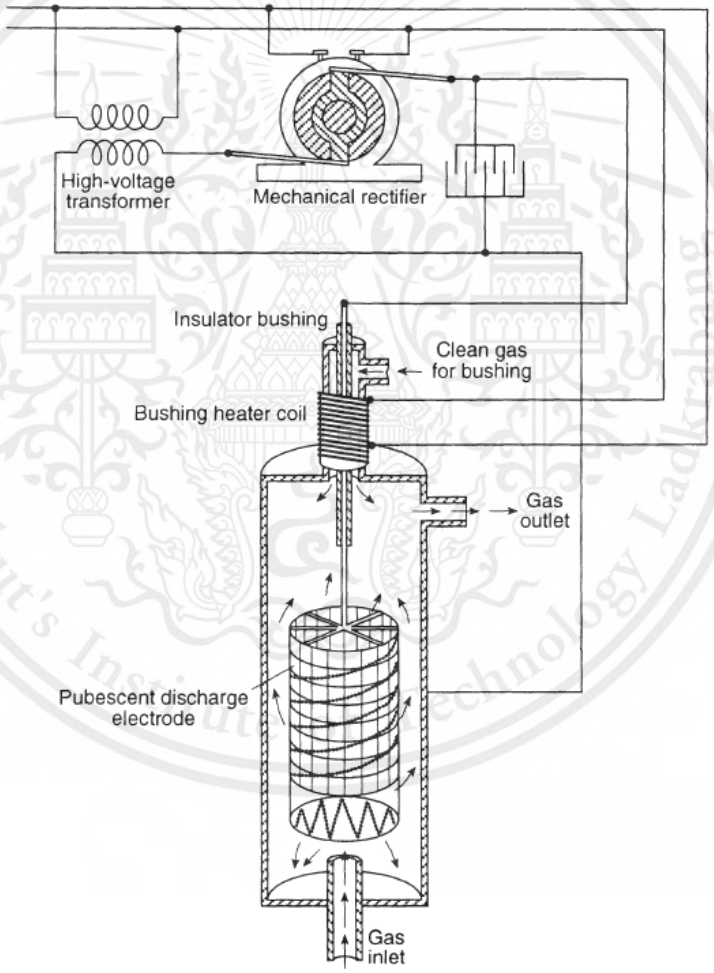

Figure 2.17 Illustration from Cottrell's first electrostatic precipitation patent, No. 895729 (1908).

Source: Parker, K. (1997). Applied electrostatic precipitation. Springer.

2.4.2 Its usage

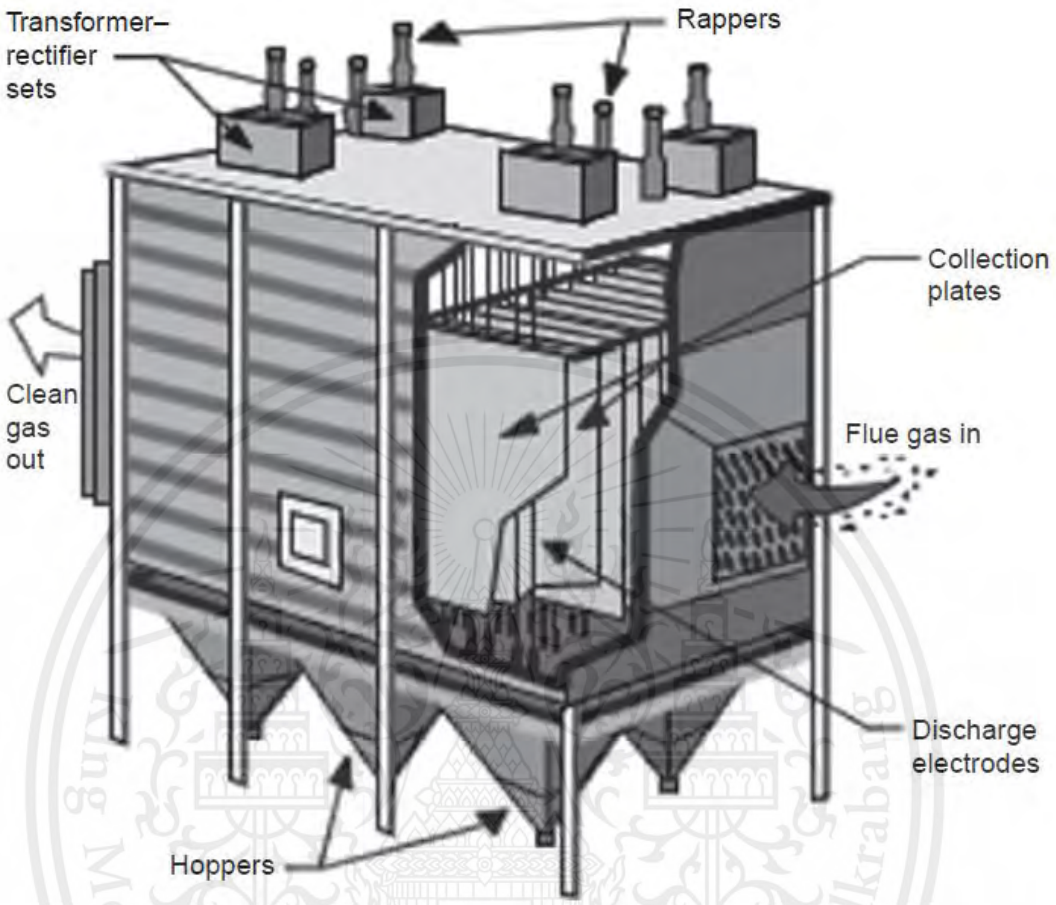

Figure 2.18 Commercial plate-type ESP. U.S. Environmental Protection Agency. Basic concepts in environmental sciencesdmodule 6: air pollutants and control techniques. http://www.epa.gov/eogapti1/module6/matter/control/control.htm; [accessed 30.06.07].

Source: Vallero, D. (2014). Fundamentals of air pollution. Academic Press

Electrostatic precipitators were originally used as a recovery of process material. Nowadays, it is used in industrial scale such as power plant, cement plant, any industrial involving emissions of particulate matter. Electrostatic precipitator uses the high-intensity electric field to ionize the dust particles in the air stream, the dust particles are collected by oppositely charged collecting plate. The dust particles, once

collected are removed from the collector plates periodically by hammering the collectors by a different mechanism.

Electrostatic precipitators offer an advantage such as

1. It can easily handle high temperature gases which makes it suitable for boilers, furnaces, etc.
2. Small pressure drops.
3. High collection efficiency, if it was designed correctly according to the size and types of particulate matter on that location.
4. Can be used to collect wet pollutants using wet ESP system.
5. Handle a wide range of particle sizes ranging from fine to coarse.
6. If properly designed and constructed, the operating and maintenance course are considerably lower than other types of systems.

Electrostatic precipitators have disadvantages such as

1. The initial cost is the highest compared to other types of particulate matter control systems.
2. A large amount of space is required for this system.
3. Not flexible to move once it was installed.
4. ESP is not suitable for combustible particles such as grain or wood dust.
5. They cannot be used to collect gaseous pollutants.

2.4.3 Types of Electrostatic Precipitator

2.4.3.1 Single and two stage plate type

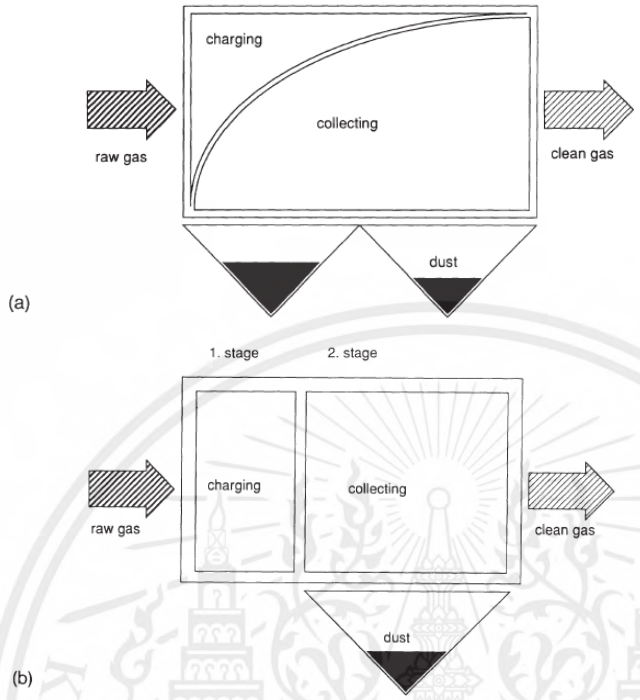

Figure 2.19 (a) Single-stage precipitator (b) Two-stage precipitator

Source: Parker, K. (1997). Applied electrostatic precipitation. Springer.

There are two main types of Electrostatic precipitator as shown in Figure 2.19, which are single and two stages. The difference is that in the two-stage system steps 1 and 2 are executed separately whereas in the single-stage system, step 1 and 2 are executed together with another steps.

However, the single-stage system is much more popular in industries mainly because of the cost that is initially cheaper to build single-stage, also the size needed to build single-stage is much lower than two-stage whereas they need another chamber to charge particles separately. Where the two-stage system is more suited to use in an application that is in smaller scale and its ability to capture more fine particulate matter is better than the single-stage system.

2.4.3.2 Plate vs Tube Electrostatic Precipitator

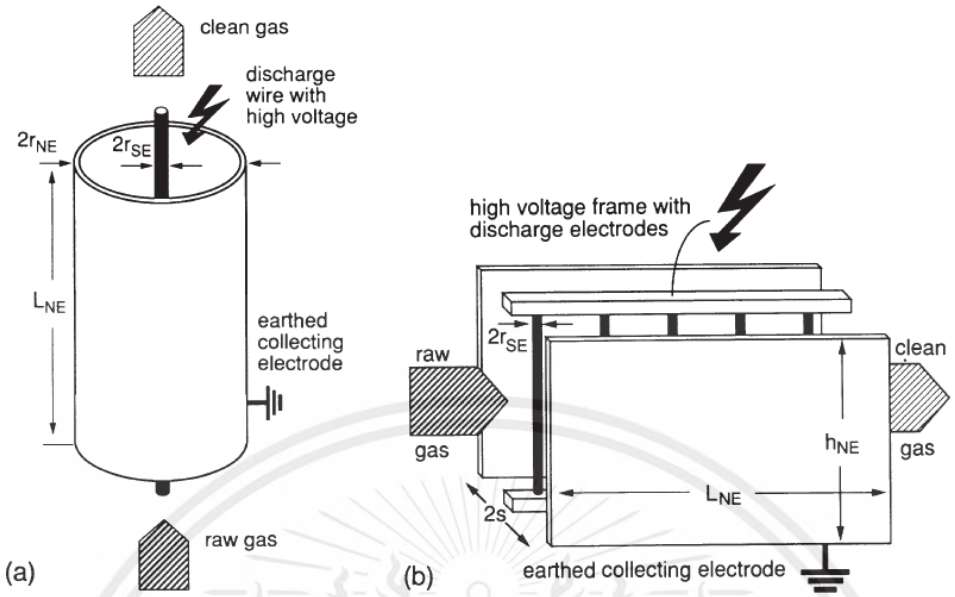

Figure 2.20 (a) Tube-type ESP (b) Plate-type ESP

Source: Parker, K. (1997). Applied electrostatic precipitation. Springer.

Tube-type and plate-type electrostatic precipitators (ESP) are the two most common designs for controlling particulate matter emissions from various industries. Both have their own unique advantages and disadvantages and are designed based on the type and size of particulate matter.

For tube-type ESP, the tube and discharge wire are orientated along the gravitational axis, and it is usually cleaned by using liquid running down the tube of ESP. With this reason, tube-type is more suited to use with processes that use self-draining liquid particles. Most importantly, it is more suited to capture bigger particles and dust that is coarse particles, and since it's a tube, allowing it to handle higher gas flowrate than the plate type. Lastly, it can be designed compactly. They are often used in cement production, steel manufacturing, etc.

For plate-type ESP, it has a flat plate configuration where the collection plates are aligned parallel to the gas flow direction. It is often use when the compact design is not a priority. Plate-type does a better job on capturing finer Particulate Matter (PM) and in the same time it is also good at capturing bigger PM, plate-type ESP is a good idea when a wide range of PM size is taken into consideration. They are often used in coal-fired power plants, chemical manufacturing, etc.

2.4.4 Ion production

2.4.4.1 Introduction

When a critical electric field strength has been overcome, there's a large number production of charge carriers in a gas phase. This can be created by using a high voltage electrode with an appropriate gap to the ground, when the applied voltage exceeds some value, an electrical current between the two electrodes can be measured which indicates a corona discharge. Where this is called the corona onset voltage as shown in Figure 2.21. If the voltage is increased further, this will lead to an increase in electrical current, then the spark-over occurs.

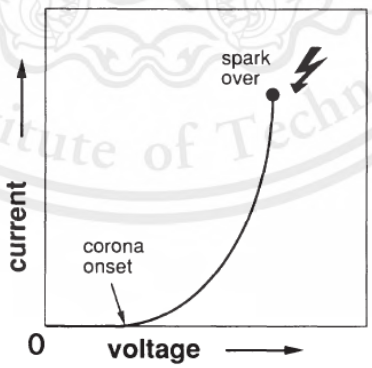

Figure 2.21 Current-Voltage Relationship

Source: Parker, K. (1997). Applied electrostatic precipitation. Springer.

2.4.4.2 Corona discharge

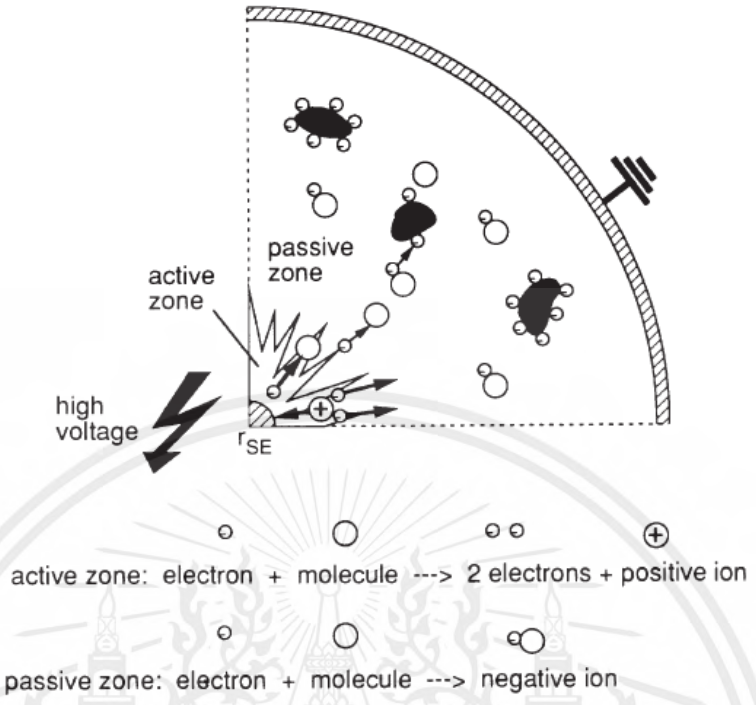

Figure 2.22 Principle of a corona discharge.

Source: Parker, K. (1997). Applied electrostatic precipitation. Springer.

According to the diagram on figure 2.22 shows a basic principle of a corona discharge. Corona discharge occurs if a conducting electrode in the shape of a sharp point (or a thin wire) is held at a sufficiently high potential, maybe 2-20 kV, the breakdown field strength may be exceeded in a region of a few millimeters around the electrode. There are two zones when corona discharge occurs, that is the active zone and the passive zone. These are the regions where different electrical and physical phenomena occur during the corona discharge process.

The active zone, known as "corona zone," is the region where the electrical breakdown or ionization of the surrounding air or gas occurs due to the high voltage applied between the high voltage electrode with a gap to the ground. In this zone, the

electric field is strong enough to take electrons from air molecules which will create free electrons and positive ions.

The passive zone, known as "non corona zone," is the region beyond the active zone where the electric field strength is not enough for electrical breakdown or ionization of the air or gas which will leave negative ion.

In general, the discharge electrode can be operated on **negative or positive** polarity. For a given geometry, however, the corona initiation voltage and the electrical breakdown of the gas occur at higher voltages for negative energization than for positive. Because of these higher electrical field strengths, most industrial applications prefer negative corona, that is discharge electrodes are energized with negative high voltage and the collecting plates (positive) are grounded. However, there are some drawbacks between positive and negative coronas. A positive corona generates much less ozone than the corresponding negative corona, as the reactions which produce ozone are relatively low energy. Therefore, the greater number of electrons of a negative corona leads to increased production. However, as discussed above, electrical breakdown of gas occurs at much higher electric field strength for negative corona compared to positive corona. Negative corona would be more efficient in capturing particulate matter, trade-off with more ozone production. That is the reason why most industrial size ESP prefer to use negative corona.

2.4.4.3 Resistivity of particulate matter

The resistivity of PM is a measure of its resistance to electrical conduction, is considered important factors as it could affect the collection efficiency. Once the particle has been collected, it begins to lose its charges to the plate. This transfer of charge completes the electrical circuit which produces current flow. If the resistivity is too low (the dust is a good conductor), the electrostatic charge will be drained off too quickly and that dust could re-entrain into the gas. If the resistivity Is too high (the dust is a good insulator), the charge would not drain off at the collecting plates which causes "**back corona**" (Refer to the next section).

The resistivity of a material is determined experimentally by establishing a current flow through a slab of the material (Figure 2.23). The resistivity P is equal to the resistance times the area normal to the current flow divided by the path length, as shown in Eq. (2.21).

$$P = \frac{RA}{L} = \frac{V}{I} \cdot \frac{A}{L} \tag{2.21}$$

Where P = Resistivity $(\Omega - cm)$

R = Resistance (Ω)

A = Area normal to the current flow (cm^2)

L = Path length in the direction of current flow (cm)

V = Voltage (V)

I = Current (A)

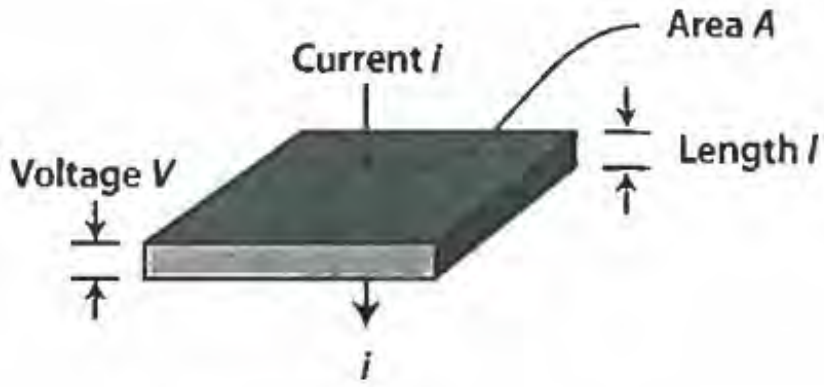

Figure 2.23 Determination of resistivity.

Source: C. David Cooper, & Alley, F. C. (2010). Air Pollution Control. Waveland Press.

The resistivity of materials ranges from 10^{-3} to $10^{14}\ \Omega - \text{cm}$, for coal fly ashes, resistivity usually ranges from 10^{5} to $10^{13}\ \Omega - \text{cm}$, the resistivity of dry cement dust can exceed $10^{13}\ \Omega - \text{cm}$. ESP design and operation are difficult for resistivities above $10^{11}\ \Omega - \text{cm}$.

The major factors influencing fly-ash resistivity are temperature and chemical composition (of the fly ash and of the combustion gases). The conductivity of the dust layer is derived from two effects: volume conduction through the material itself, and surface conduction via adsorbed gases or liquids. Volume conduction decreases with increased temperature, whereas surface conduction increases with temperature.
A highly resistive dust increases the occurrence of electrical sparking in the precipitator and forces a lower operating voltage. A serious back corona can develop, which reduces both particle charging and collection. The effect of resistivity are more significant above $10^{11}\ \Omega - \text{cm}$.

2.4.4.4 Back corona

The dust layer on a collecting plate has a certain resistivity. A high resistivity (low electrical conductivity) of the dust layer may generate back-corona on the collecting plate. As illustrated in Figure 2.24.

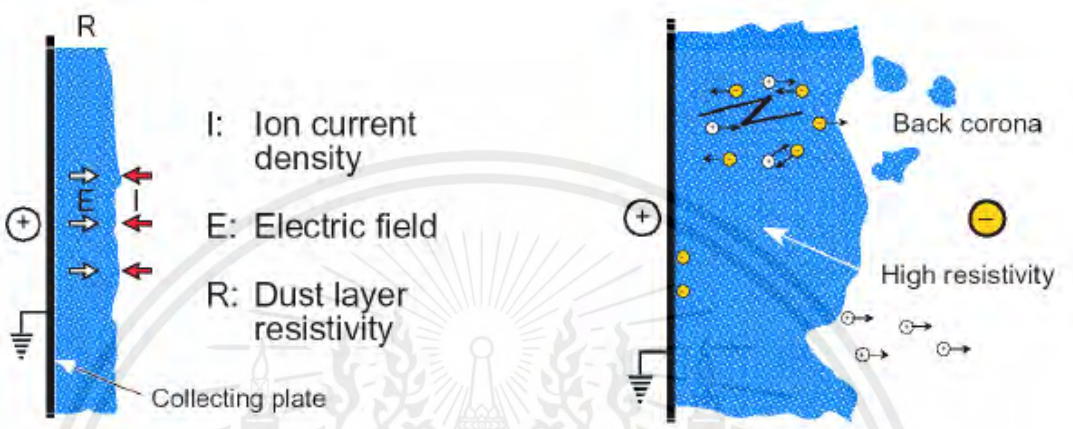

Figure 2.24 Corona current, I, penetrating the dust layer generates ionization, back-corona, along the collecting plate.

Source: Francis, S. L., & Bradburn, K. M. (2007). Electrostatic Precipitators for Industrial Applications.

The corona current through the dust layer on the collecting plate multiplied with the apparent resistivity of the dust generates a voltage (electrical field) drop through the dust layer. Depending on the gas conditions and dust properties (size, shape, compactness etc.) the field strength in the layer may lead to a breakthrough of the gas, local sparking in the dust layer and positive and negative ions are generated. The positive ions travel to the discharge electrode and may discharge any negatively charged particles on their way. Therefore, the collecting efficiency decreases. This is further aggravated by the re-entrainment of dust due to the sparking. Examples of I/V curves under back-corona condition are seen in Figure 2.25.

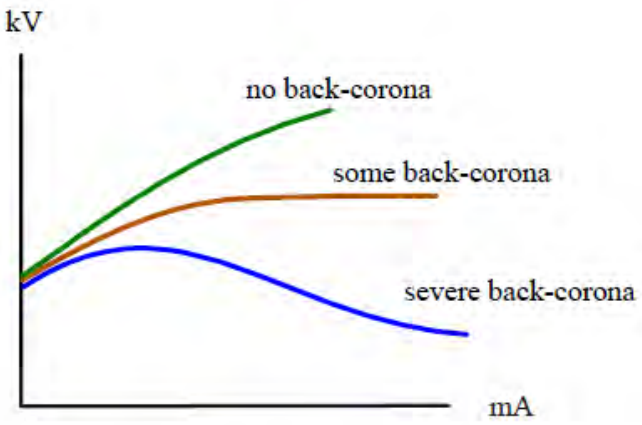

Figure 2.25 Typical I/V curves with and without back-corona conditions.

Source: Francis, S. L., & Bradburn, K. M. (2007). Electrostatic Precipitators for Industrial Applications

2.4.4.5 Corona initiation field strength

The electric field required to initiate a continuous ionization process depends on the ionization energy of gas species and the mean free path between collisions. The mean free path is related to the gas state then the corona initiation field strength is a function of gas density. Below is a semi-empirical relationship between the initiation field strength E_0, relative gas density δ, the discharge wire radius r_{SE} and empirical constants, A and B.

$$\mathrm{E_0} = \mathbf{A}\delta + \mathrm{B}\sqrt{\delta/\mathrm{r_{SE}}} \tag{2.22}$$

$$\delta = \frac{\rho_2}{\rho_1} = \frac{p_2}{p_1} \cdot \frac{T_1}{T_2} \tag{2.23}$$

At normal conditions, $T_1 = T_0 = 273\ K$ and $p_1 = p_0 = 1\ bar$

Empirical constant for ESP, $A = 3.2 \times 10^6\ V/m$, $B = 9 \times 10^4\ V/m^{1/2}$

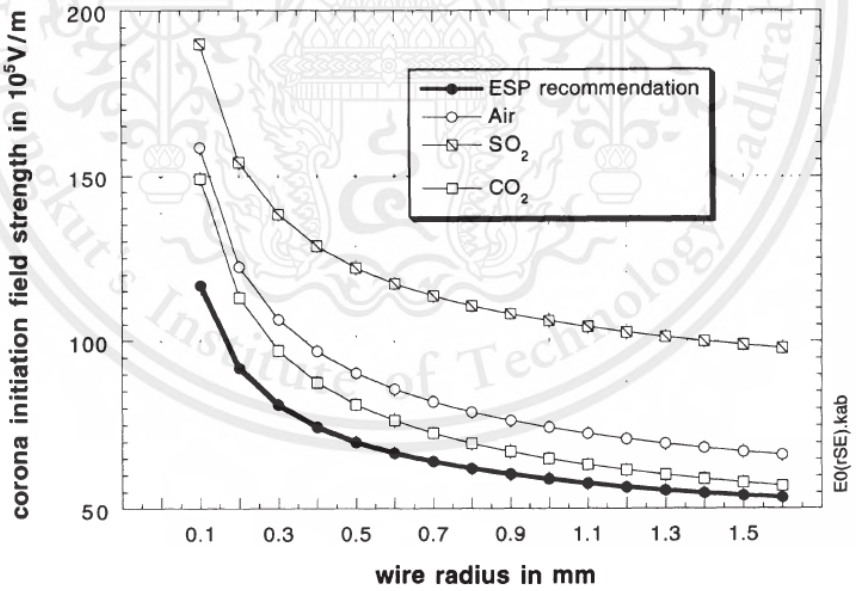

Figure 2.26 Corona initiation field strength $\boldsymbol{E_0}$ as a function of wire radius

Source: Parker, K. (1997). Applied electrostatic precipitation. Springer.

2.4.5 Particle charging

The charging process is divided into a field charging region, for particles > 1 μm, and a diffusion charging region for particles < 0.1 μm. While field charging requires the presence of an electrical field, which drives the free movable charge carriers, the diffusion process is based on randomly moving gas ions caused by temperature and described by the kinetic gas theory, i.e. Brownian motion.

2.4.5.1 Cochet's charging model

The particle saturation charge is given by the below equation by Cochet. This calculation gives the electric field strength (E), where the electrical permittivity of the particle material ε_r needs to be specified.

$$Q_p^{\infty} = \left\{(1 + 2\lambda/d_p)^2 + \left(\frac{2}{1+2\lambda/d_p}\right) \cdot \left(\frac{\varepsilon_r - 1}{\varepsilon_r + 2}\right)\right\} \cdot \pi\varepsilon_0 {d_p}^2 E \tag{2.24}$$

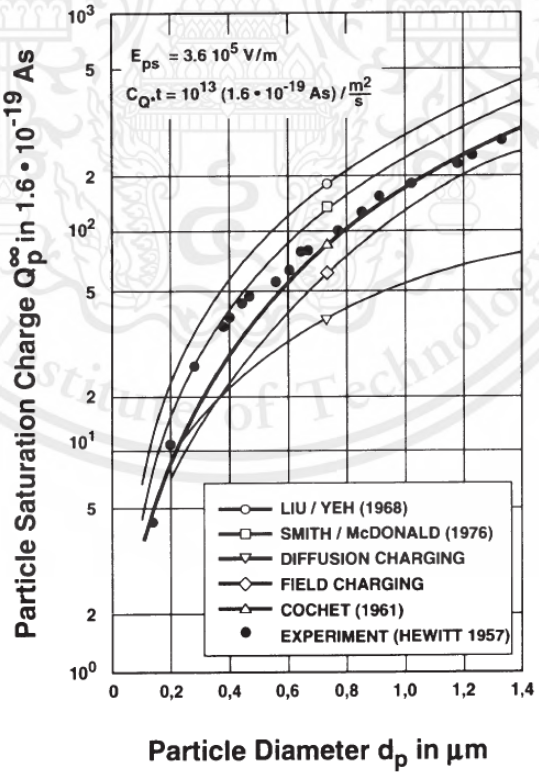

Figure 2.27 Plot of particle diameter versus particle saturation charge.

Source: Parker, K. (1997). Applied electrostatic precipitation. Springer.

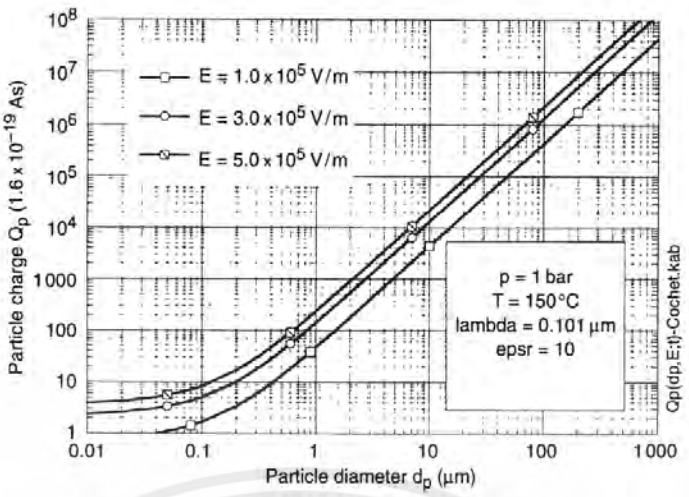

Figure 2.28 Plot of particle diameter versus particle saturation charge.

Source: Parker, K. (1997). Applied electrostatic precipitation. Springer.

2.4.5.2 Time dependence and saturation charge

Time dependence of charging process is described by using the time constant τ_Q for the charging process. The dynamic charging behavior is independent of particle size when constant electric field is considered.

$$Q_P(T) = Q_P^{\infty} \cdot \frac{T}{T+\tau_Q} \tag{2.25}$$

$$\tau_Q = \frac{4\varepsilon_0}{c_Q b} \approx \frac{4\varepsilon_0}{j_{NE}/E} \tag{2.26}$$

However, before time dependence can be calculated, the time constant (τ_Q) needs to be specified from the electrical conditions. According to the Ohm's law that the concentration of gas ions (c_Q) is expressed in terms of current density, electric field, and mobility, given approximately in equation (2.10). Mostly for typical electrical states, the time constant (τ_Q) has a value of ≤ 10 ms. The figure below shows the relationship of charging process with respect to time constant 1, 10 and 100ms. As observed, the particles will reach 90% of their saturation charge within 10ms under typical electrical conditions.

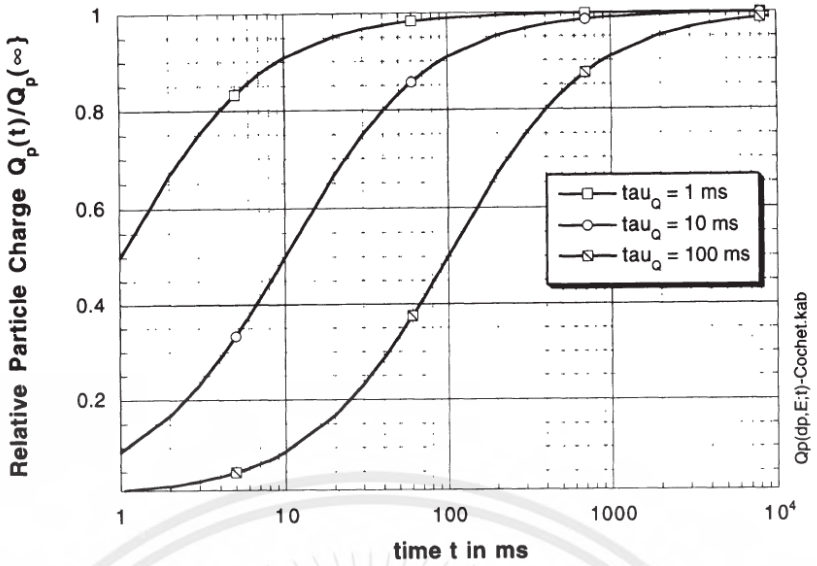

Figure 2.29 Plot of relative particle charge versus time.

Source: Parker, K. (1997). Applied electrostatic precipitation. Springer.

2.4.5.3 Equation of motion

To analyze the motion of particles inside ESP, the balancing of all forces components are needed. It comprises of the momentum force $\overrightarrow{F_T}$, the electrical force $\overrightarrow{F_{el}}$. and drag force $\overrightarrow{F_w}$, given by below equations.

$$\overrightarrow{F_T} = -m\vec{a} \tag{2.27}$$

$$\overrightarrow{F_{el}} = Q_p\vec{E} \tag{2.28}$$

$$\overrightarrow{F_D} = c_w(Re) \cdot A_{pr} \cdot \frac{\rho_F}{2} \cdot v_{rel} \cdot \vec{v}_{rel} \tag{2.29}$$

The sum of all forces are equal to zero.

$$\overrightarrow{F_D} + \overrightarrow{F_{el}} + \overrightarrow{F_w} = 0 \tag{2.30}$$

2.4.5.4 Theoretical migration velocity

Recall section 2.2.2.3 Drag, where the drag force on particle was introduced.

$$F_D = \frac{3\pi\mu_g v_p d_p}{C_C} \tag{2.15}$$

Where μ_g = Gas viscosity $(g \cdot cm^{-1} \cdot s^{-1})$

d_p = Particle diameter (cm)

ρ_g = Gas density $(g \cdot cm^{-3})$

v_p = Particle velocity relative to the gas $(cm \cdot s^{-1})$

C_C = Cunningham slip factor

Combining with the equation of motion equation yields the theoretical migration velocity (w). Where particle velocity v_p will be written as w

$$\frac{dw}{dt} + \frac{3\pi\mu_g d_p}{m \cdot C_C} w = \frac{Q_P^{\infty}}{m} E \tag{2.31}$$

$$w(t) = w_{th}\left\{1 - e^{\left(-\frac{t}{\tau_p}\right)}\right\} \tag{2.32}$$

$$\tau_p = \frac{m_p \cdot C_C}{3\pi\mu_g d_p} = \frac{\rho_p \cdot {d_p}^2}{18\mu_g} \cdot C_C \tag{2.33}$$

$$w_{th} = \frac{Q_P^{\infty} E}{3\pi\mu_g d_p} \cdot C_C \tag{2.34}$$

Taking $w(t = 0) = 0$ as the initial condition, the solution of equation (2.31) can be found. This describes the time dependence of the particle migration velocity (equation 2.32). The relaxation time τ_p characterizes the dynamic behavior of the particle (equation 2.33) and w_{th} is the theoretical migration velocity, which is the steady state velocity of the particle (equation 2.34).

The theoretical migration velocity is plotted in Figure 2.30 as a function of particle size for three different electric field strengths, a temperature of 150°C and an electrical permittivity of ε_r= 10. The theoretical migration velocity shows a minimum located at 0.35 µm. For larger particles the increase of w_{th} proceeds linearly with particle size. For smaller particles the increase in w_{th} is more pronounced.

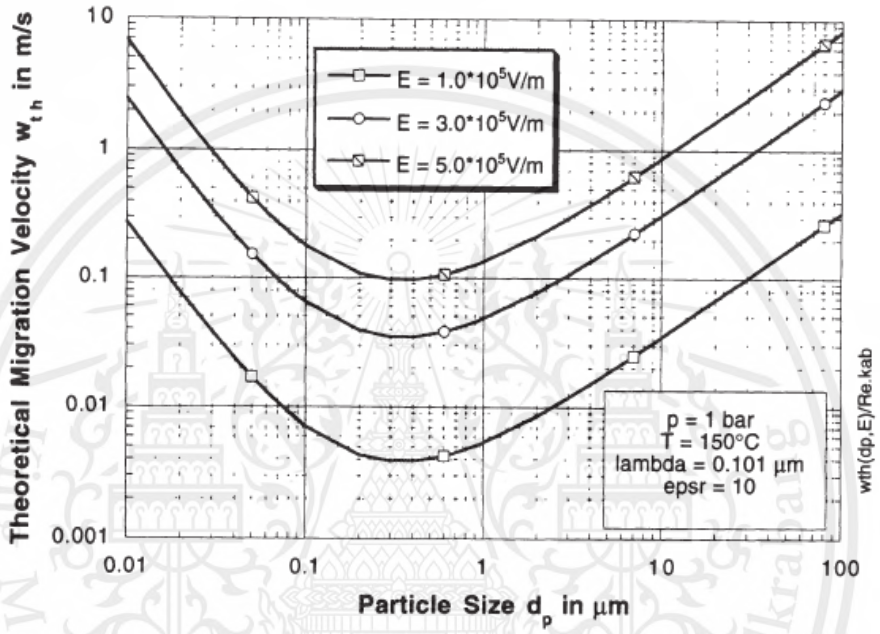

Figure 2.30 Plot of theoretical migration velocity as a function of particle size for three different electric field strengths.

Source: Parker, K. (1997). Applied electrostatic precipitation. Springer.

This figure shows an effective theoretical particle migration velocity in a charging process, where is around 0.5 to 8 m/s. Electric field intensity in the range of $1 - 5 \times 10^5\,\mathrm{V/m}$.

2.4.6 Particle Collection

After the particles have been charged, these particles will be moving toward the collection process in the next step. Particle Collection uses the principle of electric field to repel the charged particles into the opposite polarity collecting plate.

2.4.6.1 Charged particles motion in a uniform Electric Field

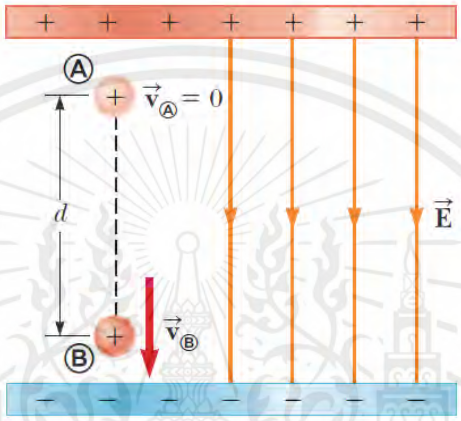

Figure 2.31 A proton accelerates from A to B in the direction of the electric field.

Source: Serway, R. A., & Jewett, J. W. (2013). Physics for Scientists and Engineers with Modern Physics. Cengage Learning.

Starting with the conservation of energy equation.

$$\Delta K + \Delta U = 0 \tag{2.35}$$

$$\left(\frac{1}{2}mv^2 - 0\right) + (e\Delta V) = 0 \tag{2.36}$$

The final speed of particle is given as.

$$v = \sqrt{\frac{-2e\Delta V}{m}} = \sqrt{\frac{-2e(-Ed)}{m}} = \sqrt{\frac{2eEd}{m}} \tag{2.37}$$

Where v = Particle velocity $(m \cdot s^{-1})$

e = Particle charge $(1.6 \times 10^{-19} C)$

ΔV = Potential difference (V)

E = Electric field $(V \cdot m^{-1})$

d = Gap between + and – (m)

m = Particle mass (kg)

Where mass of the particle is found from the relation of density.

$$\rho = \frac{m}{V} \tag{2.38}$$

Assuming the dust particles are sphere.

$$V = \frac{4}{3}\pi {r_p}^3 = \pi \frac{{d_p}^3}{6} \tag{2.39}$$

Mass of each particle is given by.

$$m = \rho\pi \frac{{d_p}^3}{6} \tag{2.40}$$

Where ρ = Particle density $(kg \cdot m^{-3})$

d_p = Particle diameter (m)

2.5 Air Flow measurement

2.5.1 Pitot tube

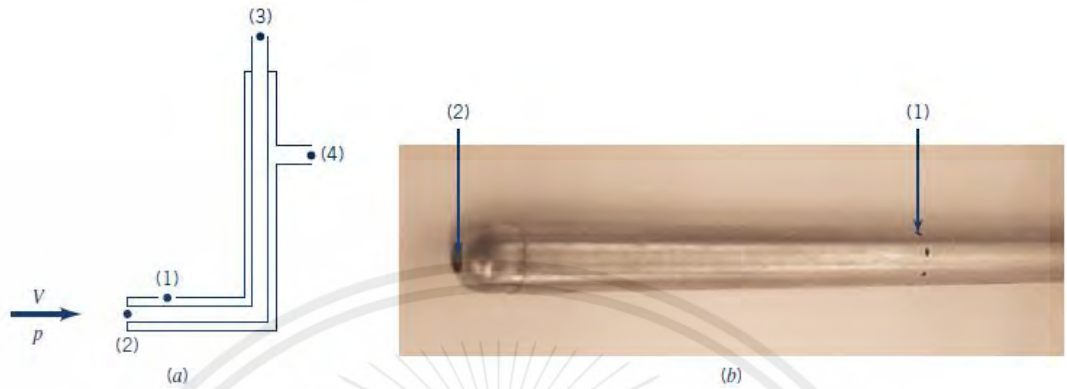

Figure 2.32 The Pitot-static tube.

Source: Munson, B. R., Rothmayer, A. P., Okiishi, T. H., & Huebsch, W. W. (2012). Fundamentals of Fluid Mechanics. Wiley.

There are 2 types of pressure which are static and dynamic. According to Figure 2.32, Pressure at point 4 equals to the static pressure whereas pressure at point 3 equals to the static pressure combined with the dynamic pressure, with these relationships, velocity of fluid can be found. Given by equation 2.41.

$$P_3 = P + \frac{1}{2}\rho v^2 \tag{2.41}$$

Where effect of elevation is negligible yields.

$$P_4 = P_4 = P \tag{2.42}$$

Combining equations 2.41 and 2.42 yields the fluid velocity.

$$v = \sqrt{\frac{2(P_3 - P_4)}{\rho}} = \sqrt{\frac{2(\Delta P)}{\rho}} \tag{2.43}$$

2.5.2 Hot wire Anemometer

Figure 2.33 Hot wire anemometer

Source: Agarwal, T. (2021, February 17). Hot Wire Anemometer : Construction, working & its Applications. ElProCus - Electronic Projects for Engineering Students. https://www.elprocus.com/what-is-a-hot-wire-anemometer-its-working/

A hot wire anemometer is an instrument used to measure the velocity of the fluid. The measurement is done by measuring the loss of heat within the wire that is situated in the fluid stream. These devices use a thin wire and it is heated up electrically to some stage of temperature approximately higher than the range of ambient temperature. This wire gets cool once the air flows throughout it because the resistance of metal mainly depends on the temperature. Resulting in a relation between the resistance of the wire and the speed of the fluid flow. However, the wind have a cooling effect on the wire, so it measures the rate of cooling by either the constant current or the constant temperature configurations.

In the constant current mode, a current will heat the wire. The wind flow will change the temperature of the heated wire. Since the temperature is proportional to the wind flow rate, the anemometer can measure wind speed from this constant current method. Exposure of the heated wire to airflow will alter the temperature. In this mode, there is a danger of burning the wire.

In Constant temperature mode, the hot wire anemometers maintain the wire at a constant temperature. The device must pull more current to keep the temperature steady because the wind flow decreases the wire's heat. Then, the device will determine the current pull needed to maintain a constant temperature to measure wind speed.

Advantages of Hot wire Anemometer

1. Quick response
2. Low starting threshold
3. Portable and easy to operate.

Disadvantages of Hot wire Anemometer

1. Not appropriate in an area where there’s high temperature fluctuations.
2. Not suitable in dirty environments as dust can damage the hot wire.

2.6 Particulate Matter Sensor (PMS5003)

Figure 2.34 PMS5003

PMS5003 is a digital particle concentration sensor, which can be used to obtain the number of suspended particles in the air, i.e. the concentration of particles, and output them in the form of digital interface. This sensor can be inserted into variable instruments related to the concentration of suspended particles in the air or other environmental improvement equipment to provide correct concentration data in time.

Laser scattering principle is used for this sensor, i.e. produce scattering by using laser to radiate suspending particles in the air, then collect scattering light in a certain degree, and finally obtain the curve of scattering light change with time. In the end, equivalent particle diameter and the number of particles with different diameter per unit volume can be calculated by microprocessor based on MIE theory.

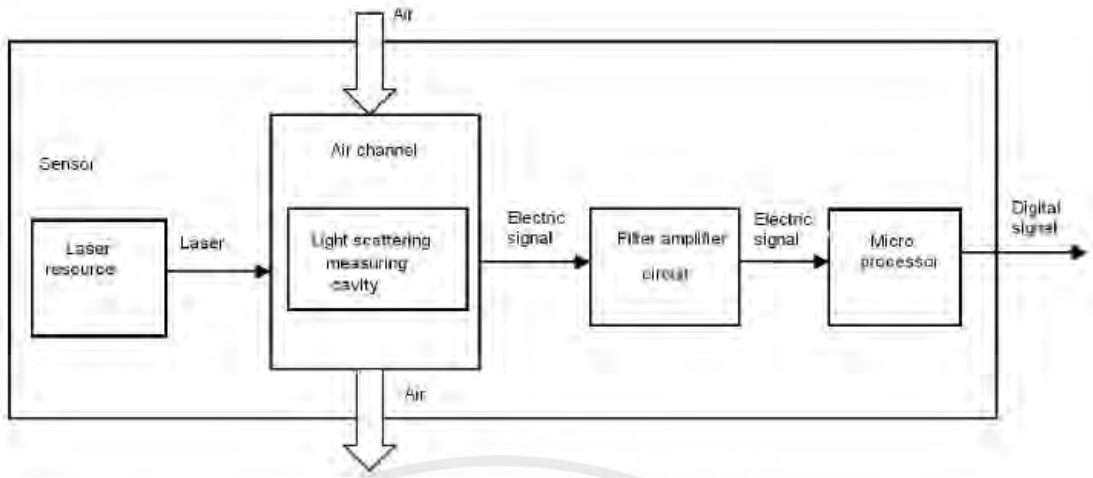

Figure 2.35 Functional block diagram of PMS5003

Source: PMS5003 datasheet

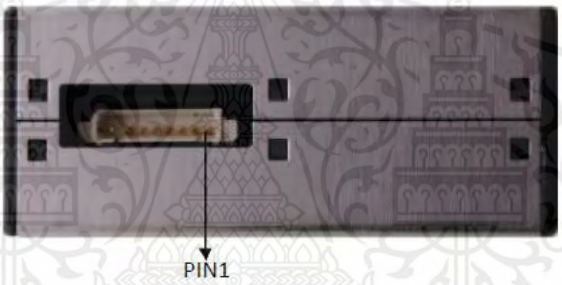

PIN1	VCC	Positive power 5V
PIN2	GND	Negative power
PIN3	SET	Set pin /TTL level@3.3V，high level or suspending is normal working status, while low level is sleeping mode.
PIN4	RX	Serial port receiving pin/TTL level@3.3V
PIN5	TX	Serial port sending pin/TTL level@3.3V
PIN6	RESET	Module reset signal /TTL level@3.3V，low reset.
PIN7/8	NC	

Figure 2.36 PMS5003 sensor pin

Source: PMS5003 datasheet

Parameter	Index	unit
Range of measurement	0.3~1.0；1.0~2.5；2.5~10	Micrometer（μ m）
Counting Efficiency	50%@0.3μ m 98%@>=0.5μ m	
Effective Range（PM2.5 standard）	0~500	μ g/m³
Maximum Range（PM2.5 standard）*	≥1000	μ g/m³
Resolution	1	μ g/m³
Maximum Consistency Error (PM2.5 standard data)*	±10%@100~500μ g/m³ ±10μ g/m³ @0~100μ g/m³	
Standard Volume	0.1	Litre（L）
Single Response Time	<1	Second（s）
Total Response Time	≤10	Second（s）
DC Power Supply	Typ:5.0 Min:4.5 Max: 5.5	Volt（V）
Active Current	≤100	Milliampere（mA）
Standby Current	≤200	Microampere（μ A）
Interface Level	L<0.8 @3.3 H>2.7@3.3	Volt（V）
Working Temperature Range	-10~+60	℃
Working Humidity Range	0~99%	
Storage Temperature Range	-40~+80	℃
MTTF	≥3	Year（Y）
Physical Size	50×38×21	Millimeter（mm）

Figure 2.37 PMS5003 specification

Source: PMS5003 datasheet

2.7 NodeMCU ESP8266

Figure 2.38 NoduMCU ESP8266

Source: NodeMCU ESP8266 datasheet

NodeMCU is an open-source Lua based firmware and development board specially targeted for IoT based Applications. It includes firmware that runs on the ESP8266 Wi-Fi SoC from Espressif Systems, and hardware which is based on the ESP-12 module. NodeMCU runs on 3.3 V logic level which matches the PMS5003 sensor.

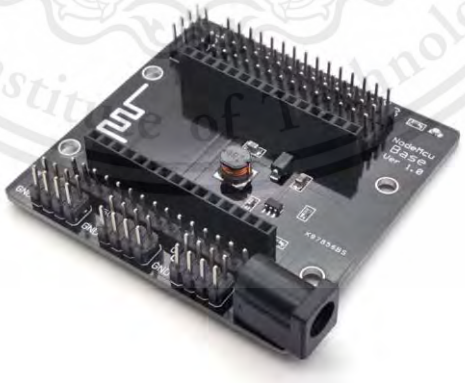

Figure 2.39 NodeMCU ESP8266 Extension board

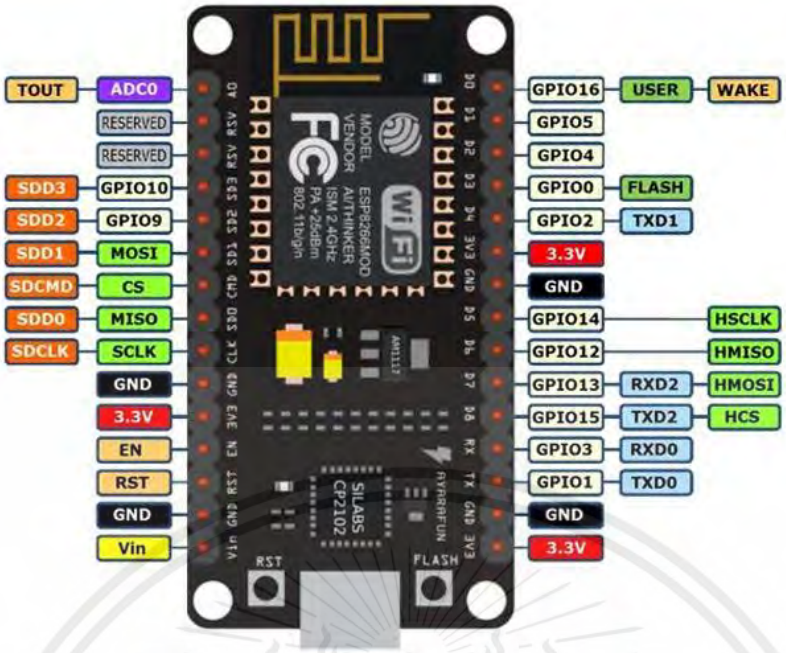

Figure 2.40 NodeMCU ESP8266 Pin definitions

Source: NodeMCU ESP8266 datasheet

The full specification of NodeMCU ESP8266 is given as follows.

- Microcontroller: Tensilica 32-bit RISC CPU Xtensa LX106
- Operating Voltage: 3.3V
- Input Voltage: 7-12V
- Digital I/O Pins (DIO): 16
- Analog Input Pins (ADC): 1
- UARTs: 1
- SPIs: 1
- I2Cs: 1
- Flash Memory: 4 MB
- SRAM: 64 KB
- Clock Speed: 80 MHz

2.8 Duct calculation

Bernoulli equation is defined as

$$P_1 + \frac{\rho v_1^2}{2} + \rho g z_1 + P_H = P_2 + \frac{\rho v_2^2}{2} + \rho g z_2 + \Delta P \quad (2.44)$$

Where P = Pressure (Pa)

ρ = Fluid density (kg/m^3)

v = Fluid velocity (m/s)

E = Electric field $(V \cdot m^{-1})$

P_H = Head pump (Pa)

ΔP = Total Pressure loss (Pa)

The terms head and pressure are often used interchangeably. However, head is the height of a fluid column supported by fluid flow, whereas pressure is the normal force per unit area. For liquids, it is convenient to measure head in terms of the flowing fluid. With a gas or air, however, it is customary to measure pressure on a column of liquid.

Static pressure or static head refers to $P/\rho g$

Velocity pressure refers to $\rho\, v^2/2$ while velocity head refers to $v^2/2g$. Although velocity head is independent of fluid density, velocity pressure is not.

$$P_v = \rho\, v^2/2 \quad (2.45)$$

Where P_v = Velocity pressure (Pa)

v = Fluid velocity (m/s)

Given ρ = $1.204\ kg/m^3$ at standard condition of air

Total pressure refers to the sum of static pressure and velocity pressure.

$$P_t = P_s + P_v \tag{2.46}$$

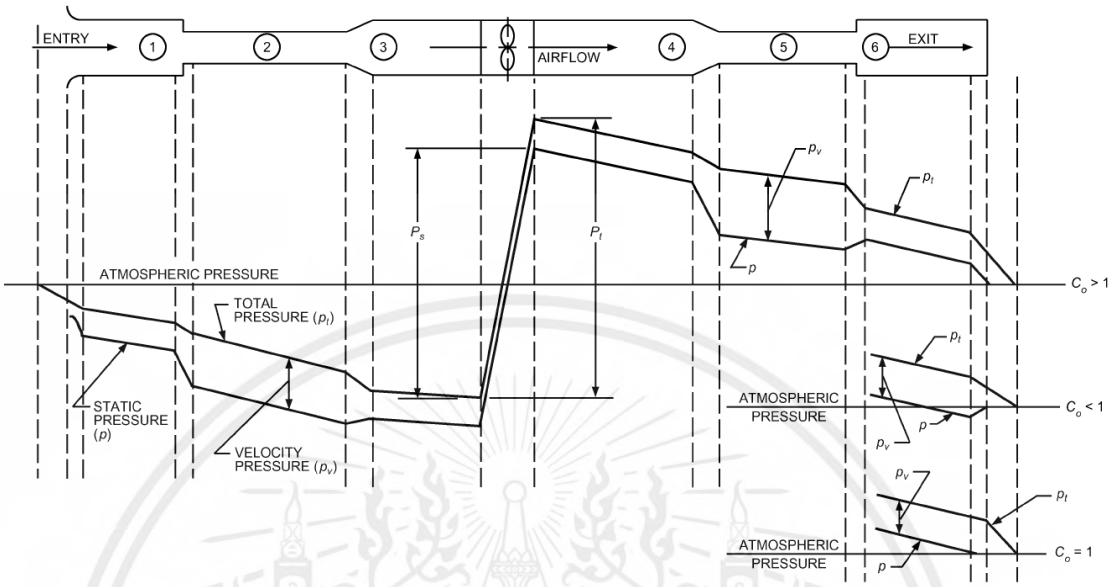

Figure 2.41 Pressure changes during flow in ducts

Source: 2021 ASHRAE Handbook: Fundamentals. (2021).

Friction factor is calculated using Colebrook's equation.

$$\frac{1}{\sqrt{f}} = -2.0 \log\left(\frac{\varepsilon/D}{3.7} + \frac{2.51}{Re\sqrt{f}}\right) \tag{2.47}$$

Where f = Friction factor

ε = Relative roughness

D = Pipe diameter (m)

For rectangular duct, the hydraulic diameter is defined as

$$D_h = \frac{4A}{U} \tag{2.48}$$

Where A = Duct cross section area

U = Duct perimeter

Reynold number is determined from the relation.

$$\mathrm{Re} = \frac{\rho v D}{\mu} \tag{2.49}$$

Where Re = Reynold number

μ = Fluid dynamic viscosity

Major loss is calculated from the relation.

$$\Delta P_{major} = f\frac{L}{D}\frac{\rho v^2}{2} \tag{2.50}$$

Minor loss is calculated from the relation.

$$\Delta P_{minor} = C_0 \cdot \frac{1}{2}\rho v^2 \tag{2.51}$$

Where C_0 = Minor loss coefficient

CHAPTER 3

RESEARCH METHODOLOGY

3.1 Commercial ESP

Since most of the ESP units are discussed according to an industrial scale ESP. The basic working principle is also applicable for smaller size ESP. However, there are parameters and design considerations where they are completely different. We decided to buy a commercial ESP that is smaller size from a manufacturer in China, to test the machine's characteristics and efficiency when it's smaller size as some of the parameters needs to be adjusted which may change the operating conditions which affect the efficiency of the machine. This will give us a basic idea of how to design our customized ESP.

Figure 3.1 Commercial ESP

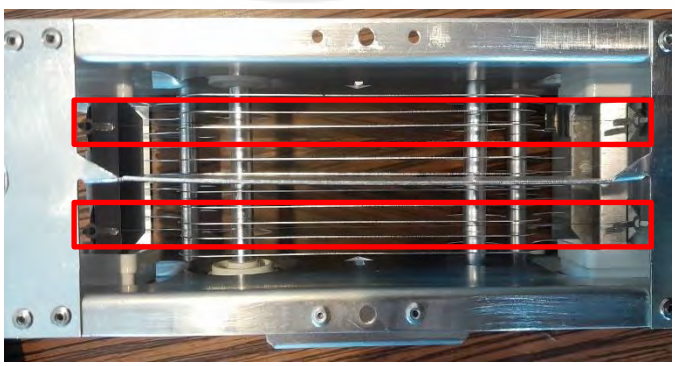

Figure 3.2 Commercial ESP Front view (Electrode charging side)

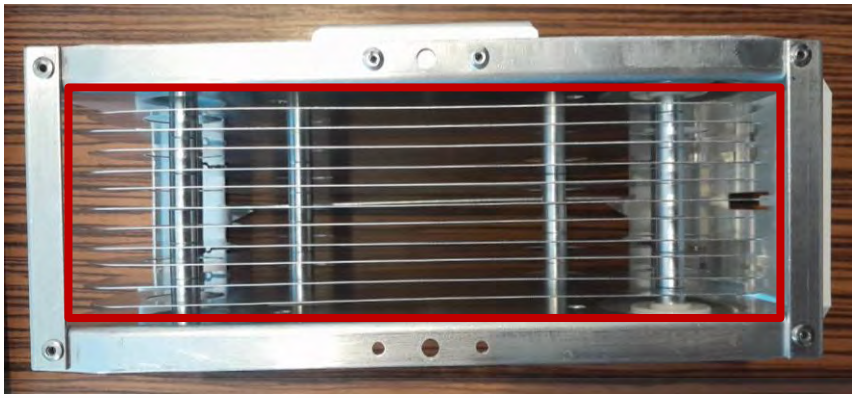

Figure 3.3 Commercial ESP Rear view (Collecting plate side)

Figure 3.4 High Voltage power supply unit (4/8 kV)

This commercial ESP designs such that the input voltage into charging and collecting sides are done separately. As seen in Figure 3.4 that the high voltage power supply outputs 2 High voltage values which are 4 and 8 kV.

3.1.1 Basic ESP Machine Testing

We wanted to make sure if the machine we bought was able to perform correctly. Wood pallets were used to construct the support for ESP unit where it's facing vertically. Incense was introduced to let the smoke blow towards the ESP unit. When the ESP system is powered, the smoke coming from the incense should be reduced confirming that the ESP unit works correctly.

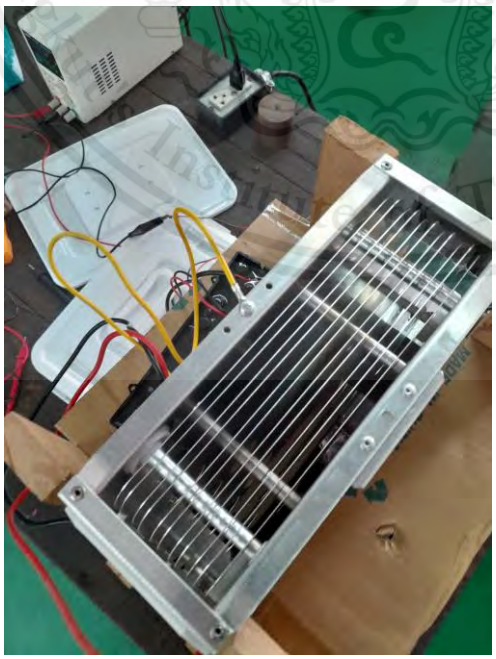

Figure 3.5 Incense blowing experiment setup

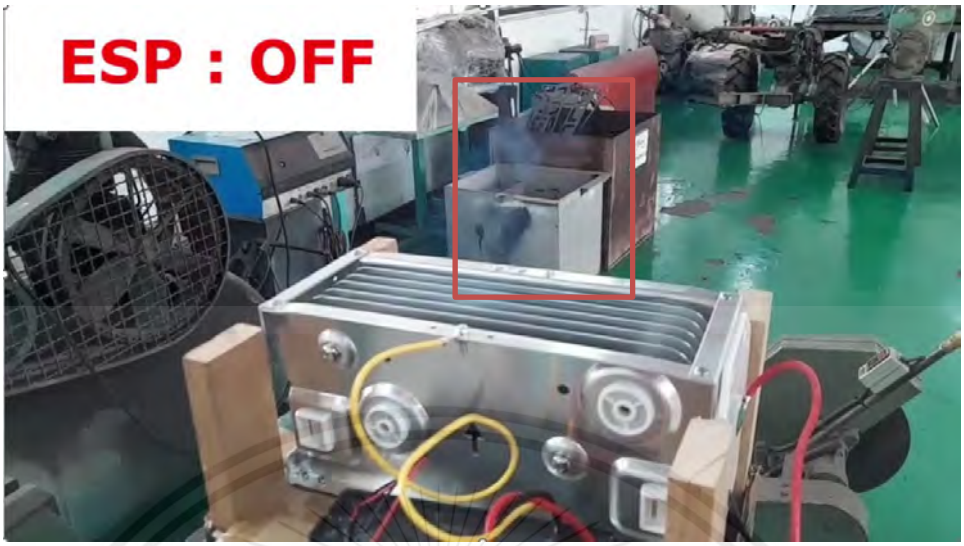

Figure 3.6 Incense blowing experiment (ESP Power off).

Figure 3.7 Incense blowing experiment (ESP Power on).

Around 10 of incense were used, it was fired at the bottom of the test rig, the smoke was constantly blowing upward towards the ESP. Once the power supply is turned on, energizing the high voltage converter, so did the charging and collecting process has begun, the smoke significantly gone away. Refer to Figure 3.6 once when the system is off.

3.1.2 ESP Testing for its efficiency

After the previous test has confirmed the unit performed correctly. Another important parameter such as flowrate and efficiency were to be determined. By utilizing a testing rig for the ESP system. By placing the PMS5003 (PM sensor) both at inlet and outlet side, where the difference in PM can be directly related to collection efficiency, the fan is placed at the outlet which induced the flow through the system, pitot tube is used to measure the flowrate of the system.

All parts are designed using SolidWorks which will be 3d printed.

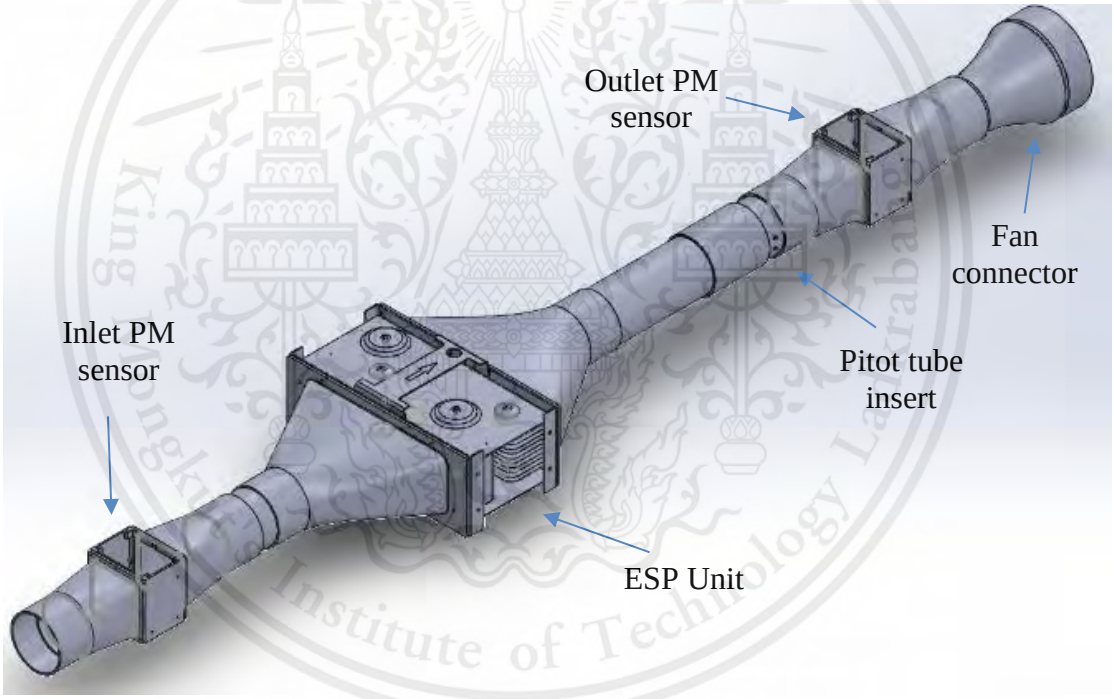

Figure 3.8 Commercial ESP test rig.

As seen on Figure 3.8 that the pipe on the center has a small diameter. Since the pitot tube was used to measure the air speed, pitot tube is not effective to measure air speed below 5 m/s practically, Thus, the pipe diameter must be reduced to increase the flow velocity.

The manufacturer recommends running this ESP at a volume flowrate of 100 m^3/h. To make sure that the velocity in the pipe would be more than 5 m/s. Thus, the maximum pipe diameter could be.

$$A = \frac{Q}{v}$$

Where $$A = \frac{\pi d^2}{4}$$

Then $$d = \sqrt{\frac{4Q}{\pi v}} = \sqrt{\frac{4(100\,\frac{m^3}{h}\cdot\frac{1h}{3600\,s})}{\pi\cdot(5\,m/s)}} = 0.0841\,m = 84\,mm$$

The maximum pipe diameter is 84 mm and any larger diameter than this value would cause velocity to be lower than the threshold of 5 m/s causing error in measurement using pitot tube.

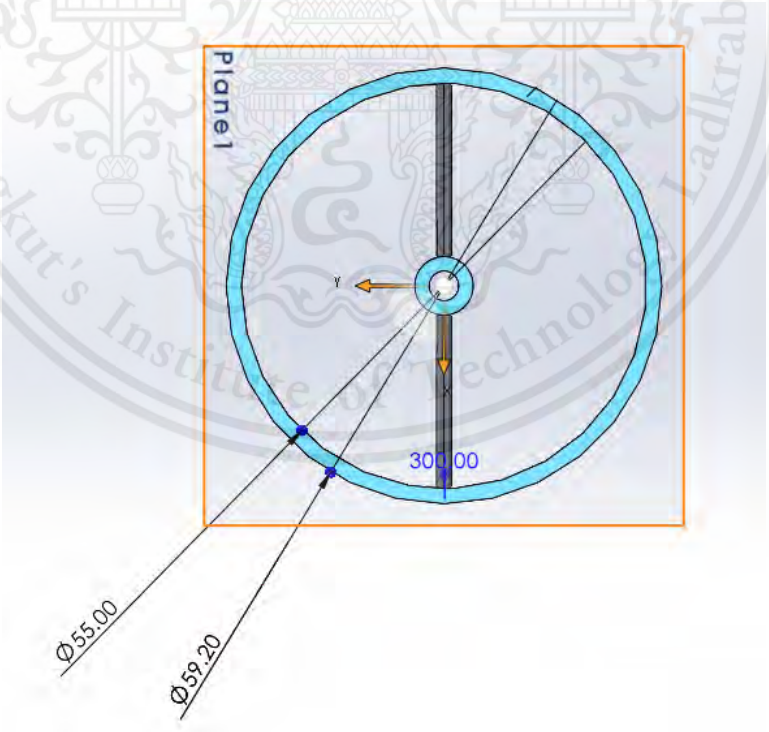

Figure 3.9 Pitot tube holder front view.

Figure 3.10 Pitot tube.

Figure 3.11 Air flow meter (Pitot tube)

Figure 3.10 shows a pitot tube used in this experiment, inserted in the direction of air flow. Air flow meter in figure 3.11 reads the pressure difference where it automatically calculates the air velocity according to equation 2.43.

Figure 3.12 Axial flow fan 290 m^3/h

This axial flow fan claims a volumetric flow rate of 290 m^3/h and a head of 150 Pa is used to induce the airflow through the system.

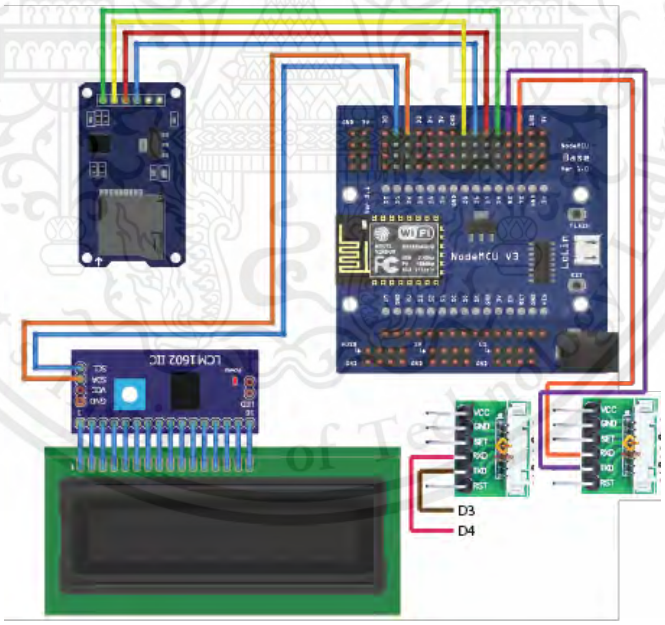

Figure 3.13 PM concentration data logger schematic.

The data logger includes two PM sensors, LCD, ESP8266, and SD card module. These are programmed by Arduino IDE software.

Below is the Arduino code for the data logging.

```
#include <SPI.h>
#include <SD.h>
#include "PMS.h"
#include <LiquidCrystal_I2C.h>
#include <SoftwareSerial.h>
LiquidCrystal_I2C lcd(0x27, 16, 2); // I2C address 0x27, 16 column and 2 rows
SoftwareSerial pmsSerial(0, 2); // Create a SoftwareSerial instance for the second se
PMS pms(Serial);
PMS pms1(pmsSerial);
PMS::DATA data;
File myFile;
const int chipSelect = D8;

void setup() {
 // Open serial communications and wait for port to open:
 Serial.begin(9600);
  Serial1.begin(9600);  // GPIO2 (D4 pin on ESP-12E Development Board)
   pmsSerial.begin(9600);
 lcd.init(); // initialize the lcd
lcd.backlight();

 while (!Serial) {
  ; // wait for serial port to connect. Needed for native USB port only
 }

 if (!SD.begin(chipSelect)) {
  Serial.println("initialization failed!");
  while (1);
 }
 myFile = SD.open("test.txt", FILE_WRITE);

 // if the file opened okay, write to it:
```

```
 if (myFile) {

   myFile.println("Start PM logging");
   myFile.println(" ");
   // close the file:
   myFile.close();
  }

}

void loop() {

 if (pms.read(data))
  {

   lcd.setCursor(0, 0);
    lcd.print(data.PM_AE_UG_1_0);
   lcd.setCursor(5, 0);
   lcd.print(data.PM_AE_UG_2_5);
    lcd.setCursor(10, 0);
   lcd.print(data.PM_AE_UG_10_0);

    myFile = SD.open("test.txt", FILE_WRITE);
  if (myFile) {
   myFile.println(" ");
   myFile.print(data.PM_AE_UG_1_0);
   myFile.print(",");
   myFile.print(data.PM_AE_UG_2_5);
   myFile.print(",");
   myFile.print(data.PM_AE_UG_10_0);
   myFile.print(",");
   myFile.close(); // close the file
  }
```

```
  delay(100);
 }

 if (pms1.read(data))
 {

  lcd.setCursor(0, 1);
   lcd.print(data.PM_AE_UG_1_0);
     lcd.setCursor(5, 1);
  lcd.print(data.PM_AE_UG_2_5);
     lcd.setCursor(10, 1);
  lcd.print(data.PM_AE_UG_10_0);

   myFile = SD.open("test.txt", FILE_WRITE);
 if (myFile) {
  myFile.print(data.PM_AE_UG_1_0);
  myFile.print(",");
  myFile.print(data.PM_AE_UG_2_5);
  myFile.print(",");
  myFile.print(data.PM_AE_UG_10_0);

  myFile.close(); // close the file
 }

  delay(1000);
 }
}
```

According to the code, the data is logged every 1.1 minute interval.

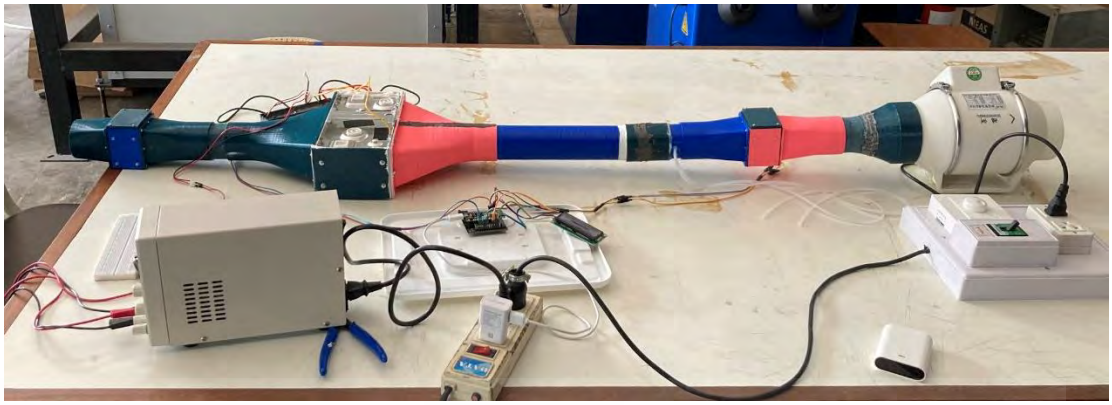

Figure 3.14 Complete ESP experiment setup.

All ducts and connectors are printed using PLA material. All parts are customized design for each component. The connection between ducts and ESP uses the screw along with the gasket to prevent air leakage.

The results of this test experiment are as follows.

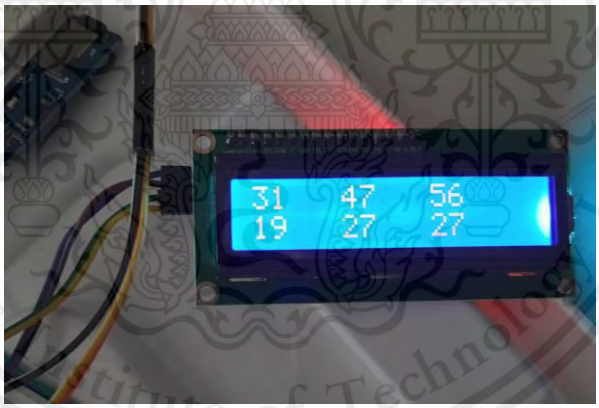

Figure 3.15 PM concentration reading on LCD.

This PMS5003 (PM sensor) outputs concentration value of PM1, PM2.5 and PM10 respectively in the unit of $\mu g/m^3$. The first row shows the value from the inlet PM sensor where the second row shows the value from the outlet sensor. The outlet sensor needs to have lower PM concentration to confirm the device's functionality.

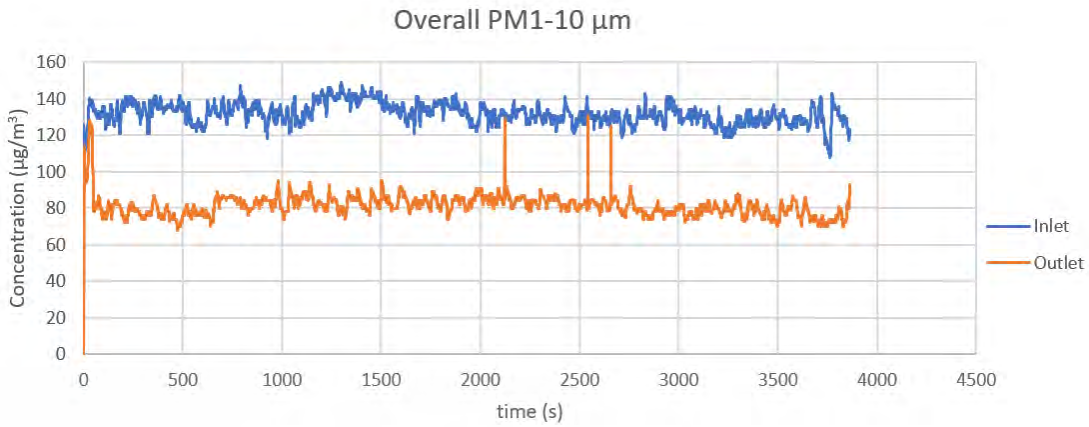

Figure 3.16 Graph showing concentration between inlet and outlet sensor.

The value of PM1, PM2.5 and PM10 are all summed up to be single value. Getting an efficiency around 38%. However, after the test, the air leak was inspected at the outlet side, which would induce the outdoor air into the stream. Thus, making PM outlet sensor reads higher value, lowering the efficiency.

3.1.3 Characterization test

According to the last test, there were leaks causing a lowered ESP collecting efficiency. The spray bottle of water is used to spray when the machine is operating (Only fan is on) and spray onto the duct, if there were bubble sucked into the pipe where it indicates the leaks. Epoxy and glues are then used to close all leak gaps.

This test was done to determine whether the machine's efficiency would drop over a long period of time running or not.

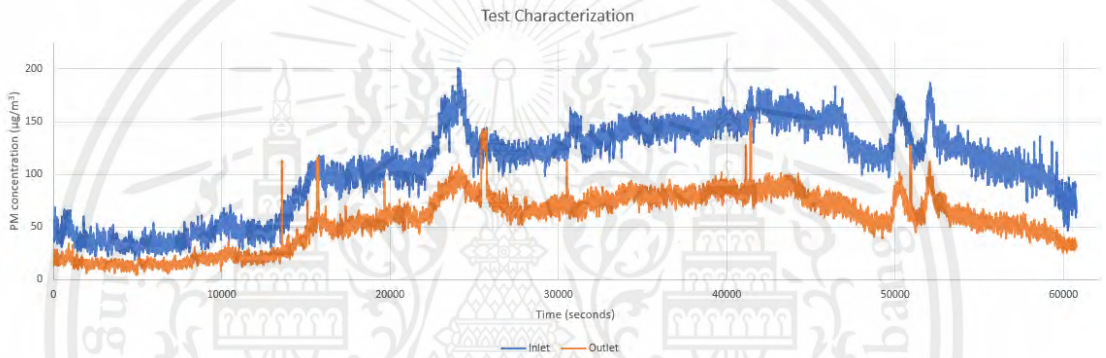

Figure 3.17 Inlet versus Outlet PM concentration (Characterization)

According to Figure 3.17 shows the inlet concentration versus outlet concentration. The machine was running for 16 hours. However, there was an increase in PM concentration for 10 hours indicating that the ambient PM concentration has been rising over that period.

The calculated efficiency of the ESP is 48% after the leak test was done. Another observation is that the efficiency of the system tends to stay in the same range over the operating period and did not reveal any significant drop in efficiency over the running period.

3.2 Final Customize design ESP

3.2.1 Basic Considerations

According to the objective that we wanted to build a PM collector machine with minimal contamination (No fabric filter). The commercial ESP was able to collect PM with efficiency 48%. However, the collector plate is secured to the frame and hence non removable. The final design would allow the collector plate to be removable for easier PM collection.

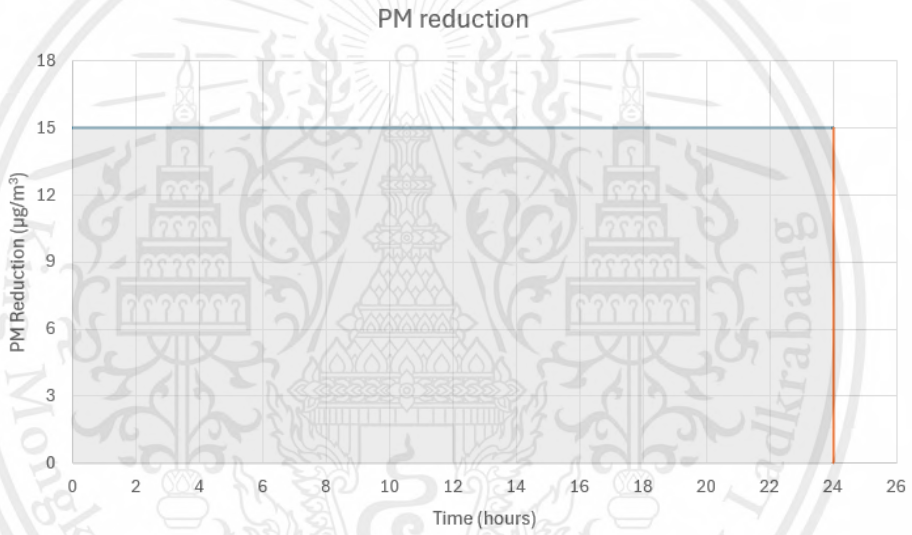

Figure 3.18 PM Constant Reduction with Respect to Time

According to the previous section of determining the average efficiency of the ESP system, concluded that the efficiency is around 48%. However, there's an improvement that could be made to raise efficiency up higher. Hence, an efficiency of 50% is assumed.

This device should be able to collect PM according to the objective even if the PM concentration is low. Assuming the inlet PM concentration is 30 $\mu g/m^3$ and given

the efficiency of the ESP is 50%. Thus, an outlet PM concentration would be 15 $\mu g/m^3$. Where this concludes the constant reduction in PM concentration of 15 $\mu g/m^3$.

As for requirements, the collection of PM total accumulated mass would not be less than 100 mg within 24 hours timeframe.

Area under the curve is given as ;

$$\text{Area} = (15\ \mu g/m^3)(24\ \text{hours}) = 360\ \mu g \cdot h/m^3$$

The amount of collected PM mass in mg shall be executed if the Area under the curve $(\mu g \cdot h/m^3)$ is multiply by volume flowrate (m^3/h), it would result in a total accumulate of collecting PM mass (mg). Using this relation in Figure 3.19

According to Figure 2.30, the effective velocity for imparting charge on PM particles on ESP system is 2 m/s. The relation $Q = AV$ could be used to determine flow area for ESP system with respect to volume flowrate. Using this relation in Figure 3.20

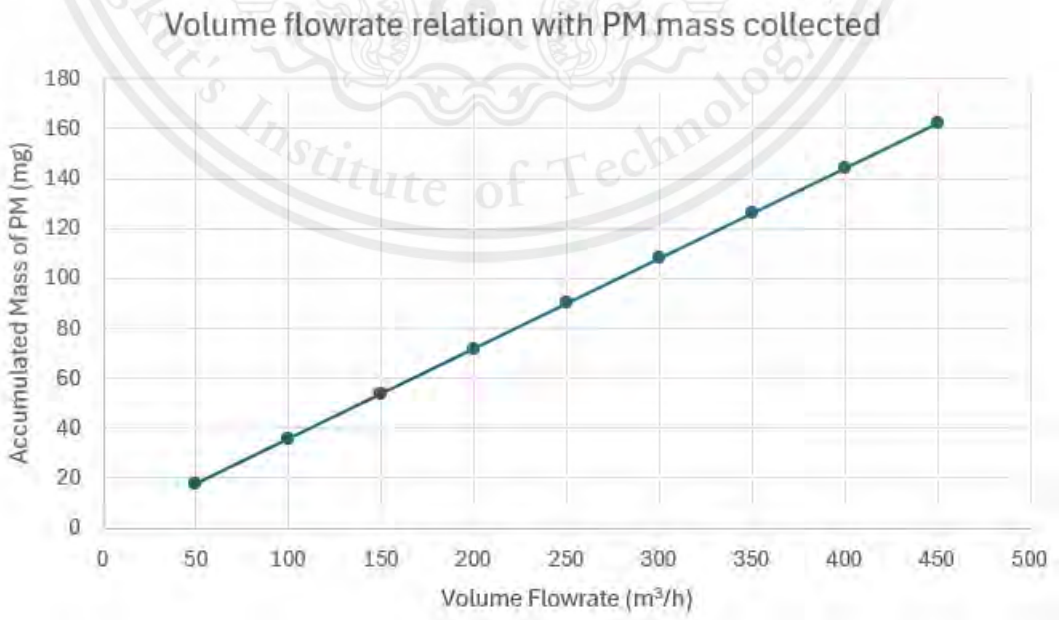

Figure 3.19 Volume flowrate relation with PM mass collected.

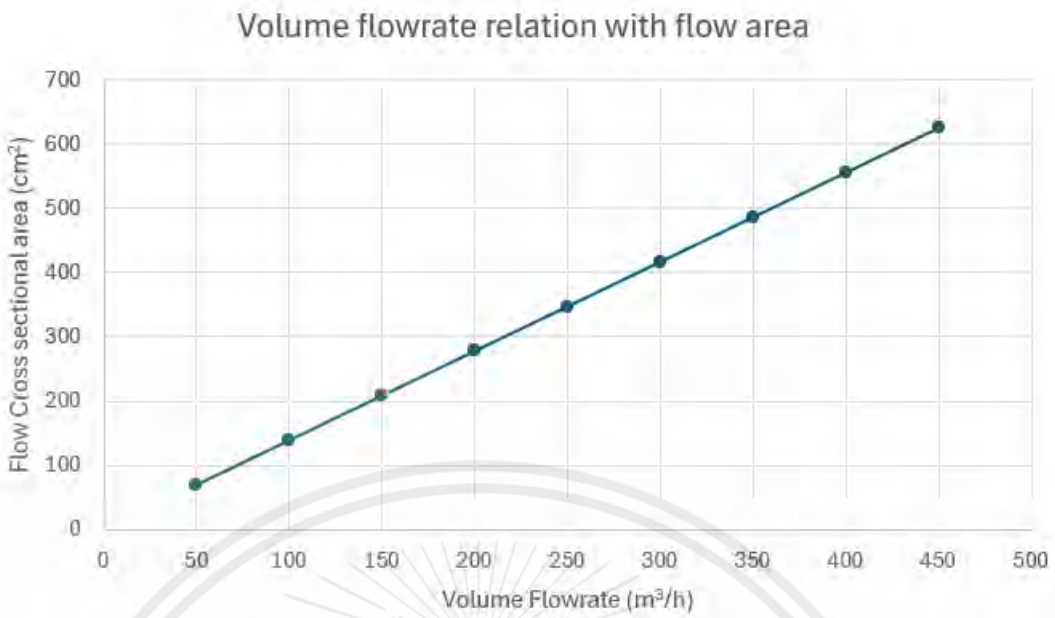

Figure 3.20 Volume flowrate relation with flow area.

Figure 3.19 shows the relation of the approximation of collected PM mass with respect to the volume flowrate into the system. According to the graph, it is more appropriate to choose the flowrate into the system of at least 300 m^3/h.

Figure 3.20 shows the relation of the volume flowrate of the system with respect to the ESP device's cross section area. After the flowrate was selected, the flow cross section area can be determined from the graph.

According to Figure 3.19, the reasonable mass of PM collection should be slightly higher than the 100 mg requirement. Hence, 120 mg was chosen as the baseline where this corresponds to the volume flowrate of around 350 m3/h. Relate this value of flowrate to Figure 3.20, the corresponding value for the ESP cross section area is approximately 500 cm^2.

3.2.2 Charging Section

According to the Figure 2.30, value for electric field intensity for ESP system varies from $1 - 5 \times 10^5\ \mathrm{V/m}$. However, if an electric field goes as high as $7.5 \times 10^5\ \mathrm{V/m}$, there's a significant increase in an ozone gas production. Thus, in this custom ESP design, $6 \times 10^5\ \mathrm{V/m}$ of electric field intensity was used for charging section.

Materials to be used as a charging electrode could be varied, two best choices for this application would be tungsten wire and copper wire. These factors such as electrical conductivity, melting point, strength, and corrosion resistance are taken into consideration when determining which materials should be used.

Electrical conductivity. Copper has an electrical conductivity value of $5.96 \times 10^7\ \mathrm{S/m}$, where tungsten wire has an electrical conductivity value of $1.79 \times 10^7\ \mathrm{S/m}$. Copper is a better electrical conductor than tungsten wire, which means that copper has lower electrical resistance than tungsten wire. However, this application is utilized on DC-High voltage, low current. Hence, this the lower conductivity of tungsten wire is not a significant trouble.

Melting point. Tungsten wire has a much higher melting point than copper wire. Tungsten has the highest melting point of all metals, at around 3,422°C, while copper has a melting point of around 1,085°C. This makes tungsten wire useful in applications where high temperatures are involved.

Strength. Tungsten wire is much stronger and more durable than copper wire. Tungsten wire is often used in applications where strength and durability are

important. Copper wire is relatively soft and malleable and is often used in applications where flexibility is important, such as in electrical wiring.

Corrosion resistance. Tungsten wire is highly resistant to corrosion, while copper wire can corrode over time. This makes tungsten wire useful in applications where exposure to harsh environments is a concern.

In this project, tungsten wire of diameter 0.2 mm is selected as the material for the charging electrode such that the benefits of higher strength, higher melting point, better corrosion resistance traded off the downside of electrical conductivity.

Figure 3.21 Configuration of Charging Electrode

The tungsten is at the positive polarity from the high voltage DC converter where the 1 mm aluminum plate is at the negative polarity from high voltage DC converter. Thus, creating positively charged particles when the air is flowing.

The power supply for the charging process outputs at 8 kVDC since this ESP runs on positive corona and does not need that very high voltage.

Figure 3.22 High Voltage Converter (8 kV Charging)

Electric field is defined by voltage divided the gap distance.

$$E = \frac{V}{d}$$

$$d = \frac{8000\ V}{6 \times 10^5\ V/m} = 13.33\ mm$$

Hence, the gap distance between electrode (Tungsten wire +) and aluminum plate (-) is 13.33 mm apart to keep this constant electric field intensity.

Figure 3.23 7 of total tungsten wire (charging electrode) configuration.

The frame is constructed by an acrylic glass of thickness 4.76 mm for the easily visualization of inside components. The charging electrode is hung by the electrode holder (Figure 3.24), along with the grounded 1 mm thick aluminum plate hanging in between those charging tungsten wire electrode.

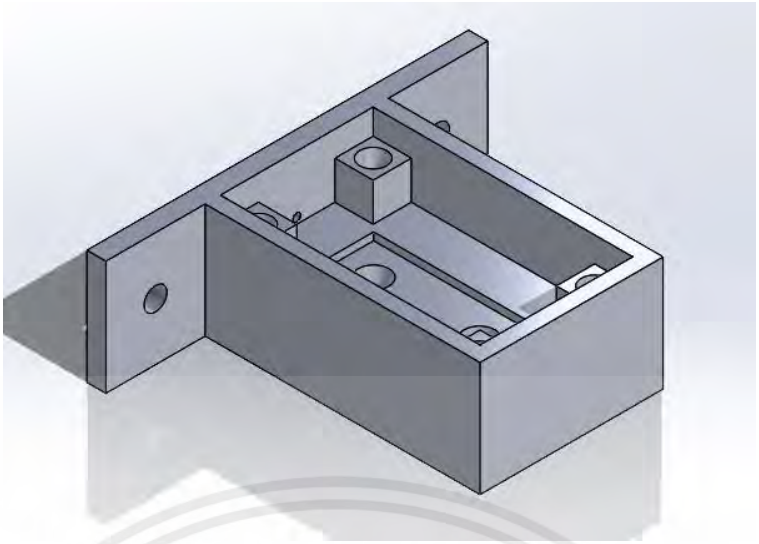

Figure 3.24 Tungsten wire electrode holder.

Figure 3.25 Construction of Charging side.

The connection is utilized by the wire terminal placed inside the electrode holder. The wire is High voltage DC wire and is rated at 10 kV maximum.

3.2.3 Collecting Section

After the particles have been positively charged, ranges of electric field are used to attract those positively charged particles. The maximum electric field that could be used is $3 \times 10^6\ \mathrm{V/m}$ as this is the electric field where the air starts to breakdown, becoming conduction and the spark occurs. This value is slightly higher than the charging section because in the charging section was a thin wire to plate configuration whereas there's a high electric field concentration over a thin wire surface and sharp edges, comparing to the collecting section that it is a plate-to-plate configuration and does not contain a thin surface, tip, or sharp edges.

The selected design electric field is $1 \times 10^6\ \mathrm{V/m}$, the cross-section area of the ESP system retrieved in section 3.2.1 had given us the idea of the length and width of the ESP system which the area is around 500 cm^2. Hence, the designed length and width of the ESP cross section is 228.48 mm length by 210 mm height where this corresponds to the area of 479.8 cm^2.

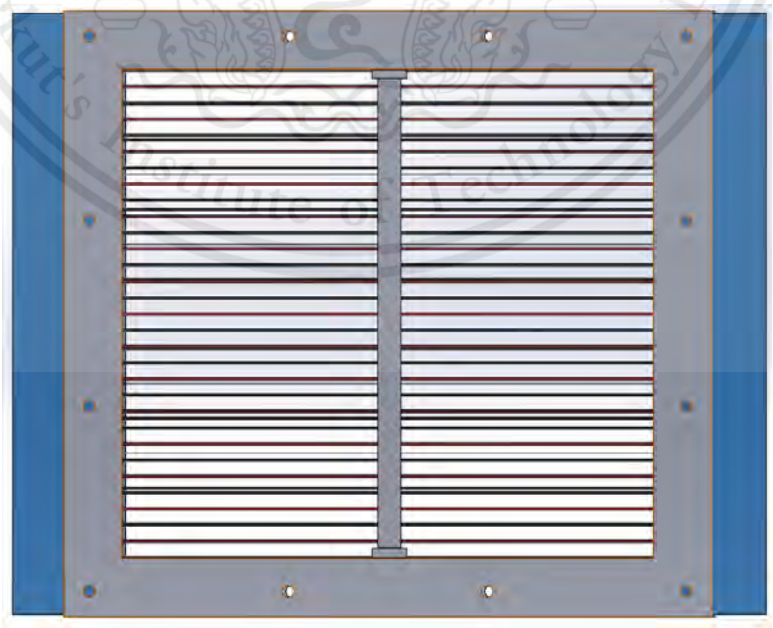

Figure 3.26 Plate gap design

There is 1 fixed variable which is the height (210mm). The gap distance of can be varied, noted that lesser the gap, particles use less time to precipitate but more collection plates are needed, hence, more collecting area.

By doing an iteration, ended up with 16 ground plates and 15 positive plates, each plate is 1 mm thick aluminum plates and are 6 mm apart. By given an electric field intensity of $1 \times 10^6\ \mathrm{V/m}$. Voltage can be determined from

$$\mathrm{E} = \frac{\mathrm{V}}{\mathrm{d}}$$

$$\mathrm{V} = (1 \times 10^6\ \mathrm{V/m})(6 \times 10^{-3}\mathrm{m}) = 6000\ \mathrm{V}$$

Figure 3.27 High Voltage Converter (6 kV Collecting)

The input to this high voltage converter is 12 VDC and it outputs 6 kVDC at 5W maximum of power.

After the electric field and gap between positive and negative plates are known, another important parameter is the plate length or known as projectile length. The particles undergo projectile motion when they enter the electric field. The necessary minimum projectile length is important whether the particles would have enough time to settle down on the negative collection plates or not.

According to Figure 2.31

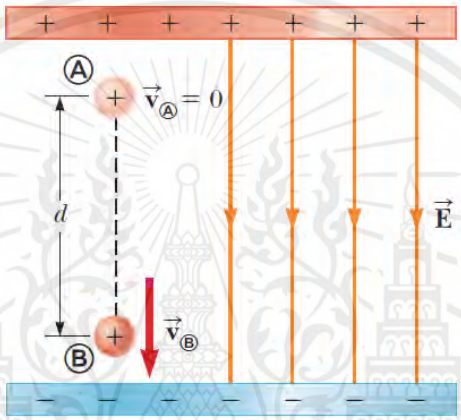

Starting with the conservation of energy equation.

$$\Delta K + \Delta U = 0 \tag{2.35}$$

$$\left(\frac{1}{2}mv^2 - 0\right) + (e\Delta V) = 0 \tag{2.36}$$

The final speed of particle is given as.

$$v = \sqrt{\frac{-2e\Delta V}{m}} = \sqrt{\frac{-2e(-Ed)}{m}} = \sqrt{\frac{2eEd}{m}} \tag{2.37}$$

This relation shall be used to calculate the y- direction velocity of particles which resulted from the pushing force from electric field.

Assuming the particles are sphere, according to equation 2.3

$$V_p = \frac{\pi {d_p}^3}{6} \tag{2.3}$$

And $m = \rho_p V_p$

Substitute these relations into equation 2.37 yields.

$$v = \sqrt{\frac{2eEd}{\rho_p V_p}}$$

$$v = \sqrt{\frac{12eEd}{\rho_p \pi {d_p}^3}} \tag{3.1}$$

Given e = Particle charge $(1.6 \times 10^{-19} C)$

E = Electric field $(V \cdot m^{-1})$

d = Gap between + and – (m)

ρ_p = Particle density (kg/m^3)

d_p = Particle diameter (m)

The equation 3.1 uses to find the velocity according to the electric field, where the mean diameter of particle is calculated as 2.5 μm as PM2.5.

Figure 3.28 shows the flow direction of particles into the series of collector plates whereas projectile length is unknown.

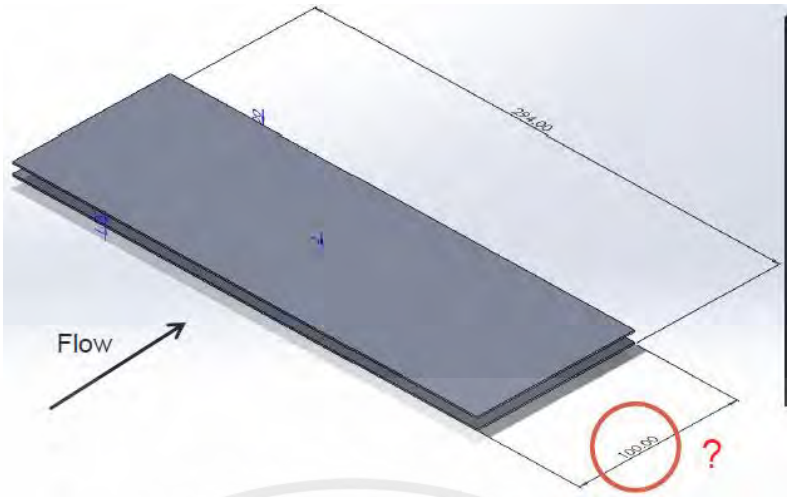

Figure 3.28 Particles flow direction into series of collection plates.

The red questions mark refers to the unknown collector plate projectile length.

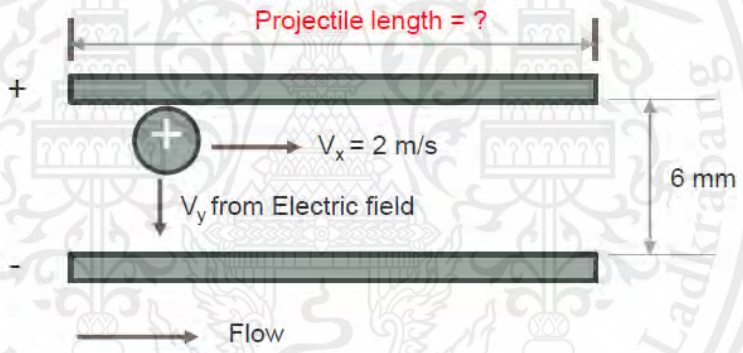

Figure 3.29 Velocity diagram for particles' projectile motion.

According to Figure 3.29, positively charged particles are travelling into the electric field where they are subjected to x and y axis velocity. X velocity refers to the velocity of the ESP system which is 2 m/s. Y velocity refers to the velocity resulted from the electric field force. The key important is to evaluate the Y velocity given the worst-case scenario that the particles have to travel 6 mm to reach the negative collection plate, then relate that time taken to travel 6 mm to the x direction, which will allow us to determine the appropriate projectile length.

$$v_y = \sqrt{\frac{12eEd}{\rho_p \pi {d_p}^3}}$$

$$v_y = \sqrt{\frac{12(1.6 \times 10^{-19}\text{C})(1 \times 10^6\ \text{V/m})(6 \times 10^{-3}\text{m})}{(2000\ \text{kg/m}^3)\,\pi(2.5 \times 10^{-6}\text{m})^3}}$$

$$v_y = 0.3425\ \text{m/s}$$

Time taken to travel 6 mm is given by $v = {}^{s}/_{t}$

$$t = \frac{d}{v_y}$$

$$t = \frac{6 \times 10^{-3}\text{m}}{0.3425\ \text{m/s}}$$

$$t = 0.017518\ \text{s}$$

By relating this time taken into the x axis displacement.

$$x = (2\ \text{m/s})(0.017518\ \text{s})$$

$$x = 0.035\ \text{m}$$

$$x = 35\ \text{mm}$$

As calculated, the minimum projectile length that the particles have to settle down on the negative plate before it starts to fly away back into the air stream. However, velocity of 2 m/s is considered at the inlet part. At the ESP's collecting section, there are areas that is used up by the collector plate thickness. An effective area is to be determined.

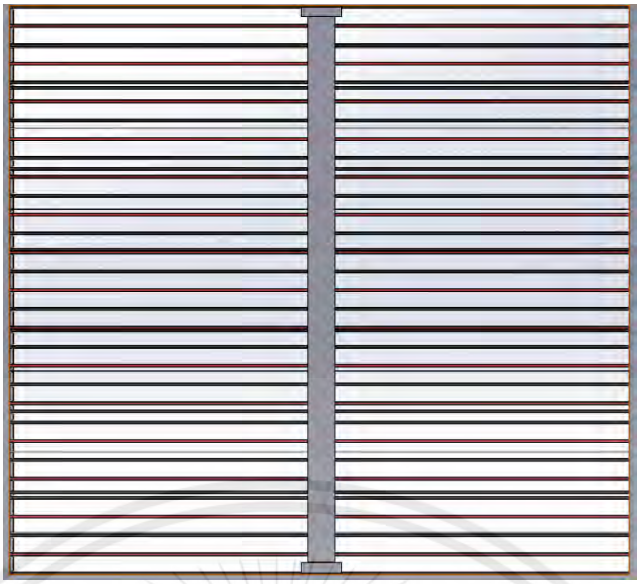

Figure 3.30 Shows an area used up by plates thickness.

Area per one block is $228.48\ \text{mm} \times 6\ \text{mm} = 1370.88\ \text{mm}^2$

Effective area is $1370.88\ \text{mm}^2 \times 30 = 41126.4\ \text{mm}^2$

Constant volume flowrate = $228.48\ \text{mm} \times 210\ \text{mm} \times 2\ \text{m/s} = 0.0959616\ \text{m}^3/\text{s}$

Velocity at each collector plate is given by the volume flowrate divided by the overall effective area.

$$v_{x,\text{eff}} = \frac{0.0959616\ \text{m}^3/\text{s}}{41126.4\ \text{mm}^2}$$

$$v_{x,\text{eff}} = 2.33\ \text{m/s}$$

By relating this time taken into the x axis displacement.

$$x = (2.33\ \text{m/s})(0.017518\ \text{s})$$

$$x = 0.04081\ \text{m}$$

$$x = 40.81\ \text{mm}$$

The x displacement is slightly higher than the x displacement when the velocity is assumed to be equal to inlet velocity which is 2 m/s.

Assuming a safety factor of 2, resulting in a displacement of 80 mm. Hence, 100 mm of projectile length is selected.

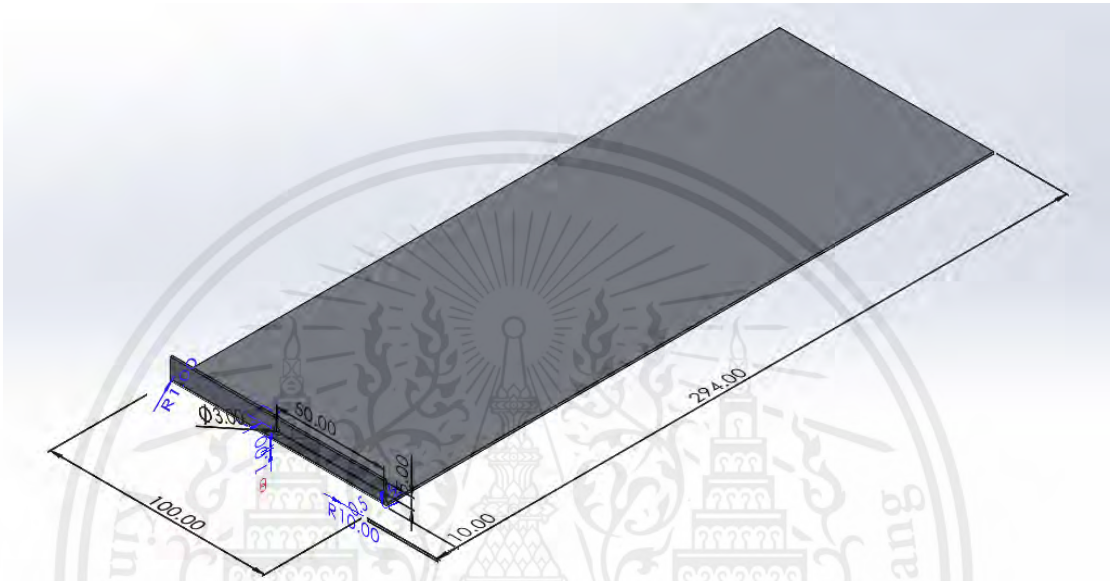

Figure 3.31 Collecting plate design.

Figure 3.31 shows the collector plate design using aluminum sheet thickness of 1 mm are bend and drill 3 mm hole at the center according to the figure.

The plates are identical for both positive and negative polarity. They are all meant to be removable unlike the previous commercial one where the plates were permanently locked into the ESP frame.

The design of the collector plate holder frame is shown in Figure 3.32. Which will be 3d printed and secured by screw and nut to the acrylic frame for both sides.

Figure 3.32 Primary collector plate holder assembly.

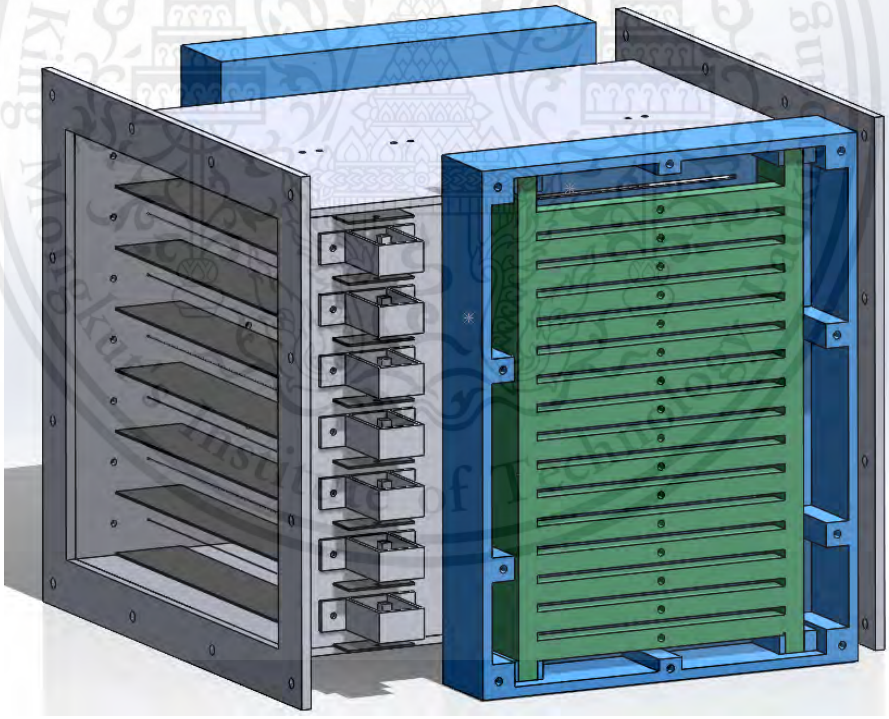

Figure 3.33 Secondary collector plate holder assembly.

Figure 3.33 shows the secondary collector plate holder, serves as the plate locker where screw is used to secure the collector plate onto the holder.

Since the plates are supported at both ends, it deflects at the center and is hard to assemble. An additional plate holder is utilized.

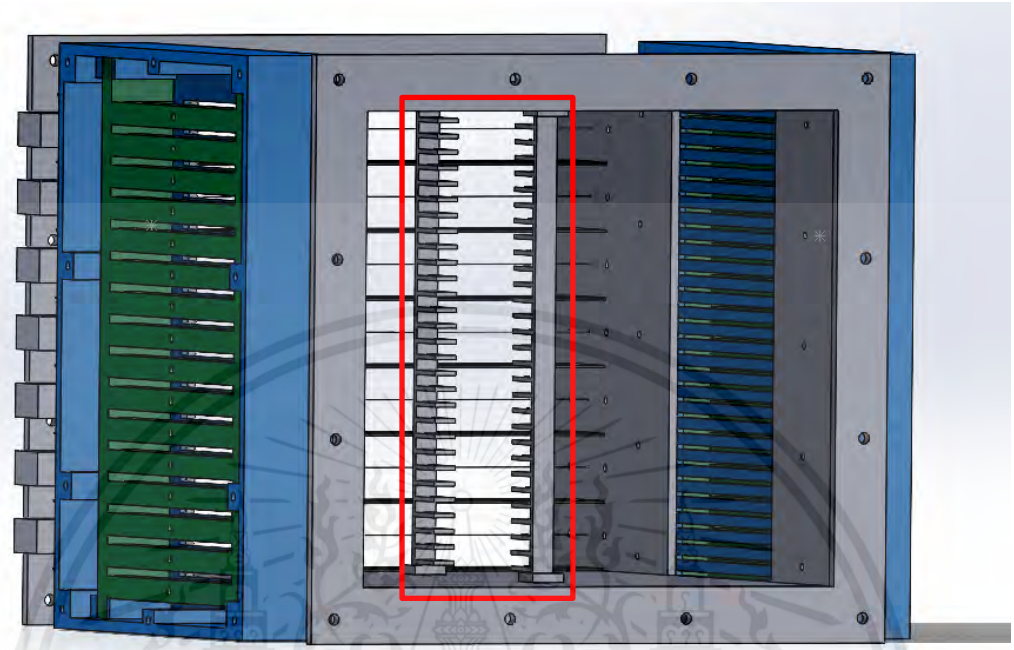

Figure 3.34 Assembly with center plate holder.

Figure 3.35 Collector plates assembly test.

Figure 3.36 Brass inserts for 3d printed part.

Brass inserts are used to make screw thread for 3d printed part. According to Figure 3.35 that the design had left a hole for the brass insert to sit into. The procedure is by simply using the soldering iron to force the brass insert into the hole.

Figure 3.37 Full collector plates assembly test.

Figure 3.37, collector plates are assembled and verify each gap if it corresponds to the design value of 6 mm.

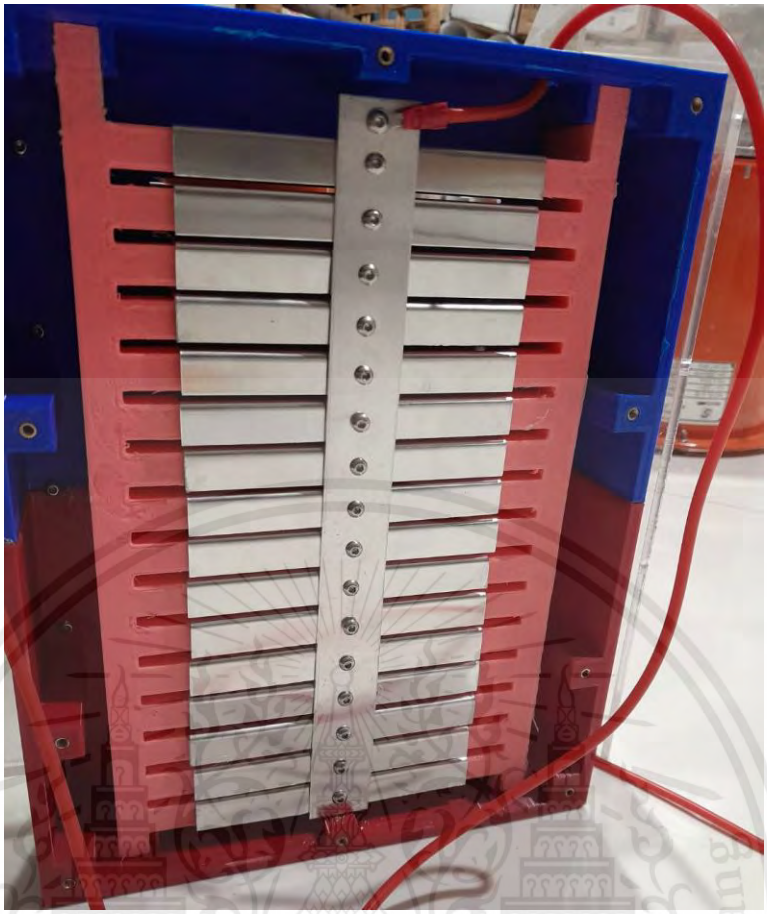

Figure 3.38 Electrical bar connector for collector plates.

The electrical bar connector is introduced for secured electrical connections and simple disassembly process. The material is the same as collector plates which is aluminum sheet of thickness 1 mm. Drilled into according to dimensions, the wire got screwed directly onto the terminal and wiring goes to the high voltage dc converter. Where the construction of the complete device and system shall be discussed in the next section.

3.2.4 Air duct

The previous section had discussed about the main parts of the system which is the ESP unit. The complete system would require an air duct, fan, and control system module. This section will discuss about the air duct design.

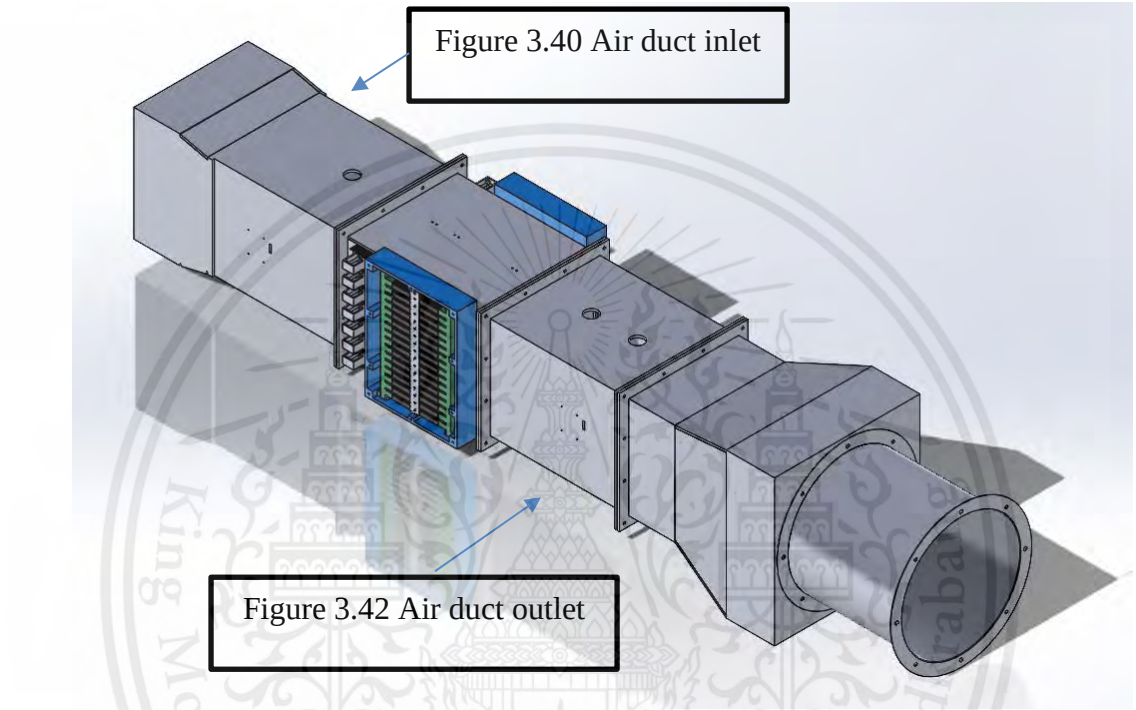

Figure 3.39 Overall assembly system.

The air duct is designed using acrylic glass of thickness 4.76 mm, laser cut and glue together with an acrylic glue, the connection between each plate is utilized by screw and nuts with gasket in between to prevent air leaks.

After the design of air ducts has been done, fan pumping power and specification can be determined by given all the duct size, air velocity, and pressure drop from equipment.

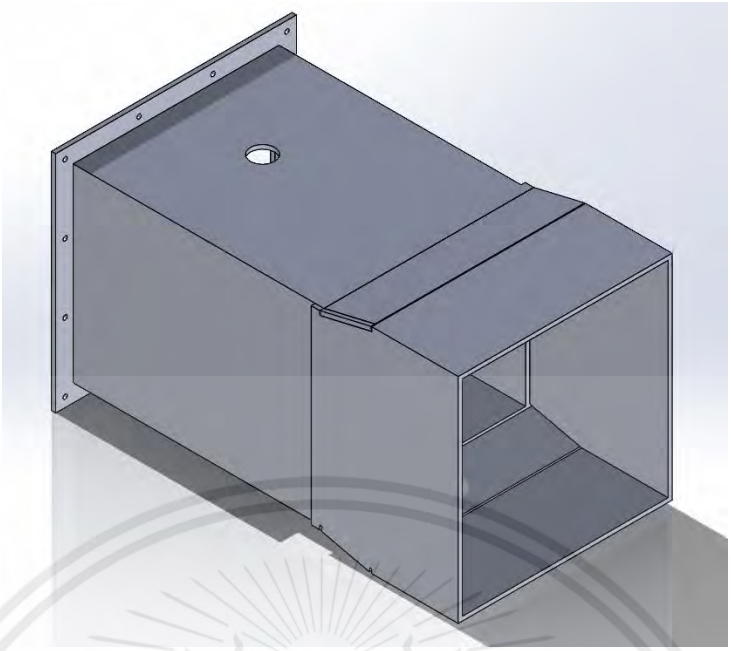

Figure 3.40 Air duct inlet

Figure 3.41 Air conditioning diffuser

Figure 3.40 shows the design of the air duct at inlet part of the system whereas the AC diffuser (Figure 3.41) is used to induce all from all directions into the system.

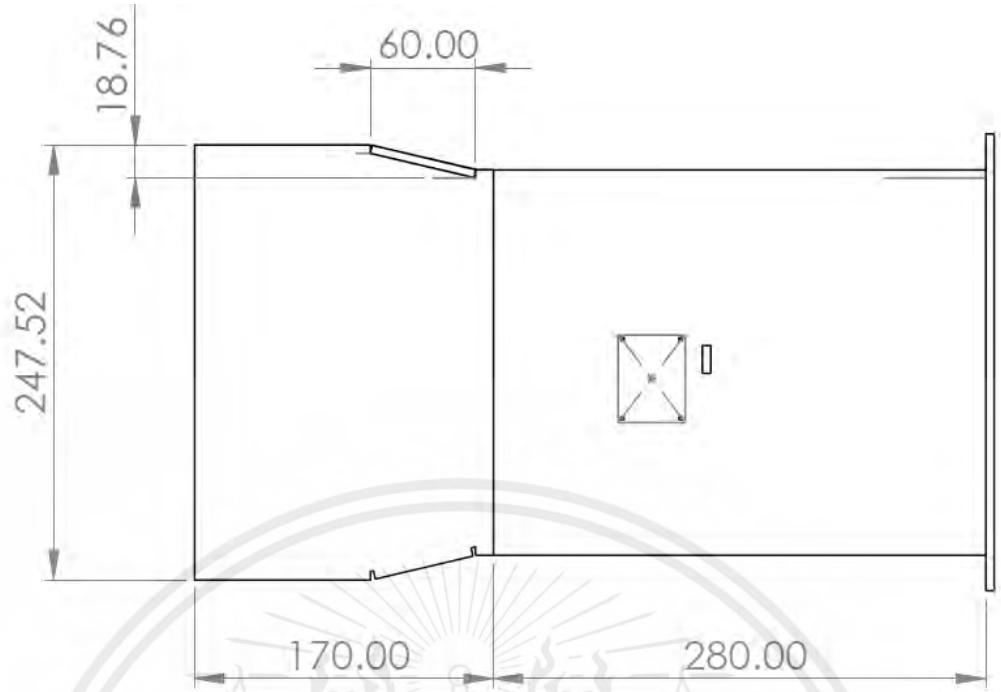

Figure 3.42 Air inlet side dimensions.

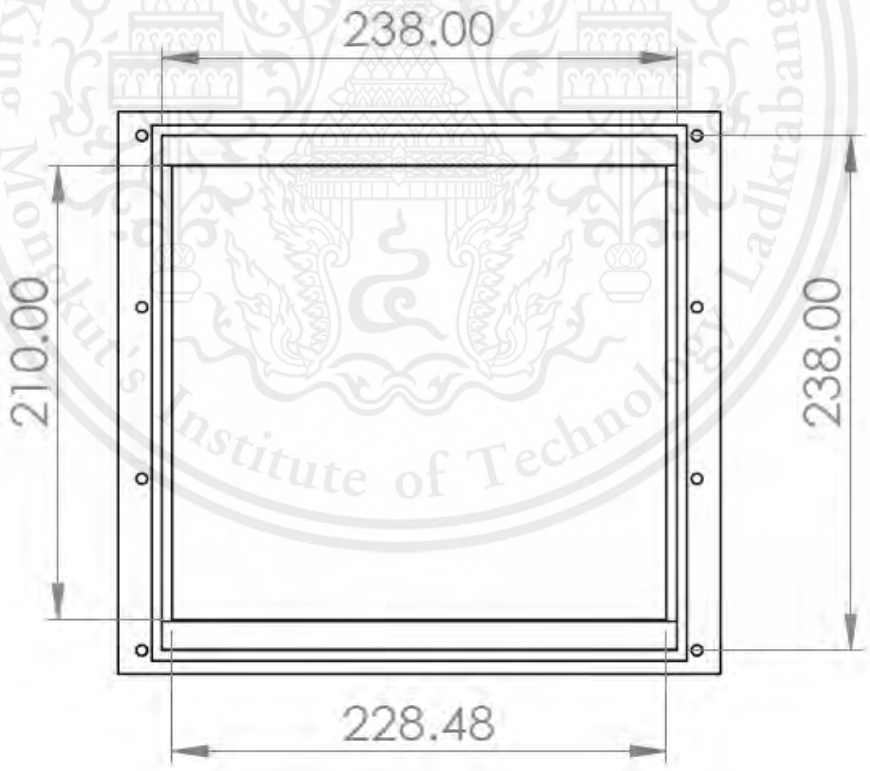

Figure 3.43 Air inlet front dimensions.

ER4-1 Transition, Rectangular, Two Sides Parallel, Symmetrical, Exhaust/Return Systems

	C_o Values												
	θ												
A_o/A_1	0	3	5	10	15	20	30	45	60	90	120	150	180
0.063	0.0	0.44	0.27	0.25	0.27	0.36	0.56	0.71	0.86	0.99	0.99	0.98	0.98
0.10	0.0	0.41	0.27	0.23	0.25	0.34	0.53	0.69	0.83	0.94	0.94	0.92	0.91
0.167	0.0	0.34	0.28	0.21	0.23	0.30	0.48	0.65	0.76	0.83	0.83	0.82	0.80
0.25	0.0	0.26	0.29	0.17	0.19	0.25	0.42	0.60	0.68	0.70	0.70	0.68	0.66
0.50	0.0	0.16	0.24	0.14	0.13	0.15	0.24	0.35	0.37	0.38	0.37	0.36	0.35
1.00	0.0	0.00	0.00	0.00	0.00	0.00	0.00	0.00	0.00	0.00	0.00	0.00	0.00
2.00	0.0	0.30	0.38	0.25	0.17	0.17	0.17	0.23	0.29	0.49	0.66	0.81	0.88
4.00	0.0	1.66	1.25	0.77	0.70	0.70	0.70	0.90	1.09	2.84	4.36	5.69	6.57
6.00	0.0	4.05	3.14	1.76	1.58	1.58	1.58	2.12	2.66	6.71	10.11	13.13	15.20
10.00	0.0	12.01	9.39	5.33	5.00	5.00	5.00	6.45	7.93	19.10	28.60	36.79	42.79

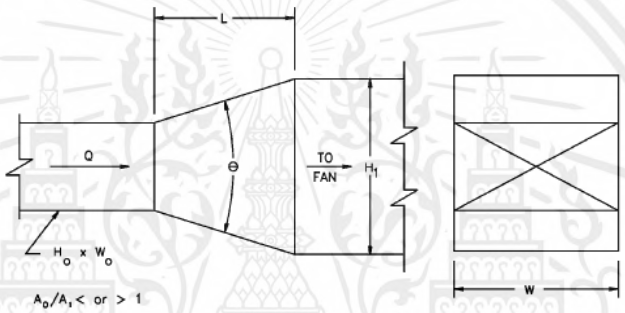

Figure 3.44 ER4-1 Table

Source: 2021 ASHRAE Handbook: Fundamentals. (2021).

Minor loss from duct fitting can be determined from ER4-1 Table according to Figure 3.44.

$$\frac{A_0}{A_1} = \frac{238 \times 238}{210 \times 228.48} = 1.1805$$

$$\theta = \tan^{-1}\left(\frac{18.76}{60}\right) = 17.36°$$

By interpolating, the corresponding value for C_0 value is 0.031

This part connects at the outlet side of the ESP unit/

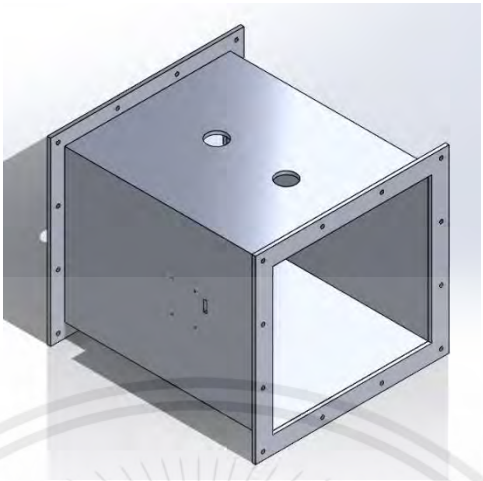

Figure 3.45 Air duct outlet.

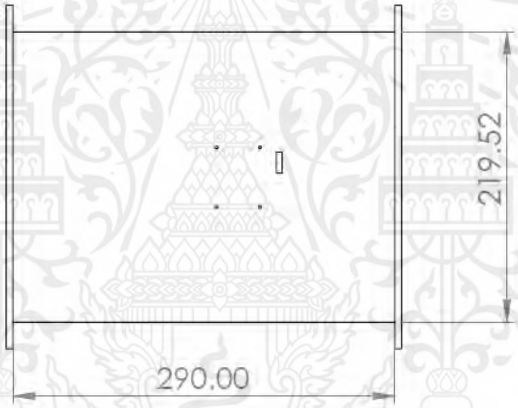

Figure 3.46 Air duct outlet side view dimensions.

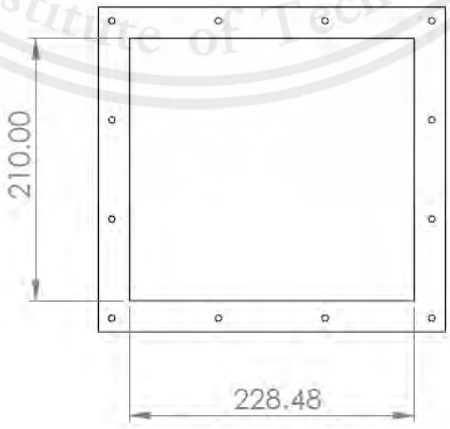

Figure 3.47 Air duct outlet front view dimensions.

The last part is the fan connection, as this system the fan is located at the outlet as it induces the flow through the ESP system. However, the fan cross section is circular and in different size to the duct. Therefore, there's a reducer duct configuration used in this part.

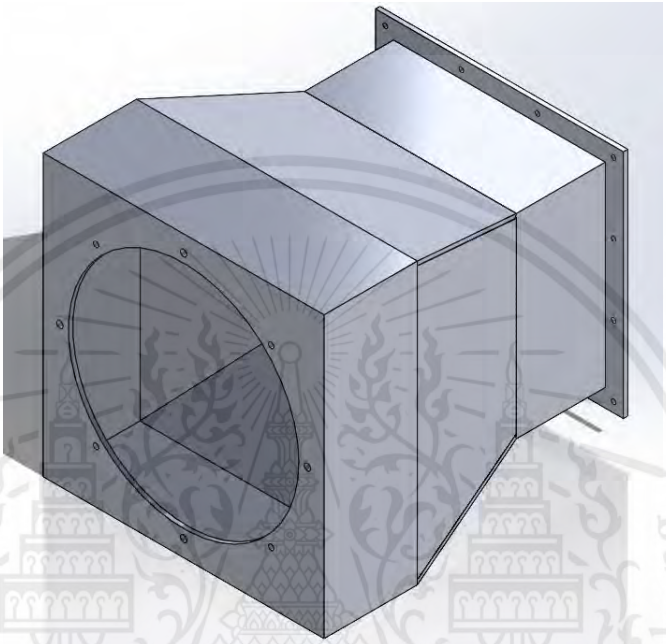

Figure 3.48 Fan connector.

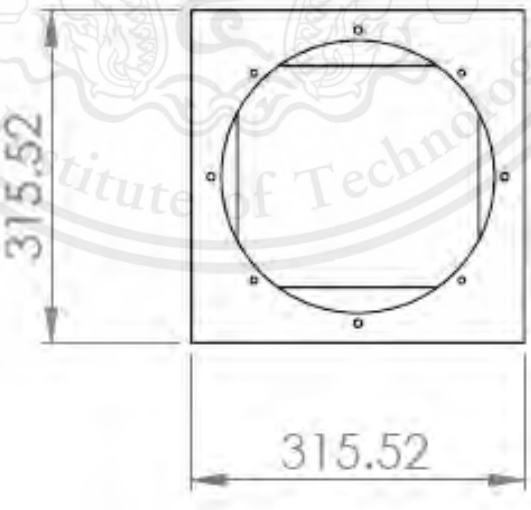

Figure 3.49 Fan connector front view dimensions.

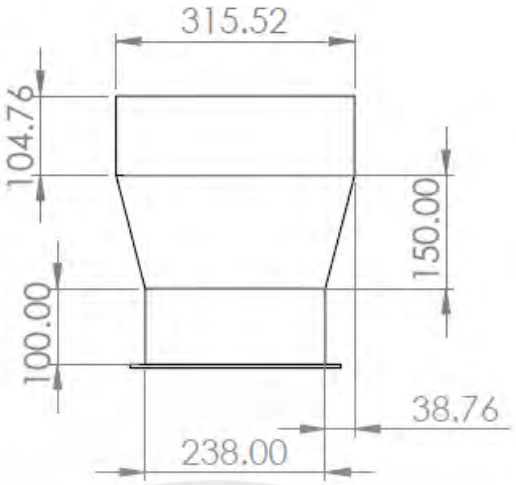

Figure 3.50 Fan connector top view dimensions.

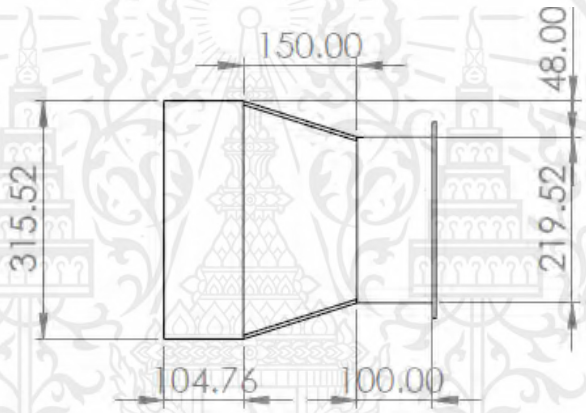

Figure 3.51 Fan connector side view dimensions.

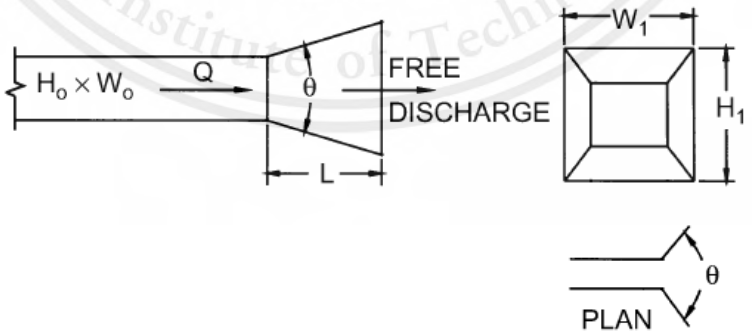

SR2-5 Pyramidal Diffuser, Free Discharge

		C_o Values									
		θ									
A_1/A_o	Re/1000	4	8	10	14	20	30	45	60	90	120
1	50	1.0	1.0	1.0	1.0	1.0	1.0	1.0	1.0	1.0	1.0
	100	1.0	1.0	1.0	1.0	1.0	1.0	1.0	1.0	1.0	1.0
	200	1.0	1.0	1.0	1.0	1.0	1.0	1.0	1.0	1.0	1.0
	400	1.0	1.0	1.0	1.0	1.0	1.0	1.0	1.0	1.0	1.0
	2000	1.0	1.0	1.0	1.0	1.0	1.0	1.0	1.0	1.0	1.0
2	50	0.55	0.65	0.68	0.74	0.82	0.92	1.05	1.10	1.08	1.08
	100	0.51	0.61	0.66	0.73	0.81	0.90	1.04	1.09	1.08	1.08
	200	0.47	0.57	0.61	0.70	0.79	0.89	1.04	1.09	1.08	1.08
	400	0.42	0.50	0.56	0.64	0.76	0.88	1.02	1.07	1.08	1.08
	2000	0.42	0.50	0.56	0.64	0.76	0.88	1.02	1.07	1.08	1.08
4	50	0.38	0.53	0.60	0.69	0.78	0.90	1.02	1.07	1.09	1.09
	100	0.33	0.49	0.55	0.66	0.78	0.90	1.02	1.07	1.09	1.09
	200	0.27	0.42	0.50	0.62	0.74	0.87	1.00	1.06	1.08	1.08
	400	0.22	0.36	0.44	0.56	0.70	0.84	0.99	1.06	1.08	1.08
	2000	0.22	0.36	0.44	0.56	0.70	0.84	0.99	1.06	1.08	1.08
6	50	0.34	0.50	0.57	0.66	0.77	0.91	1.02	1.07	1.08	1.08
	100	0.30	0.47	0.54	0.63	0.76	0.98	1.02	1.07	1.08	1.08
	200	0.24	0.42	0.48	0.60	0.73	0.88	1.00	1.06	1.08	1.08
	400	0.18	0.34	0.44	0.56	0.73	0.86	0.98	1.06	1.08	1.08
	2000	0.18	0.34	0.44	0.56	0.73	0.86	0.98	1.06	1.08	1.08
10	50	0.30	0.45	0.53	0.64	0.74	0.85	0.97	1.10	1.12	1.12
	100	0.25	0.40	0.48	0.62	0.73	0.85	0.97	1.10	1.12	1.12
	200	0.20	0.34	0.44	0.56	0.69	0.82	0.95	1.10	1.11	1.11
	400	0.16	0.28	0.40	0.55	0.67	0.80	0.93	1.09	1.11	1.11
	2000	0.16	0.28	0.40	0.55	0.67	0.80	0.93	1.09	1.11	1.11

Figure 3.52 SR2-5 Table

Source: 2021 ASHRAE Handbook: Fundamentals. (2021).

Note that 4.76 refers to the thickness of acrylic sheet.

$$\frac{A_0}{A_1} = \frac{(315.52 - 2(4.76)) \times (315.52 - 2(4.76))}{210 \times 228.48} = 1.952$$

$$\theta = \tan^{-1}\left(\frac{48}{150}\right) = 17.74°$$

By interpolating, the corresponding value for C_0 value is 0.82

3.2.5 Fan

Given that the total length of the system is 1.7 m, where the fluid velocity along the duct is 2 m/s. The duct is rectangular with a width of 228.48 mm and height 210 mm. Below is equation 2.48, use to relate the rectangular diameter.

$$D_h = \frac{4A}{U} \tag{2.48}$$

$$D_h = \frac{4(228.48 \times 210)\text{mm}}{(228.48 \times 2 + 210 \times 2)\text{mm}} = 218.85 \text{ mm}$$

Table 1 Duct Roughness Factors

1	2	3
	Absolute Roughness ε, mm	
Duct Type/Material	**Range**	**Roughness Category**
Drawn tubing (Madison 1946)	0.00046	Smooth 0.00046
PVC plastic pipe (Swim 1982)	0.009 to 0.046	Medium smooth 0.046
Commercial steel or wrought iron (Moody 1944)	0.046	
Aluminum, round, longitudinal seams, crimped slip joints, 0.91 m spacing (Hutchinson 1953)	0.037 to 0.061	
Friction chart:		
Galvanized steel, round, longitudinal seams, variable joints (Vanstone, drawband, welded. but primarily beaded coupling), 1.22 m joint spacing (Griggs et al. 1987)	0.049 to 0.098	Average 0.09
Galvanized steel, spiral seams, 3.05 m joint spacing (Jones 1979)	0.061 to 0.12	
Galvanized steel, spiral seam with 1, 2, and 3 ribs, beaded couplings, 3.66 m joint spacing (Griggs et al. 1987)	0.088 to 0.116	
Galvanized steel, rectangular, various type joints (Vanstone, drawband, welded. Beaded coupling), 1.22 m spacing[a] (Griggs and Khodabakhsh-Sharifabad 1992)	0.082 to 0.15	
Wright Friction Chart:		
Galvanized steel, round, longitudinal seams, 0.76 m joint spacing, ε = 0.15 mm	Retained for historical purposes [See Wright (1945) for development of friction chart]	
Flexible duct, fabric and wire, fully extended (Abushakra et al. 2004; Culp 2011)	0.09 to 0.9	Medium rough 0.9
Galvanized steel, spiral, corrugated,[b] beaded slip couplings, 3.05 m spacing (Kulkarni et al. 2009)	0.54 to 0.91	
Fibrous glass duct, rigid (tentative)	—	
Fibrous glass duct liner, air side with facing material (Swim 1978)	1.52	
Fibrous glass duct liner, air side spray coated (Swim 1978)	4.57	Rough 3.0
Flexible duct, metallic, fully extended	1.2 to 2.1	
Concrete (Moody 1944)	0.30 to 3.0	

[a]Griggs and Khodabakhsh-Sharifabad (1992) showed that ε values for rectangular duct construction combine effects of surface condition, joint spacing, joint type, and duct construction (cross breaks, etc.), and that the ε-value range listed is representative.
[b]Spiral seam spacing was 119 mm with two corrugations between seams. Corrugations were 19 mm wide by 6 mm high (semicircle).
[c]Subject duct classified "tentatively medium rough" because no data available.

Figure 3.53 Duct Roughness Factor

Source: 2021 ASHRAE Handbook: Fundamentals. (2021).

The roughness factor is chosen to be 0.046 mm

■ Table B.4

Physical Properties of Air at Standard Atmospheric Pressure (SI Units)[a]

Temperature (°C)	Density, ρ (kg/m^3)	Specific Weight[b], γ (N/m^3)	Dynamic Viscosity, μ (N·s/m^2)	Kinematic Viscosity, ν (m^2/s)	Specific Heat Ratio, k (—)	Speed of Sound, c (m/s)
−40	1.514	14.85	1.57 E − 5	1.04 E − 5	1.401	306.2
−20	1.395	13.68	1.63 E − 5	1.17 E − 5	1.401	319.1
0	1.292	12.67	1.71 E − 5	1.32 E − 5	1.401	331.4
5	1.269	12.45	1.73 E − 5	1.36 E − 5	1.401	334.4
10	1.247	12.23	1.76 E − 5	1.41 E − 5	1.401	337.4
15	1.225	12.01	1.80 E − 5	1.47 E − 5	1.401	340.4
20	1.204	11.81	1.82 E − 5	1.51 E − 5	1.401	343.3
25	1.184	11.61	1.85 E − 5	1.56 E − 5	1.401	346.3
30	1.165	11.43	1.86 E − 5	1.60 E − 5	1.400	349.1
40	1.127	11.05	1.87 E − 5	1.66 E − 5	1.400	354.7
50	1.109	10.88	1.95 E − 5	1.76 E − 5	1.400	360.3
60	1.060	10.40	1.97 E − 5	1.86 E − 5	1.399	365.7
70	1.029	10.09	2.03 E − 5	1.97 E − 5	1.399	371.2
80	0.9996	9.803	2.07 E − 5	2.07 E − 5	1.399	376.6
90	0.9721	9.533	2.14 E − 5	2.20 E − 5	1.398	381.7
100	0.9461	9.278	2.17 E − 5	2.29 E − 5	1.397	386.9
200	0.7461	7.317	2.53 E − 5	3.39 E − 5	1.390	434.5
300	0.6159	6.040	2.98 E − 5	4.84 E − 5	1.379	476.3
400	0.5243	5.142	3.32 E − 5	6.34 E − 5	1.368	514.1
500	0.4565	4.477	3.64 E − 5	7.97 E − 5	1.357	548.8
1000	0.2772	2.719	5.04 E − 5	1.82 E − 4	1.321	694.8

[a]Based on data from R. D. Blevins, *Applied Fluid Dynamics Handbook*, Van Nostrand Reinhold Co., Inc., New York, 1984.

[b]Density and specific weight are related through the equation $\gamma = \rho g$. For this table $g = 9.807$ m/s^2.

Figure 3.54 Physical properties of Air at Standard Atmospheric Pressure

Source: Munson, B. R., Rothmayer, A. P., Okiishi, T. H., & Huebsch, W. W. (2012). Fundamentals of Fluid Mechanics. Wiley.

According to Figure 3.54, the air dynamic viscosity at 30°C is

$1.86 \times 10^{-5}\ \mathrm{N \cdot s/m^2}$, the air density at 30°C is $1.165\ \mathrm{kg/m^3}$

Reynold number can be evaluated from equation 2.49

$$\mathrm{Re} = \frac{\rho v D}{\mu} \tag{2.49}$$

$$\mathrm{Re} = \frac{(1.165\,\mathrm{kg/m^3})(2\ \mathrm{m/s})(218.85 \times 10^{-3}\mathrm{m})}{1.86 \times 10^{-5}\ \mathrm{N \cdot s/m^2}} = 27{,}415.08$$

Which is a turbulent flow

Friction factor can be evaluated from equation 2.47

$$\frac{1}{\sqrt{f}} = -2.0\log\left(\frac{0.046\text{mm}/218.85\text{mm}}{3.7} + \frac{2.51}{27415\sqrt{f}}\right) \quad (2.47)$$

$$f = 0.024524$$

Major loss is calculated from the relation.

$$\Delta P_{major} = f\frac{L}{D}\frac{\rho v^2}{2} \quad (2.50)$$

$$\Delta P_{major} = (0.024524)\frac{(1.7\text{ m})}{(218.85\times10^{-3}\text{m})}\frac{(1.165\text{ kg/m}^3)(2\text{ m/s})^2}{2}$$

$$\Delta P_{major} = 0.4438\text{ Pa}$$

Minor loss is calculated from the relation.

$$\Delta P_{minor} = C_0\cdot\frac{1}{2}\rho v^2 \quad (2.51)$$

$$\Delta P_{minor} = (0.82+0.031)\cdot\frac{1}{2}(1.165\text{ kg/m}^3)(2\text{ m/s})^2$$

$$\Delta P_{minor} = 2\text{ Pa}$$

Hence Total head pump power is calculated from.

$$P_1 + \frac{\rho v_1^2}{2} + \rho g z_1 + P_H = P_2 + \frac{\rho v_2^2}{2} + \rho g z_2 + \Delta P$$

$$P_H = \frac{\rho(v_2^2 - v_1^2)}{2} + \Delta P$$

$$P_H = \frac{(1.165\text{ kg/m}^3)(2^2)}{2} + 2 + 0.4438 = 4.7738\text{ Pa}$$

Hence, the fan should be able to induce air at a constant flowrate of approximately 360 m^3/h and a minimum fan pressure of 4.77 Pascal.

Figure 3.55 Fan specification

This is the fan that is selected for this project. The input voltage is 220VAC, with maximum power of 250W. Maximum volumetric flowrate is 4500 m^3/h and a maximum fan pressure of 70 Pa. However, the specification of product is somewhat questionable, it's a good idea to buy over-specification produce in case it could not satisfy the conditions that is needed, which should not be a problem as the fan will be connected to a speed controller unit which shall be discussed in the electrical system section later.

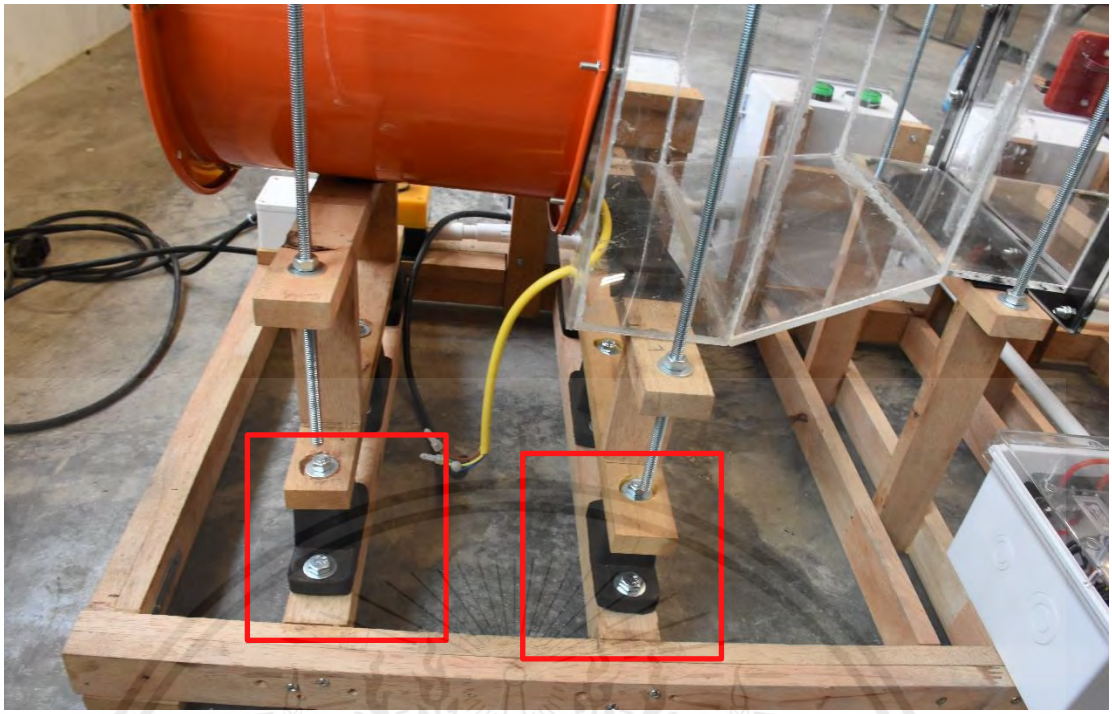

Figure 3.56 Fan vibration isolator

Since fan vibrates when operating, the vibration isolator is installed in between the fan supporter and the frame, so it could isolate the vibration to not transfer to the frame. Thus, keeping the vibrator on its body and the supporter.

Figure 3.57 Fan installation

3.2.6 Electrical system

Electrical system consists of 3 main systems which are fan system, control system (sensors), low voltage system (12VDC), and high voltage system.

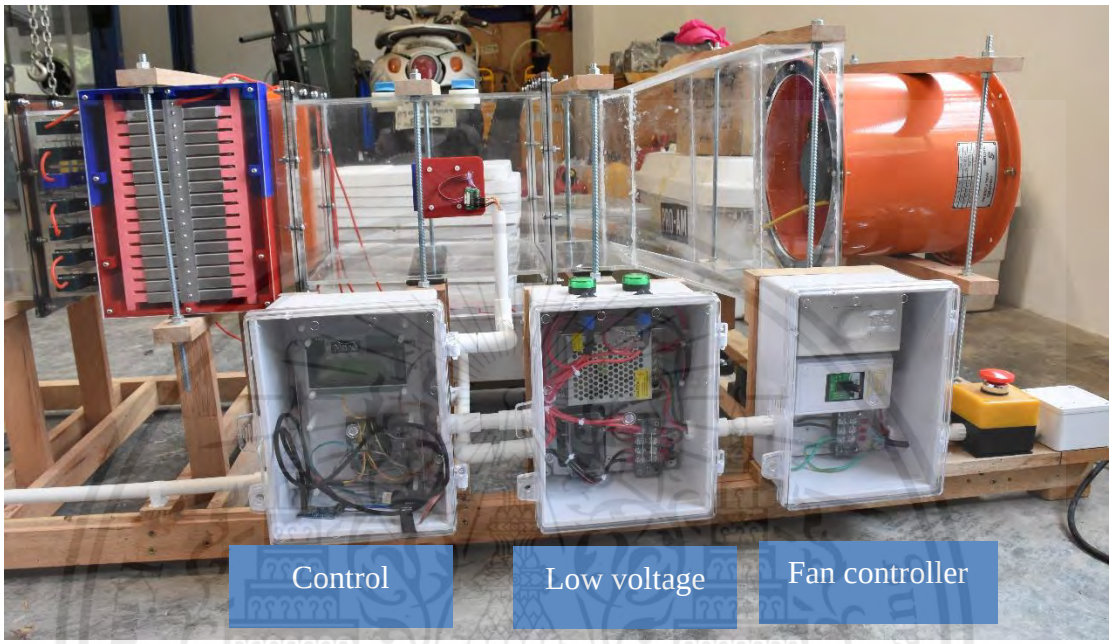

Figure 3.58 Overview of Electrical system.

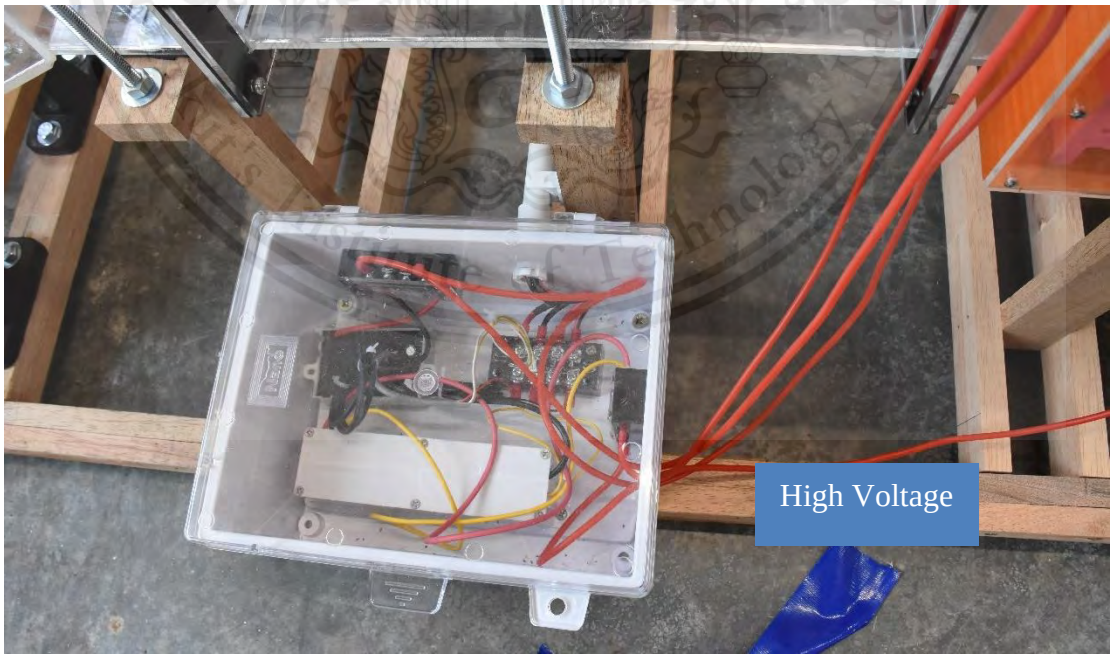

Figure 3.59 Overview of Electrical system (Rear).

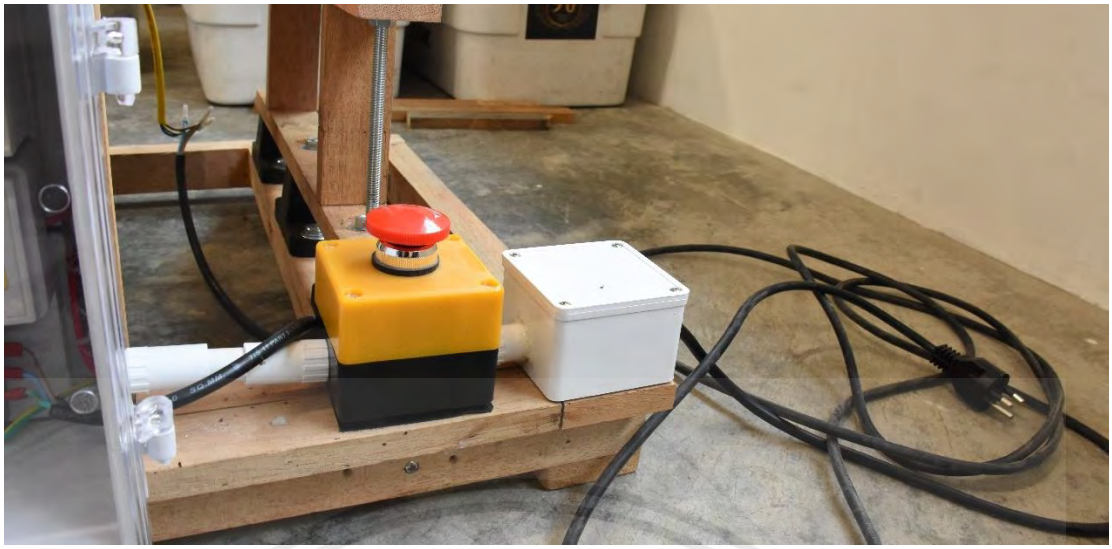

Figure 3.60 Electrical plug inlet

At the electrical inlet, 3 prong connector is used as the grounding is connected. Along with the safety switch before entering the main 10A breaker in the fan box.

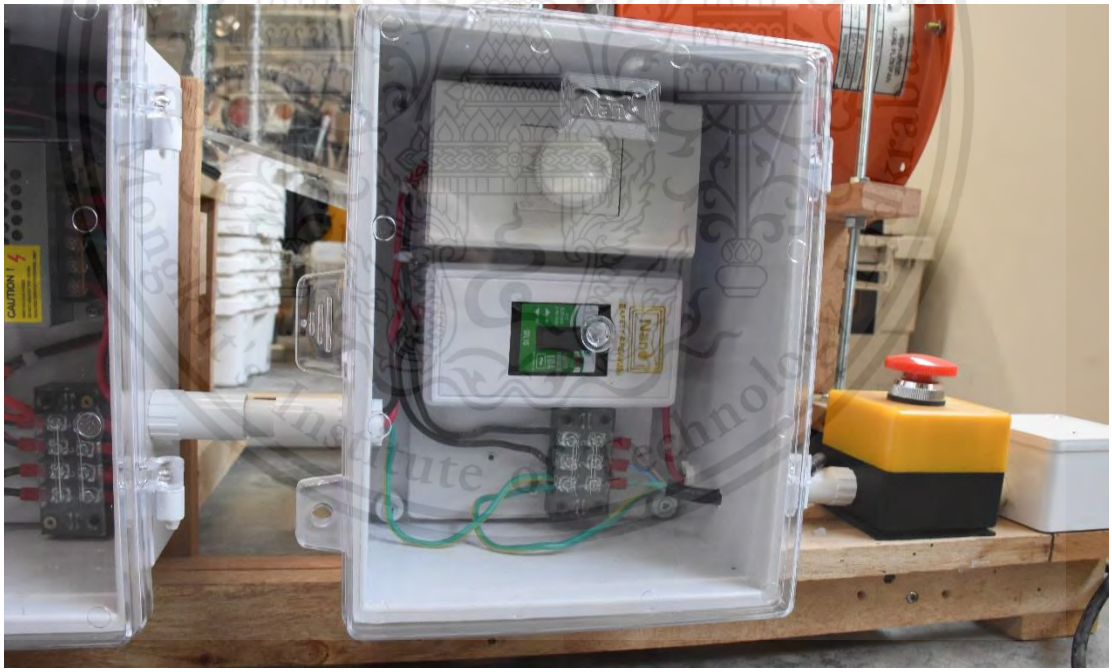

Figure 3.61 Fan control box

After passing through the safety switch, it enters the 10A circuit breaker, then got distributed to fan speed controller and to the low voltage box.

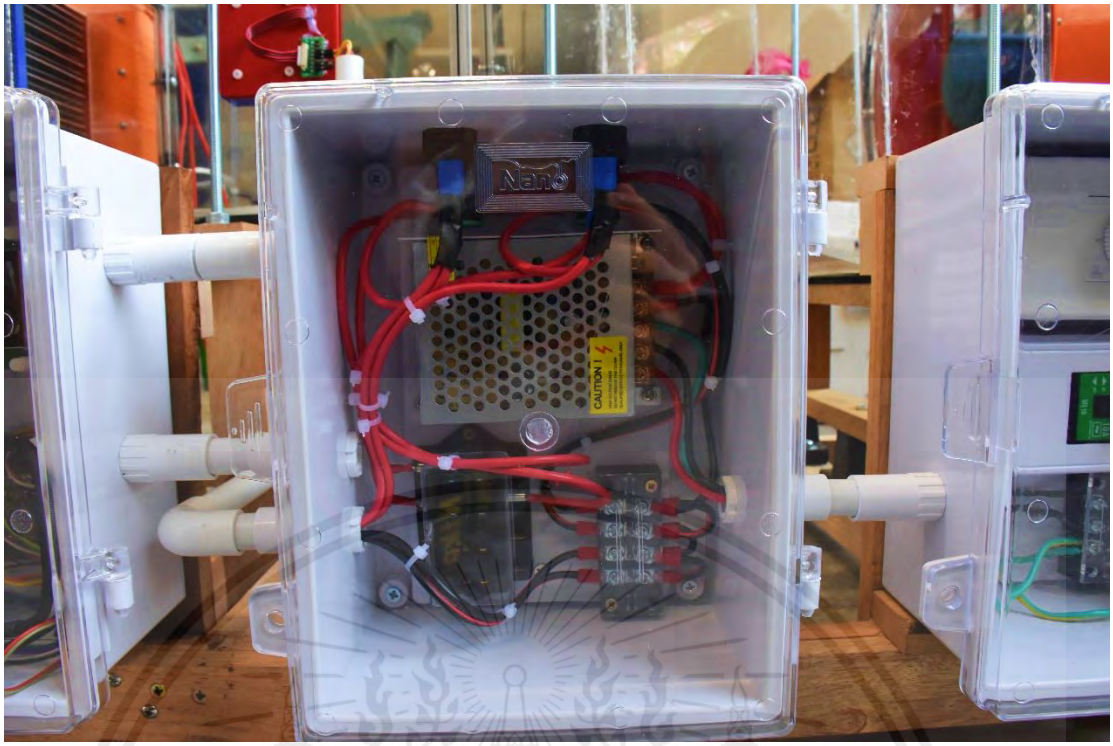

Figure 3.62 Low voltage box

220VAC firstly got into the 12V power supply where it outputs 12VDC, it then got separated into 2 channels for 12V then it got individually 1A fuse, after that it passes through the switch that is separated for the charging and collecting section.

Figure 3.63 Low voltage box top view.

It has switch and LED light to let operator knows when it's operating.

Figure 3.64 Control box

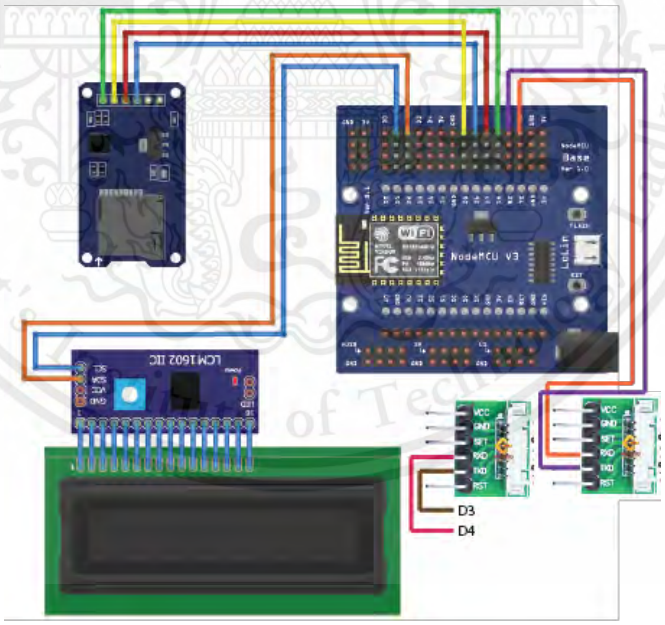

Figure 3.65 Control box circuit schematic

The control box consists of ESP8266 which is the main controller, LCD, SD card logger, and PMS5003 (PM Sensor).

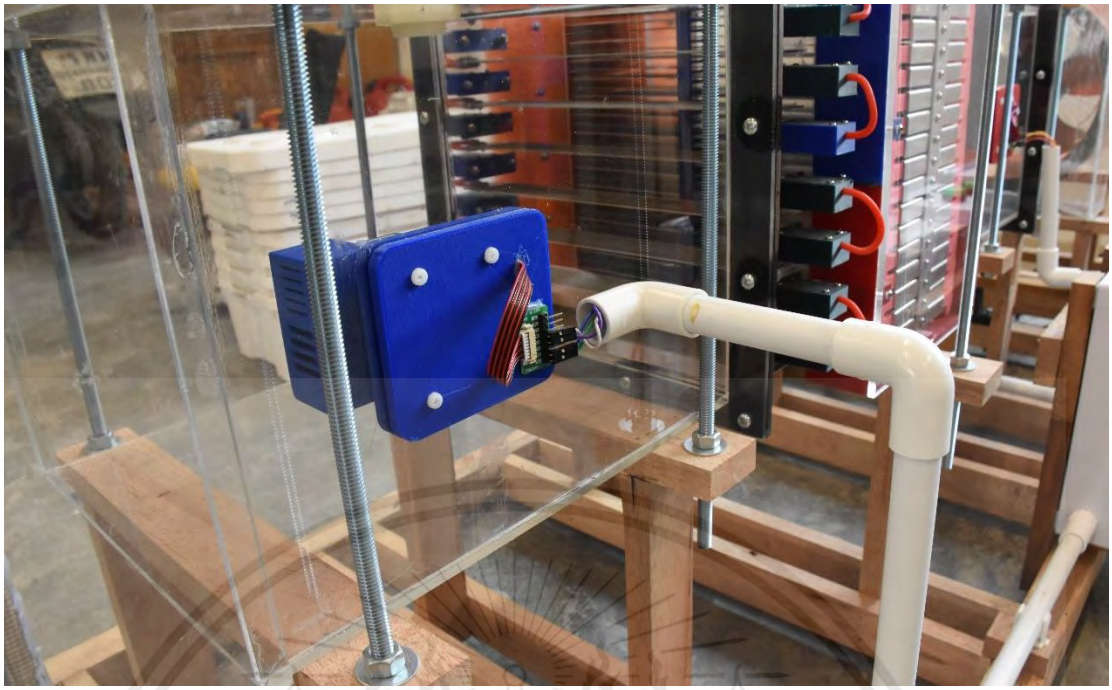

Figure 3.66 PMS5003 Sensor holder

All the wiring throughout the system has been done by white PVC electrical conduit for neat and prevent the wire from moving around which could cause the wire to become loose over time.

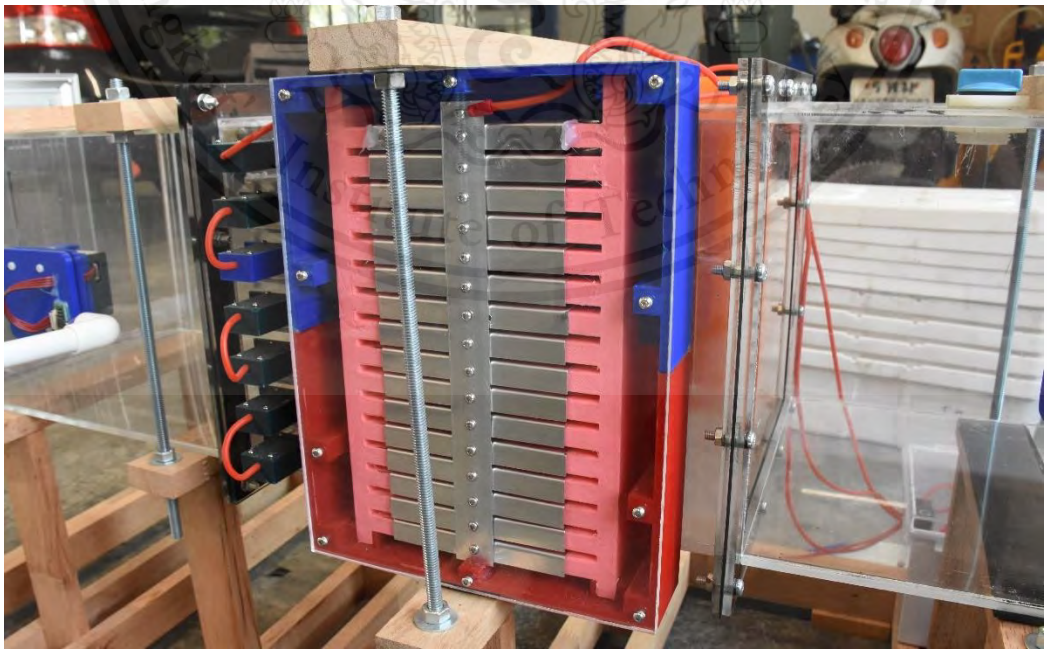

Figure 3.67 Collector plate power input

3.2.7 Overall setup

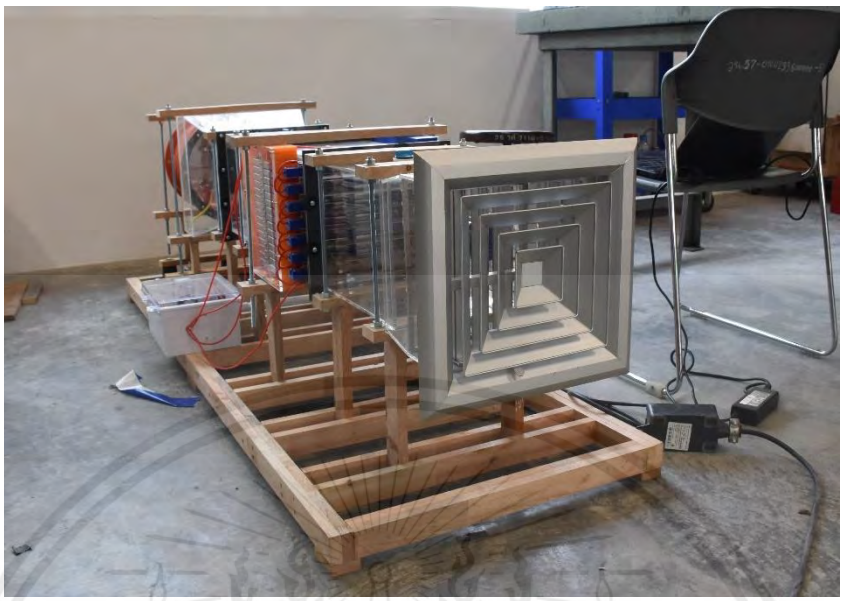

Figure 3.68 ESP complete system

Figure 3.69 ESP complete system picture 2

Wood pallets are used to construct the frame, all locking are done by clamping mechanism using thread screw. The overall system length is approximately 1.7 m.

CHAPTER 4

RESULTS AND DISCUSSION

4.1 Parametric Study (Flowrate)

This test is to investigate the relationship between the flowrate or flow velocity along the duct and the collection efficiency. The test was done twice.

The test is done within 1 hour timeframe to ensure that the PM concentration of the ambient air to be roughly the same in the range of ±10%, even though it could still fluctuate.

Test 1 was done in an average ambient PM concentration of PM1 = 23 $\mu g/m^3$, PM2.5 = 33 $\mu g/m^3$, PM10 = 37 $\mu g/m^3$. The flow velocity is varied using the fan speed controller and hotwire anemometer to measure the air velocity each time.

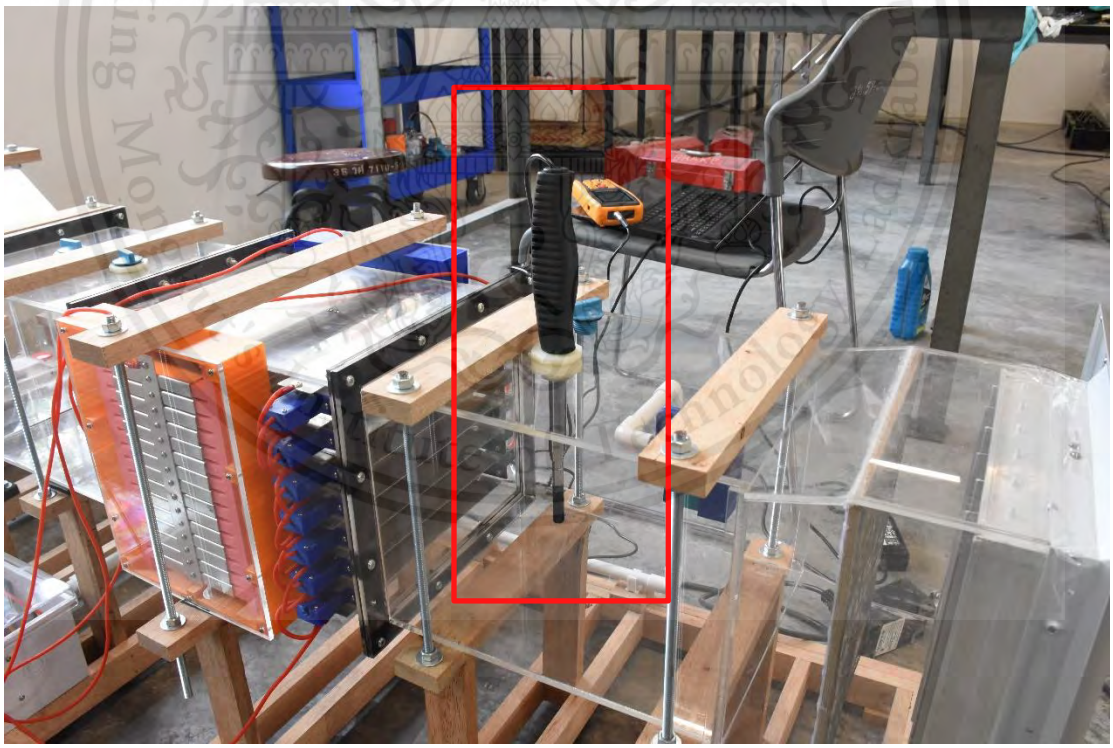

Figure 4.1 Flow velocity measurements.

Red mark shows the hot wire anemometer probe sticking into the duct, air velocity is measured at both the inlet and the outlet from ESP.

The flowrate velocity has varied 9 times. The pressure drop is calculated by.

$$\Delta P = \frac{1}{2}\rho\left(v_{outlet}^2 - v_{inlet}^2\right) \quad (4.1)$$

Inlet velocity (m/s)	Outlet velocity (m/s)	Pressure drop (Pa)
1.533	1.1	0.68405
1.7	1.25	0.7965
2.06	1.628	0.95593
2.24	1.8	1.06656
2.51	1.99	1.404
3.02	2.43	1.9293
3.21	2.52	2.37222
3.91	2.91	4.092
5.1	4	6.006

Table 4.1 Parametric Study Flowrate (Test 1)

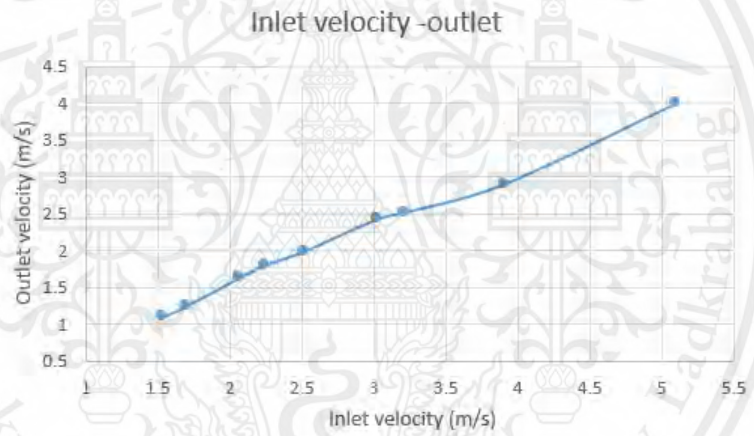

Figure 4.2 Inlet velocity versus outlet velocity (Test 1)

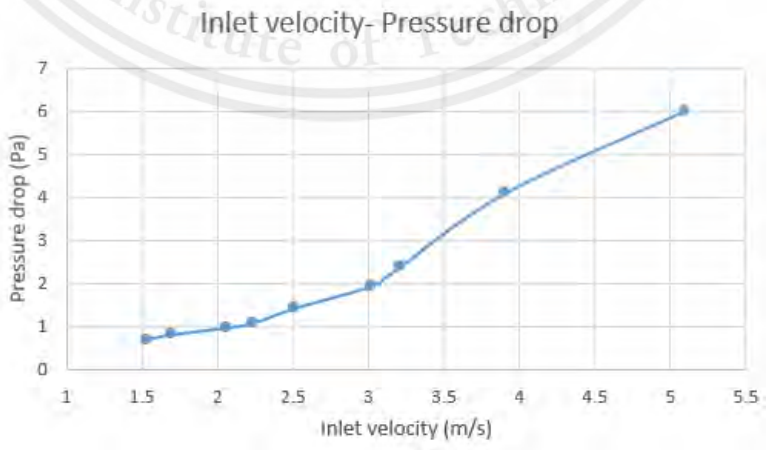

Figure 4.3 Inlet velocity versus pressure drop (Test 1)

According to Table 4.1, Figure 4.2, and Figure 4.3 shows that the flow velocity has been varied 9 times and are measured by hot wire anemometers. Observed that the higher the velocity, the higher the pressure drop across the ESP.

The collection efficiency is calculated by equation 4.2

$$\eta = \frac{\text{Inlet} - \text{Outlet}}{\text{Inlet}} \times 100 \tag{4.2}$$

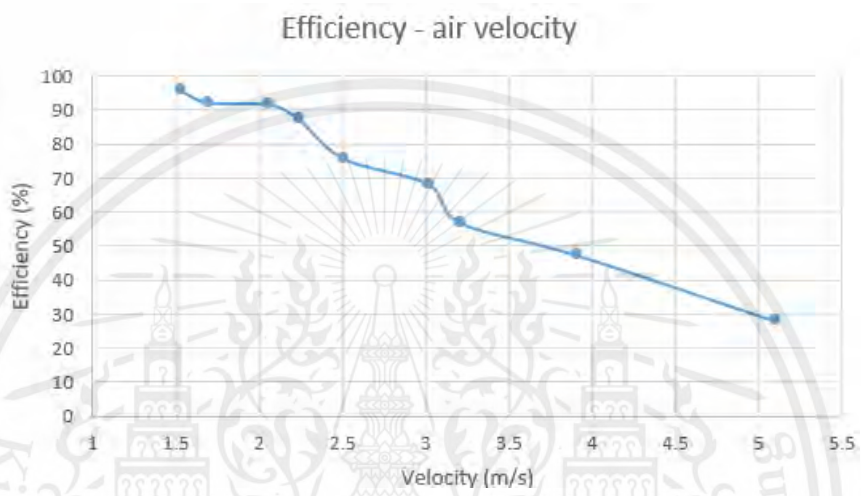

Figure 4.4 Flow velocity versus collecting efficiency (Test 1)

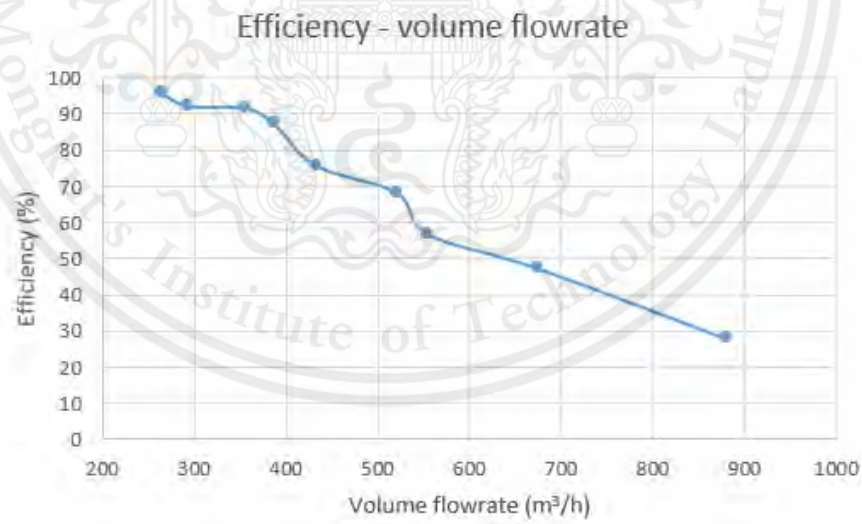

Figure 4.5 Volume flowrate versus collecting efficiency (Test 1)

Figure 4.4 shows that the collection efficiency gradually decreases with an increase in flow velocity, where this confirms with the design conditions at 2 m/s.

Figure 4.5 relates the flow velocity into the volume flowrate in m^3/h.

Test 2 was done in an average ambient PM concentration of PM1 = 47 µg/m^3, PM2.5 = 75 µg/m3, PM10 = 79 µg/m^3.

Inlet velocity (m/s)	Outlet velocity (m/s)	Pressure drop (Pa)
1.52	1.3	0.37224
1.8	1.54	0.52104
2.06	1.7	0.81216
2.37	1.87	1.272
2.72	2.15	1.66554
3.05	2.44	2.00934
3.7	2.86	3.30624
4.55	3.56	4.81734
4.98	3.95	5.51874

Table 4.2 Parametric Study Flowrate (Test 2)

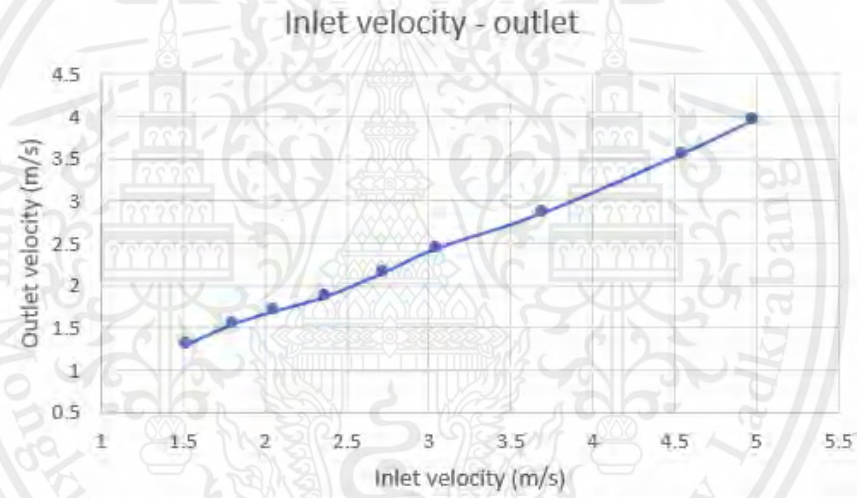

Figure 4.6 Inlet velocity versus outlet velocity (Test 2)

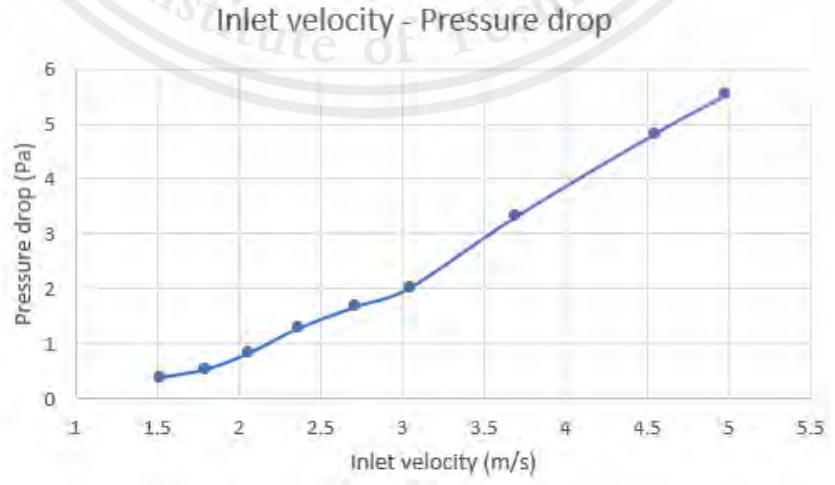

Figure 4.7 Inlet velocity versus pressure drop (Test 2)

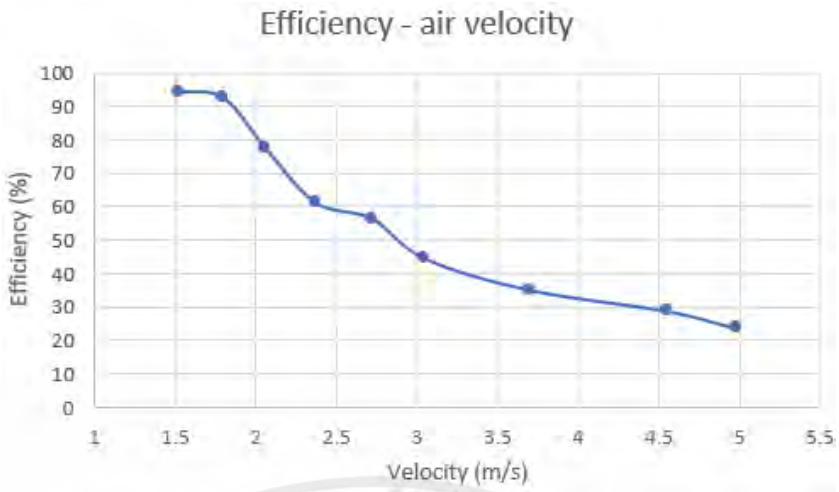

Figure 4.8 Flow velocity versus collecting efficiency (Test 2)

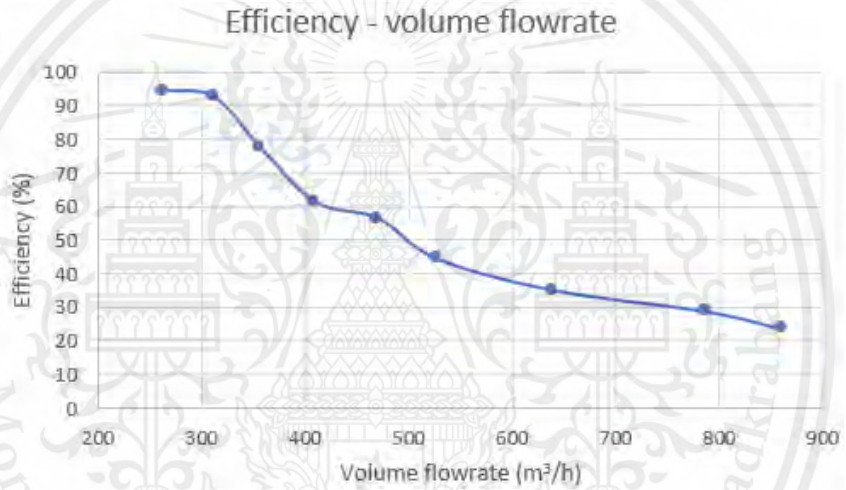

Figure 4.9 Volume flowrate versus collecting efficiency (Test 2)

After the test was done twice, the trend is accurately relatable according to the trend of the graph, the value of efficiency still differs in the range of not more than ±40%. With more velocity, more pressure drops. More velocity, less collection efficiency. However, test 1 and test 2 were done in a different ambient condition such that the PM concentration during test 2 was significantly higher than test 1. Thus, the combined graph must be illustrated for easier visualization and conclusion.

Figure 4.10 Flow velocity versus collecting efficiency (Combined)

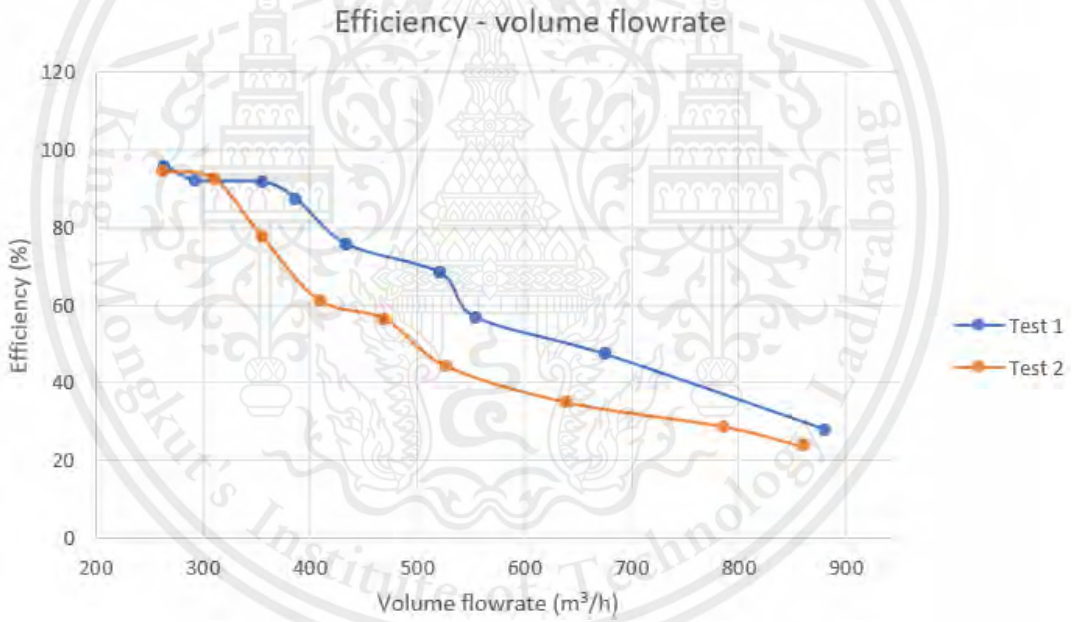

Figure 4.11 Volume flowrate versus collecting efficiency (Combined)

Test 1 was done in an average ambient PM concentration of PM1 = 23 µg/m^3, PM2.5 = 33 µg/m^3, PM10 = 37 µg/m^3. While Test 2 was done in an average ambient PM concentration of PM1 = 47 µg/m^3, PM2.5 = 75 µg/m^3, PM10 = 79 µg/m^3. As observed, the ambient PM concentration on test 2 was around 2 times higher than test 1. Thus, the PM concentration has a significant effect on collection efficiency.

4.2 PM collection test

According to section 4.1, the results reveal the device capability of collecting PM. However, those values came from the PMS5003 (PM sensor). This test would require the device to run for some time then use the paper to wipe the dust off (It's acceptable since we're not going to use the dust for analysis now) then weight on the scale to confirm how much PM it has collected.

Figure 4.12 4 digits scale

Figure 4.13 Kimtech Kimwipes

4.2.1 Test run (dry wipe)

During the operation, data was logged into the SD card every 1.6 seconds time intervals. 2 PMS5003 (PM sensor) were used at inlet and outlet. PMS5003 outputs 3 sizes of PM which will be summed up together. The difference or reduction in PM can be executed by simply subtracting outlet concentrations from inlet concentrations. The graph of PM reduction with respect to operating time can be illustrated as in Figure 4.14.

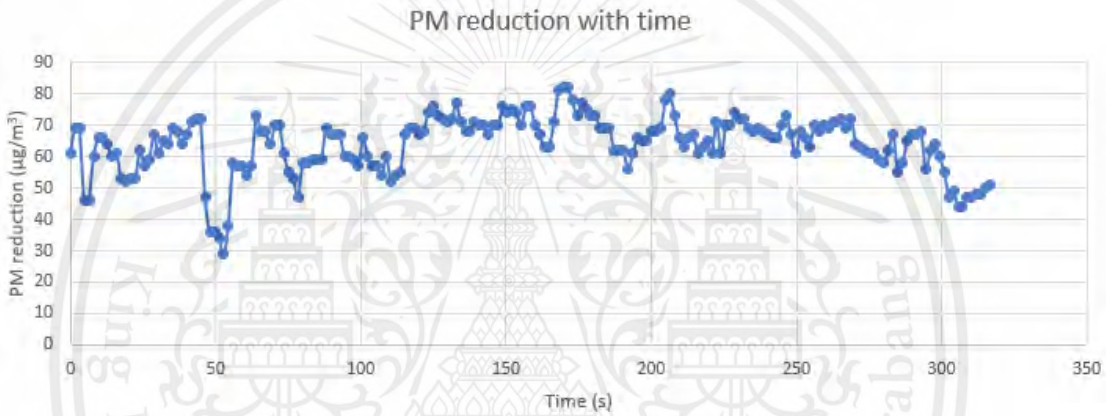

Figure 4.14 PM reduction graph (Test run dry)

For better simplicity, only the first 300 seconds of operating was used to illustrate in Figure 4.14. If the area under the graph is executed it would result in the unit of $\left(\frac{\mu g \cdot s}{m^3}\right)$ which if it is multiplied by volume flowrate (m^3/s), it would result in the accumulated value of PM collected mass which will be called integrated value later.

Microsoft Excel was used to calculate the integrated value for this test, and the result reveals that 187.23 mg of PM dust were collected during the time of 5.78 hours. However, this value came directly from the PMS5003 sensor and calculation. Practically, when collecting PM dust for usage, it's impossible to collect all of the dust that was precipitated on the collector plate.

So after the test, kimwipes (Figure 4.13) has been used for weighing apparatus. The kimwipes got folded and calculate the initial weight using the 4 digit scale as seen in Figure 4.12, after that the negative collector plate is removed one by one and use the kimwipes to wipes each plates individually.

Figure 4.15 Dust accumulation of negative collector plates surface.

After that, the kimvipes got weight on 4 digit scale again. The PM dust collected mass is executed by subtracting the weight after it has been wipes from the initial weight of kimwipes.

The result reveals that the mass of PM collected was only 16 mg comparing to the calculated value of 187.23 mg in 5.78 hours of collection.

Observed that when collection, it was very hard to wipe all the dust to settle on kimwipes paper or else the paper would get teared resulting from friction.

4.2.2 Test run (wet wipes)

According to the last test, the result was not satisfied as the weighted value was too much different from the calculated value. Based on the assumption that it was a human error where it's impossible to wipe all the dust out from collector plates.

Ethyl alcohol 95% was introduced to help the collection of PM, as it evaporates very quickly as the water content of this types of alcohol is quite low, such that it would not interfere with the result.

This test, the integrated value was 150.88 mg with the time 4.86 hours.

The alcohol is wipe onto the kimwipes and use it to wipe the collector plates, observed that the collection was better than the last test. After that, the kimwipes paper is placed in a sealed container with a small lid opening for alcohol to evaporate. We let it sit for around 1 hour and weigh it again, the result reveals it had collected 40 mg of PM. However, we let it sit for another day and weighed it again, the result was 25 mg of PM dust. Which is 6 times lesser than the integrated value, but still had some improvement over the last test (dry wipes)

Figure 4.16 Weighting process (The paper is folded).

4.2.3 Long run test 1

According to the previous tests, it's clear that it's impossible to collect all the PM dust that has been precipitated on the plates. The result from section 4.2.2 reveals that the collected PM mass was 6 times less than the calculated value. Thus, if we have an objective to collect 100 mg in 1 day, then the integrated value would need to be at least 600 mg. Hence, a long run of 24 hours is required. Since there were safety issues, it was not advice to run the device overnight unaccompanied. The device was tested for 2 days with 12 hours each and the device is off with all air ways already shut off to prevent air blowing into the system.

The collection method was by using wet wipe method and the alcohol evaporation time is set to be 1 day to ensure all the liquid has evaporated.

The integrated value is 855.79 mg with the time 26.4 hours. The weighted value is 175.5 mg. Which were 4.87 times less than the integrated value. An improvement of collecting PM has improved since last time, this may be due to higher accumulation of PM on collector plates surface, as observed that the dust accumulated together better than the last test due to more PM precipitation from long run test.

4.2.4 Long run test 2

This test run is based on the same principle as the long run test 1. Test 2 was done to confirm the validity of the experiment.

The integrated value is 641.47 mg with the time 23.645 hours. The weighted value is 166.2 mg. Thus, we have successfully met the requirements of collecting 100 mg of PM within 24 hours.

4.3 Discussion on PM dust precipitation on collector plate

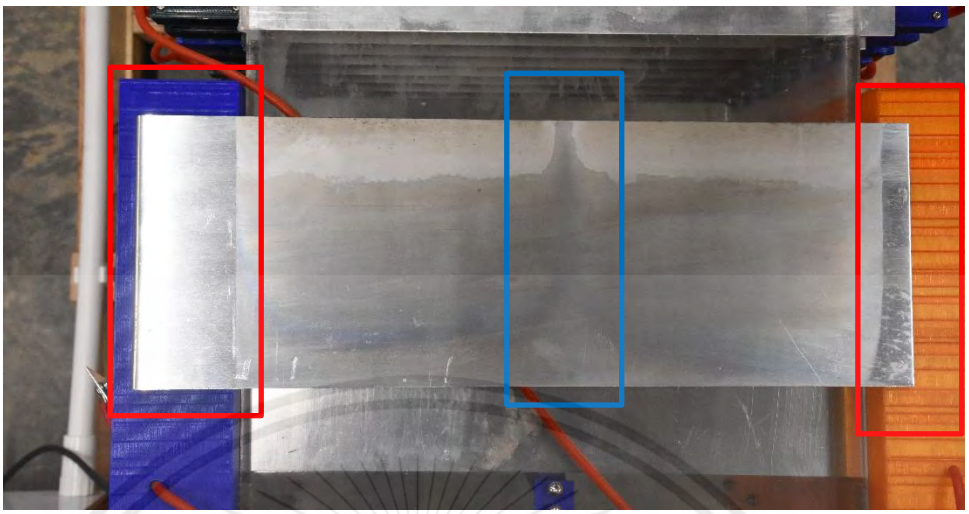

Figure 4.17 Negative collector plate dust collection picture (Front)

Figure 4.17 shows the negative collector plate with dust accumulated on the surface of the plate. The red mark reveals the area that is not inside the device, so there's no PM dust collected on that area, where it can be related directly by visualizing. The blue mark reveals that it's the area where dust does not accumulate onto which this can be explained by Figure 4.18 that at the middle of the collector plate, there's a a holder in between which may restrict the air flow toward that area.

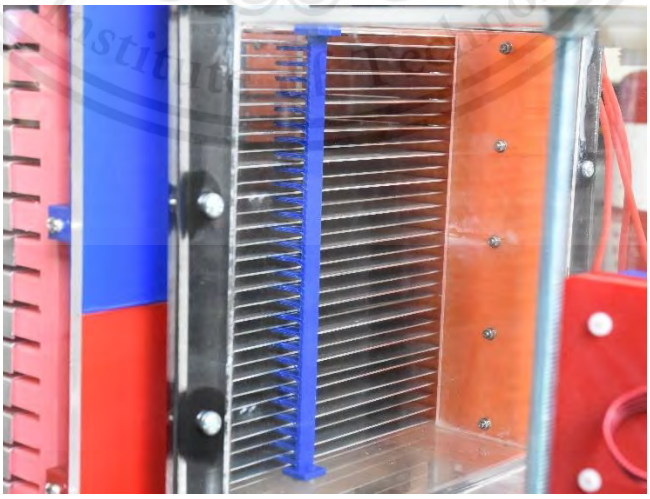

Figure 4.18 Collector plate holder in between plates

Figure 4.19 Negative collector plate dust collection picture (Back)

Figure 4.19 shows the negative collector plate but on the back size, visually, there is significantly lower dust accumulation compared to the front size. This may be due to gravitational force pushing the PM dust down and it begins to fly away.

Figure 4.20 Positive collector plate dust collection picture

Figure 4.20 shows the used positive collector plate which were little to no dust accumulation at all, where this confirms our assumption that the dust would only precipitate on negative collector plates since the positive corona was used.

4.4 Back corona effect

Figure 4.21 Back corona incident

During the operation, there was some strange sparkling noise periodically, someday it was quite frequent, sometimes not frequent. Figure 4.21 shows an incident called “Back corona” as explained in section 2.4.4.3 and 2.4.4.4 that if the resistivity of the dust is too high (the dust is a good insulator), the charge would not drain off at the collecting plates which causes “back corona” where this significantly reduced collection efficiency and could cause damage to the components.

Dust with high resistivity includes silica, coal, metal oxide, organic (wood,cotton, paper), ceramic dust, etc.

However, it’s impossible to choose the types of dust going into the ESP device. Thus, device adaptation might be necessary to prevent damage and ensure collecting efficiency.

CHAPTER 5

CONCLUSIONS AND RECOMMENDATIONS

Recall the study objectives.

1. To study basic principles of electrostatic precipitation including all design parameters.

2. To design and construct a compact size ESP that user could pull the collector plate out to use for the further analysis of PM. Target is to be able to collect 100 mg of PM in a period of not exceeding than 24 hours.

Which was successfully done throughout the project, and all documentation was listed in an organized manner in this thesis. The ESP system was able to perform correctly with considerably good efficiency and was able to collect the PM up to the target. However, the device itself is compact as it could use home electricity anywhere and it could be moved to other places, but the size of the system is relatively large, moving it would require a pickup truck. An improvement about its size should be considered, also when usage, it is not always possible to find home outlet (220VAC) everywhere, hence, battery powered would solve this problem.

This ESP has a collector plate of total 31 plates including 16 positive plates and 15 negative plates. Too many plates are harder to collect PM dust even though the higher surface area they provided; the dust would precipitate on each plate only a small amount. Collector plates gap could be higher by using higher voltage; thus, the number of plates could be reduced, also the larger gap may help reduce the back corona effect as there is more space between the gap given that the particles sizes are the same.

REFERENCES

Vallero, D. (2014). Fundamentals of air pollution. Academic Press.

Kouimtzis, T., & Samara, C. (2013). Airborne particulate matter. Springer.

Parker, K. (1997). Applied electrostatic precipitation. Springer.

C. David Cooper, & Alley, F. C. (2010). Air Pollution Control. Waveland Press.

Francis, S. L., & Bradburn, K. M. (2007). Electrostatic Precipitators for Industrial Applications.

Serway, R. A., & Jewett, J. W. (2013). Physics for Scientists and Engineers with Modern Physics. Cengage Learning.

Munson, B. R., Rothmayer, A. P., Okiishi, T. H., & Huebsch, W. W. (2012). Fundamentals of Fluid Mechanics. Wiley.

2021 ASHRAE Handbook: Fundamentals. (2021).

Agarwal, T. (2021, February 17). Hot Wire Anemometer : Construction, working & its Applications. ElProCus - Electronic Projects for Engineering Students. https://www.elprocus.com/what-is-a-hot-wire-anemometer-its-working/

Electrostatic precipitator (ESP). (2023, January 4). Ensavior : High Performance Engineering Solutions. https://ensavior.com/specialized-air-purification-system/electrostatic-precipitator-esp

APPENDIX A

Drawing of parts and fittings used in commercial ESP Testing

TITLE :	PART NUMBER :	DESIGNED BY:	DATE :	UNIT : mm
ESP FITTING FRONT	**1A**	**Panod Nilphai**	**18 April 2024**	

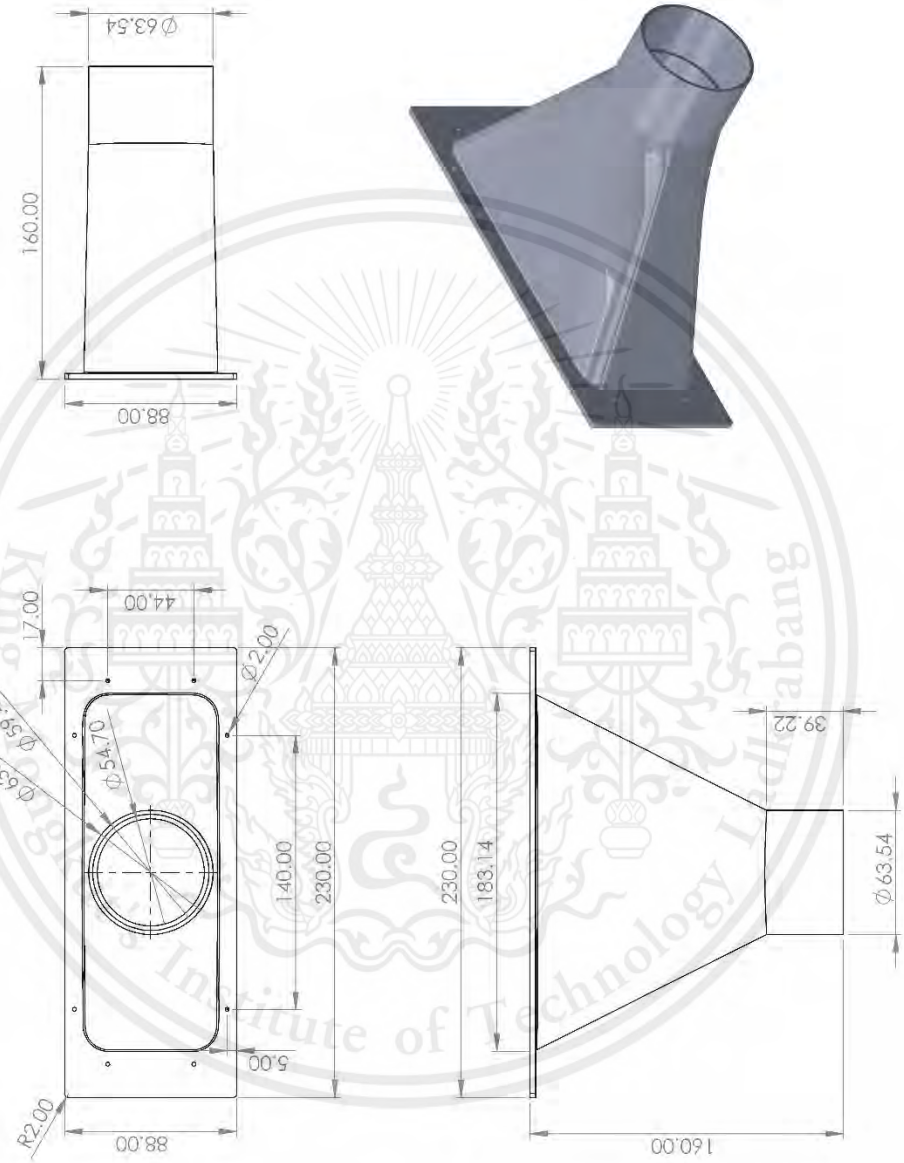

TITLE :	PART NUMBER :	DESIGNED BY:	DATE :	UNIT : mm
ESP FITTING REAR	**2A**	**Panod Nilphai**	**18 April 2024**	

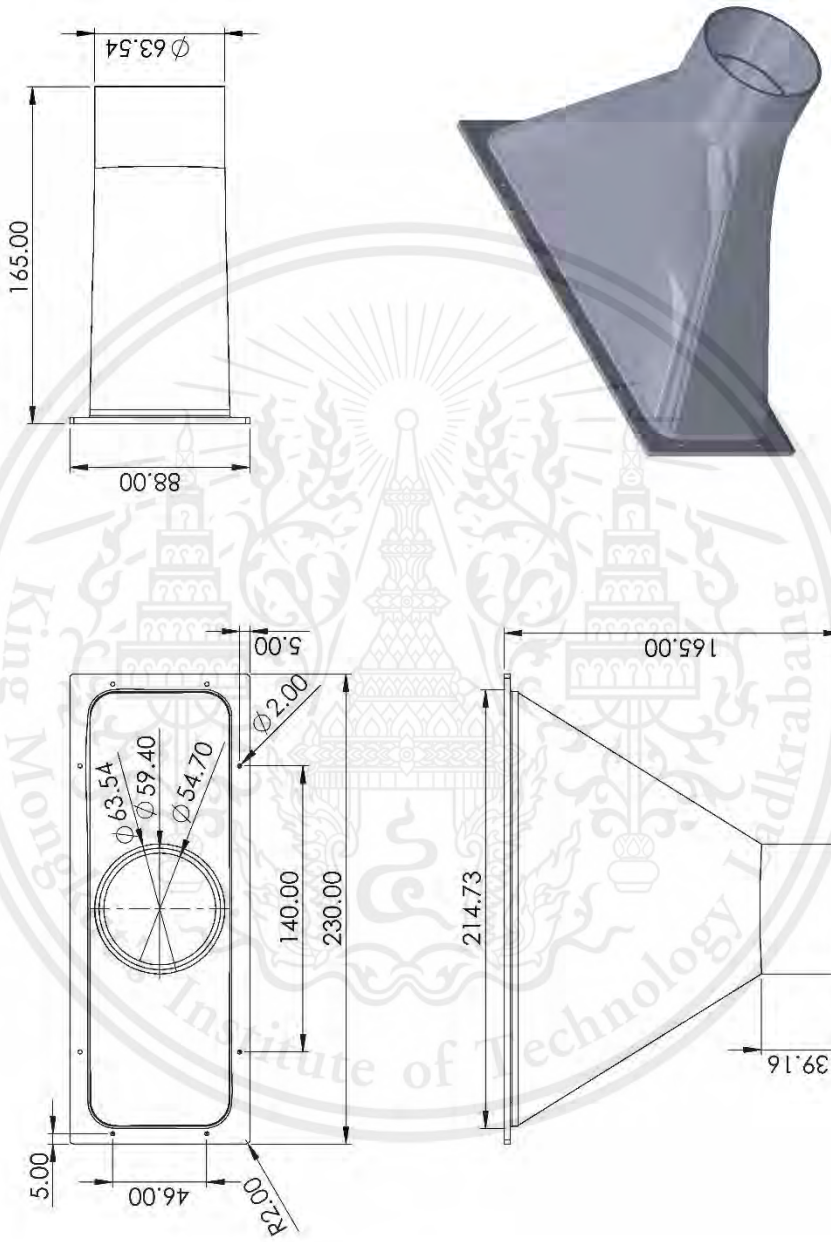

TITLE :	PART NUMBER :	DESIGNED BY:	DATE :	UNIT : mm
ADAPTER STRAIGHT	**3A**	**Panod Nilphai**	**18 April 2024**	

TITLE :	PART NUMBER :	DESIGNED BY:	DATE :	UNIT : mm
FAN CONNECTOR	**4A**	**Panod Nilphai**	**18 April 2024**	

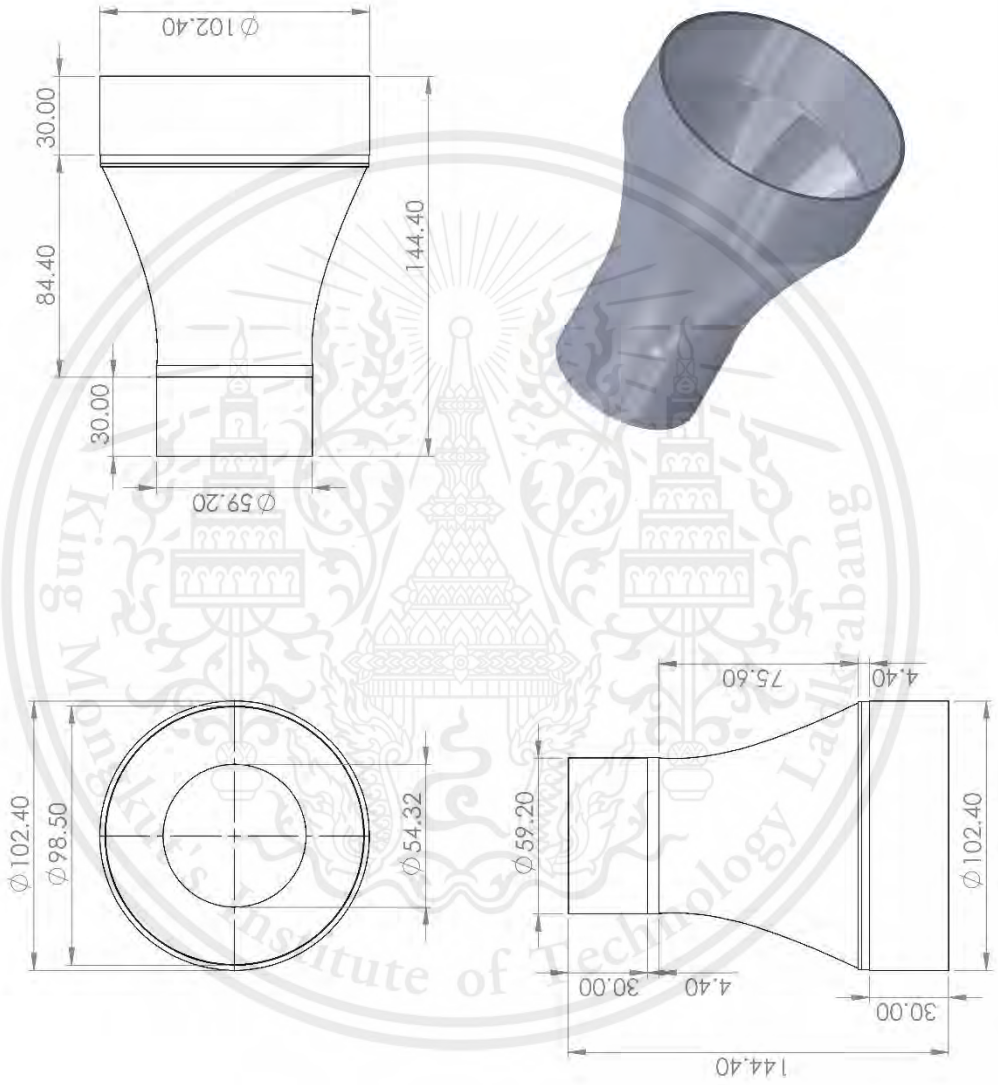

TITLE :	PART NUMBER :	DESIGNED BY:	DATE :	UNIT : mm
INLET PIPE	**5A**	**Panod Nilphai**	**18 April 2024**	

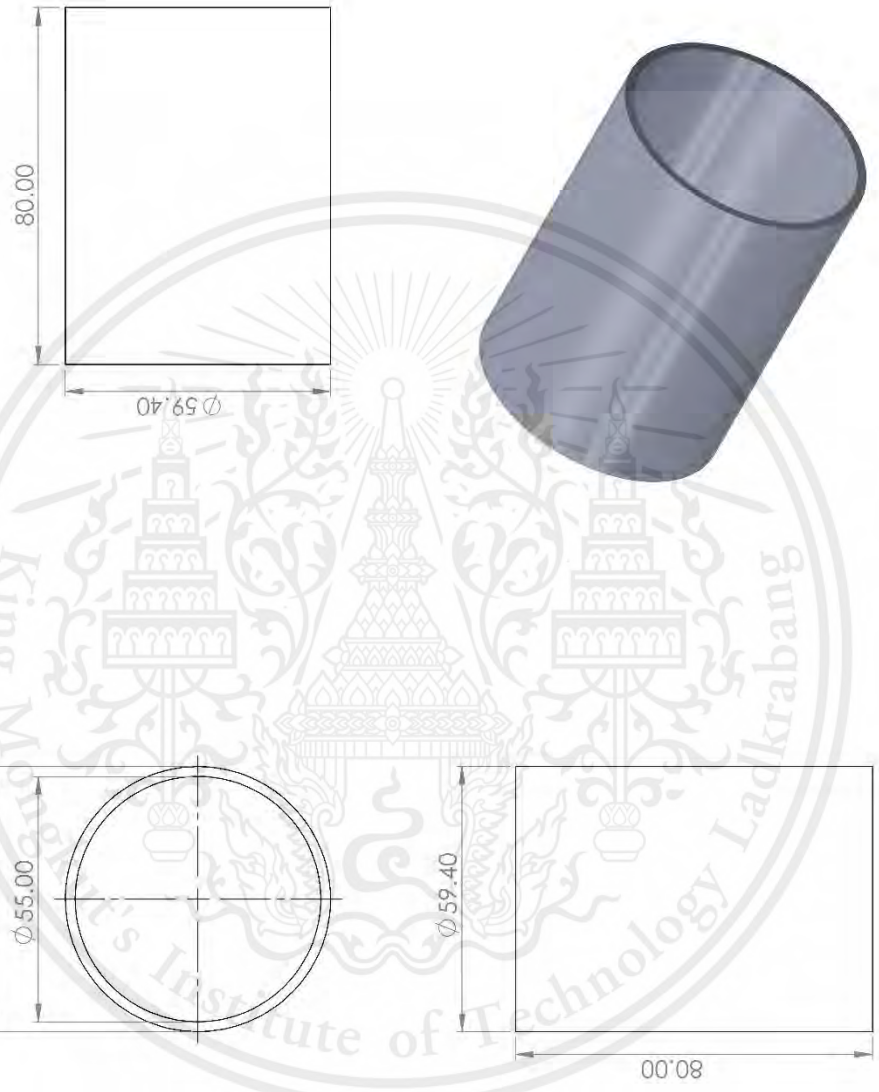

TITLE :	PART NUMBER :	DESIGNED BY:	DATE :	UNIT : mm
OUTLET PIPE	**6A**	**Panod Nilphai**	**18 April 2024**	

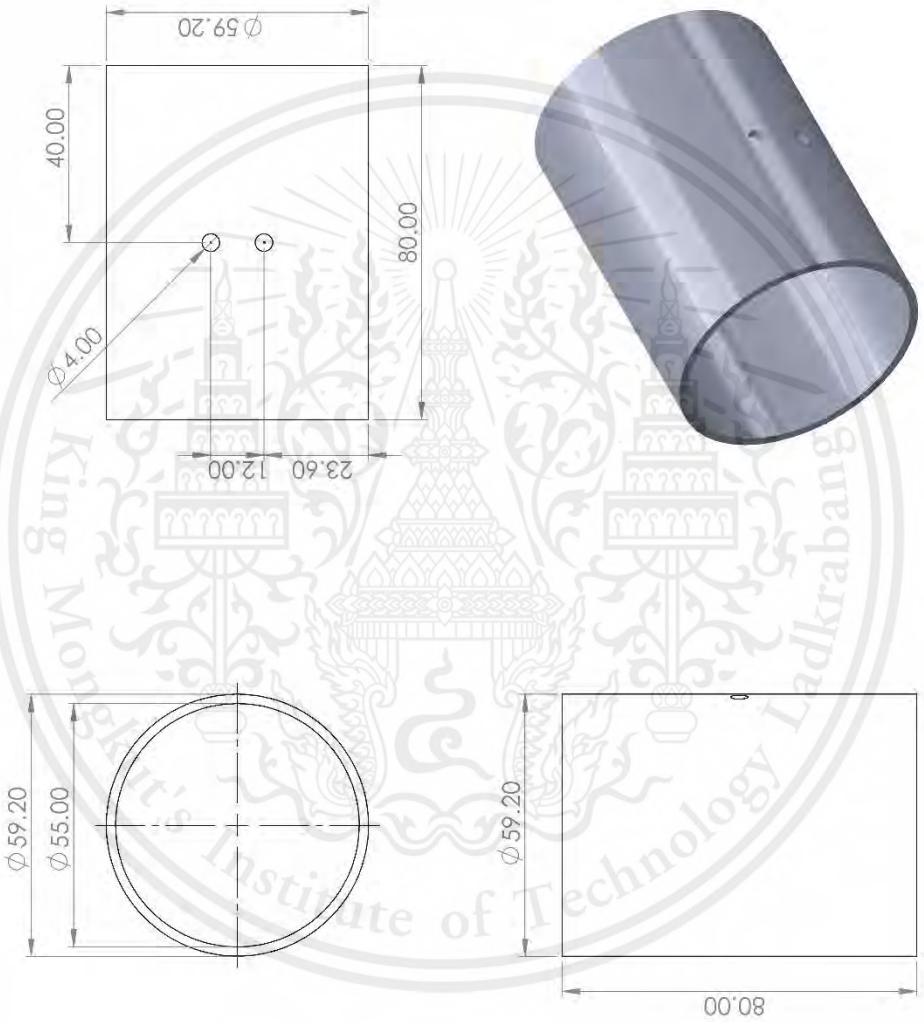

TITLE :	PART NUMBER :	DESIGNED BY:	DATE :	UNIT : mm
PITOT TUBE HOLDER	**7A**	**Panod Nilphai**	**18 April 2024**	

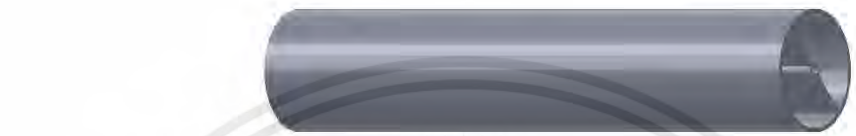

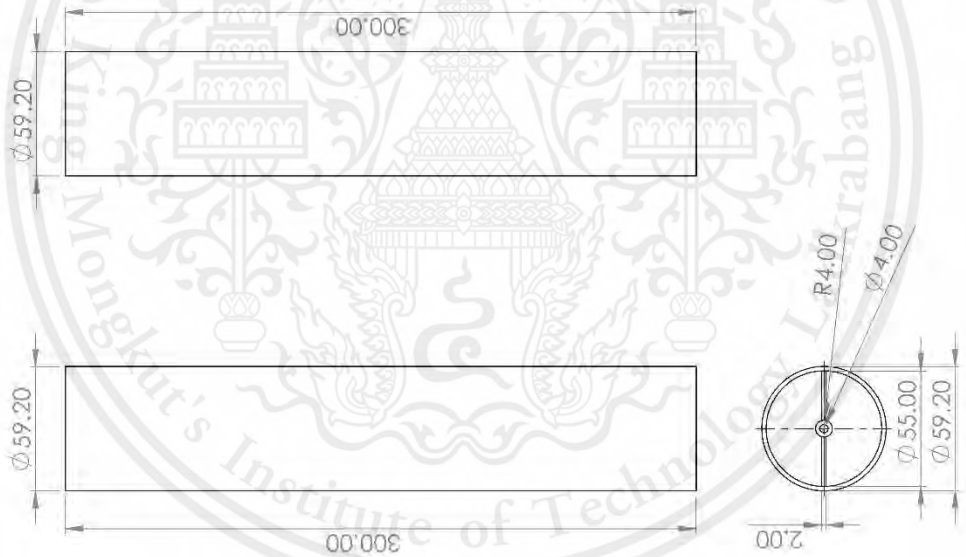

TITLE :	PART NUMBER :	DESIGNED BY:	DATE :	UNIT : mm
PM SENSOR BOX	**8A**	**Panod Nilphai**	**18 April 2024**	

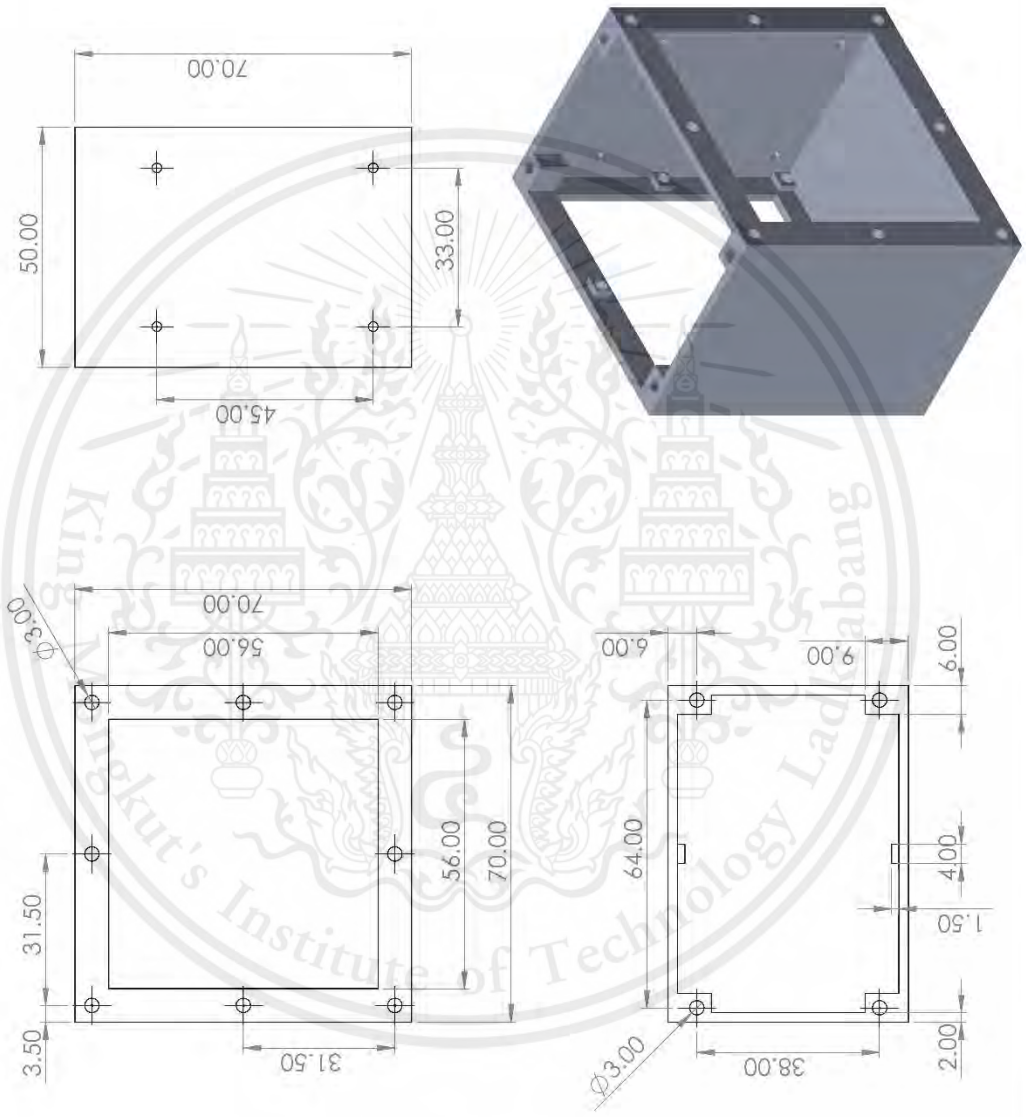

TITLE :	PART NUMBER :	DESIGNED BY:	DATE :	UNIT : mm
PM SENSOR DUCT	**9A**	**Panod Nilphai**	**18 April 2024**	

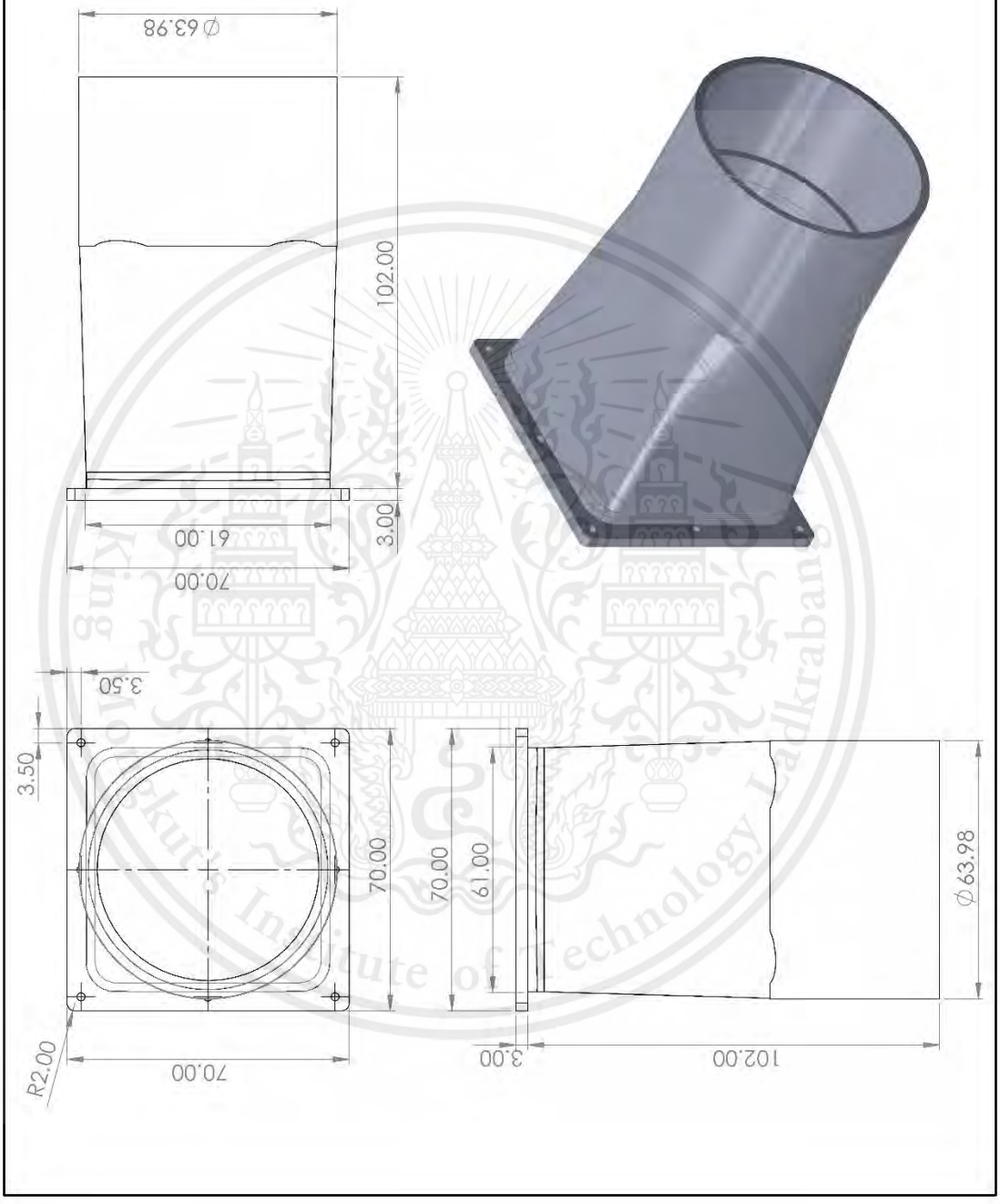

TITLE :	PART NUMBER :	DESIGNED BY:	DATE :	UNIT : mm
PM BOX ENCLOSURE	**10A**	**Panod Nilphai**	**18 April 2024**	

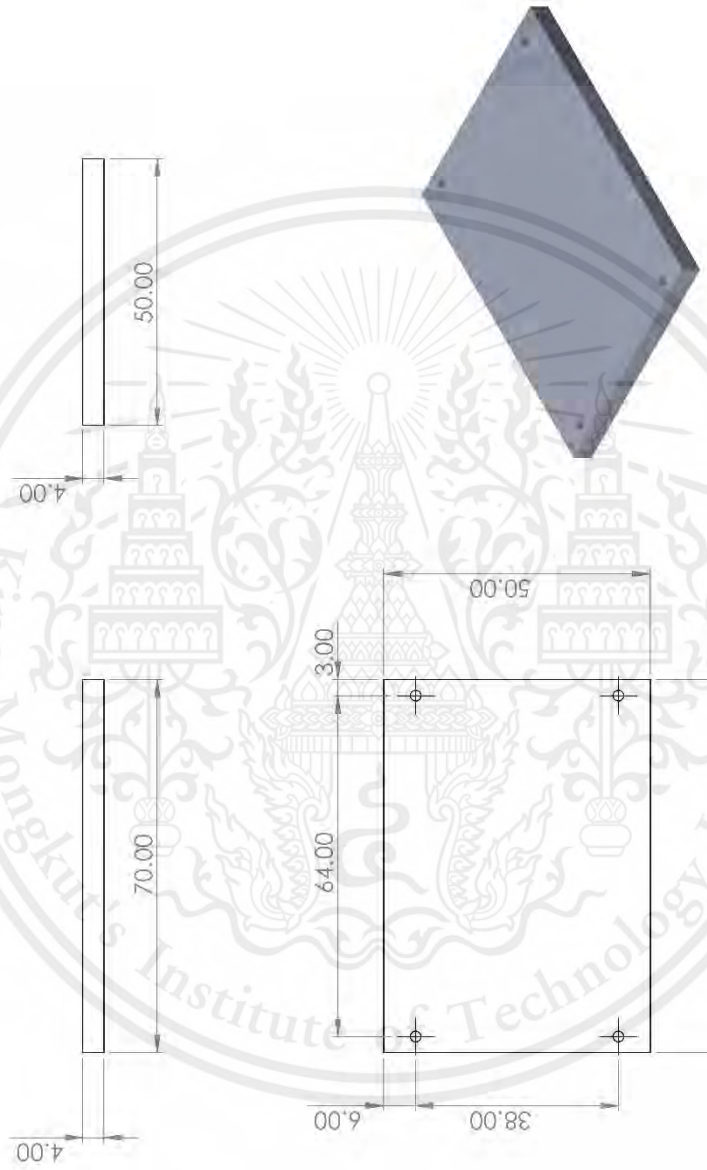

TITLE :	PART NUMBER :	DESIGNED BY:	DATE :	UNIT : mm
FULL ASSEMBLY TEST	-	**Panod Nilphai**	**18 April 2024**	

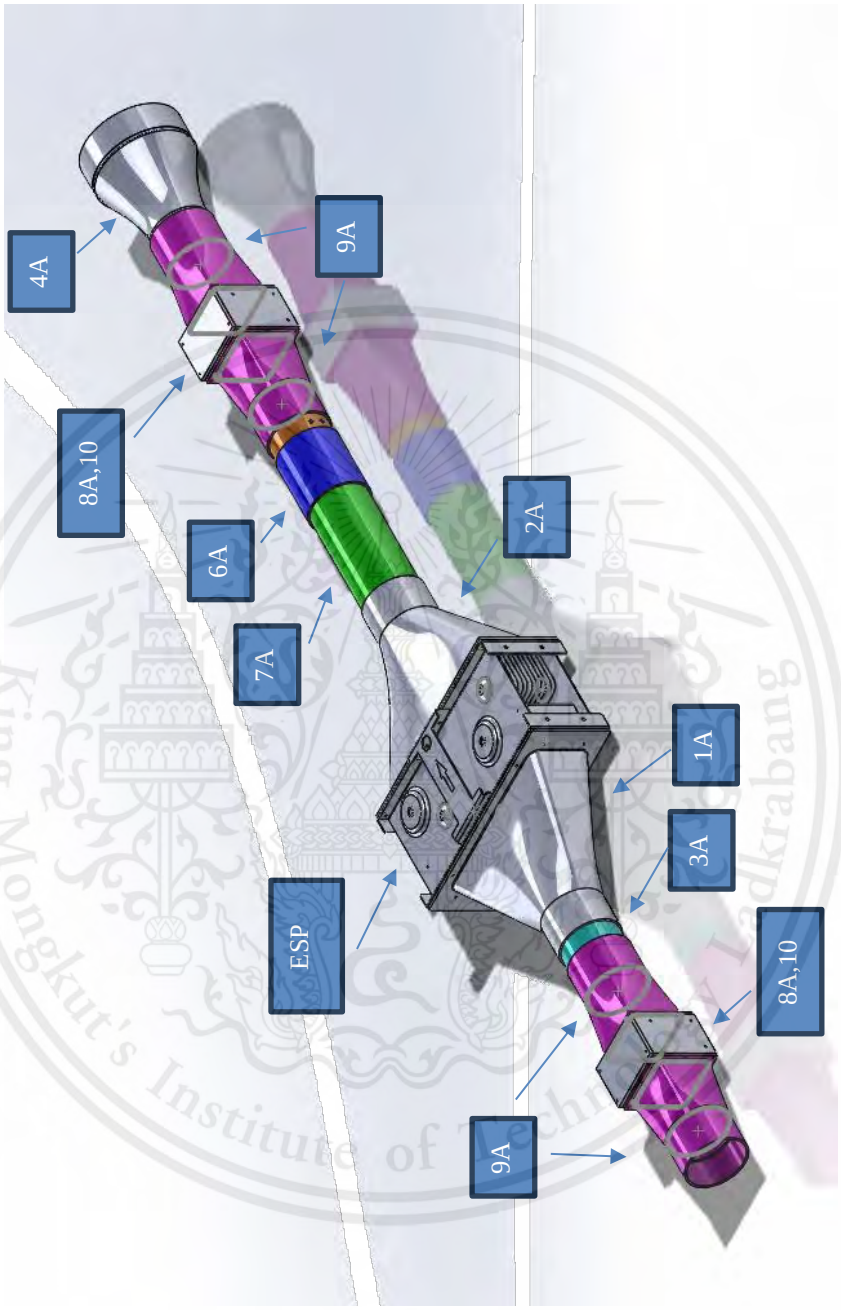

APPENDIX B

Drawing of parts and fittings used in new customized ESP unit

TITLE :	PART NUMBER :	DESIGNED BY:	DATE :	UNIT : mm
Up & Down Acrylic	**1B**	**Panod Nilphai**	**18 April 2024**	

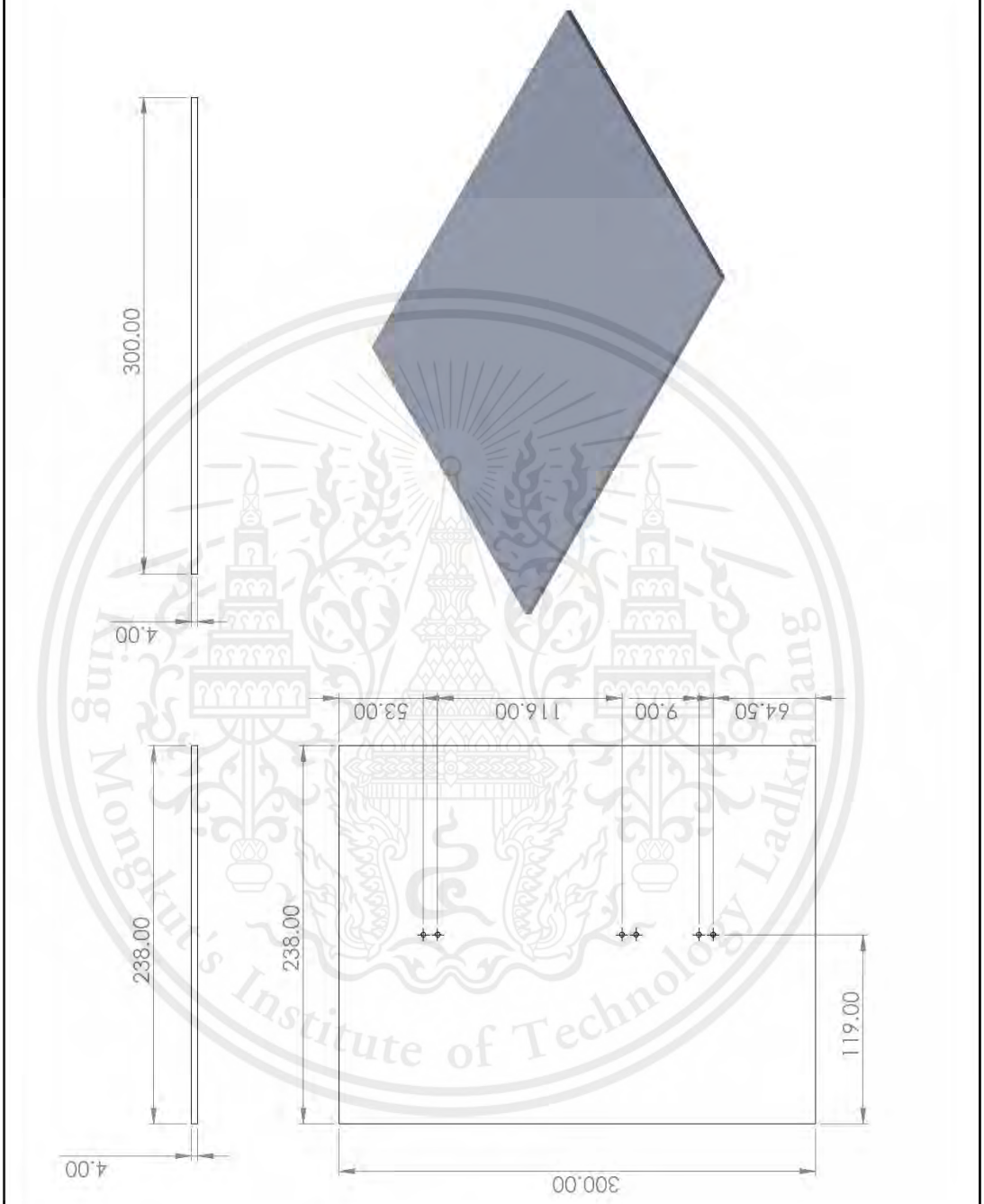

TITLE :	PART NUMBER :	DESIGNED BY:	DATE :	UNIT : mm
Left & Right acrylic	**2B**	**Panod Nilphai**	**18 April 2024**	

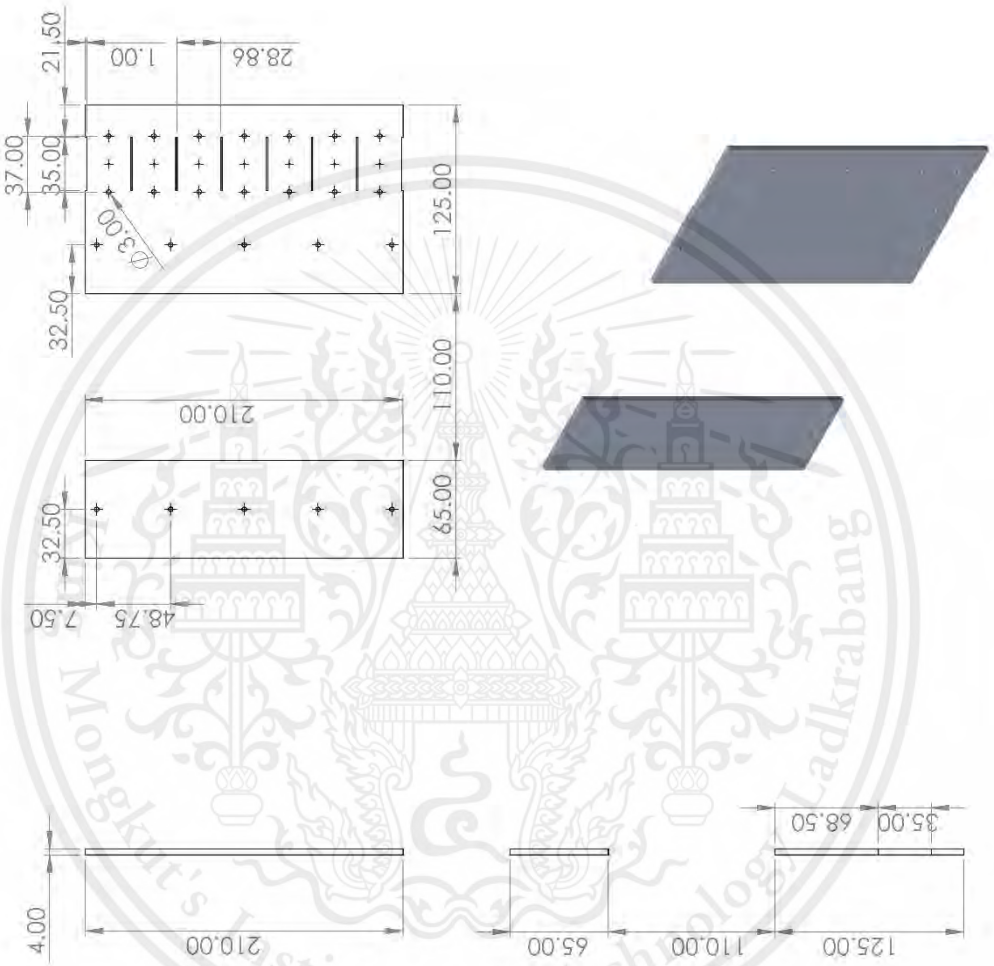

TITLE :	PART NUMBER :	DESIGNED BY:	DATE :	UNIT : mm
Electrode holder	**3B**	**Panod Nilphai**	**18 April 2024**	

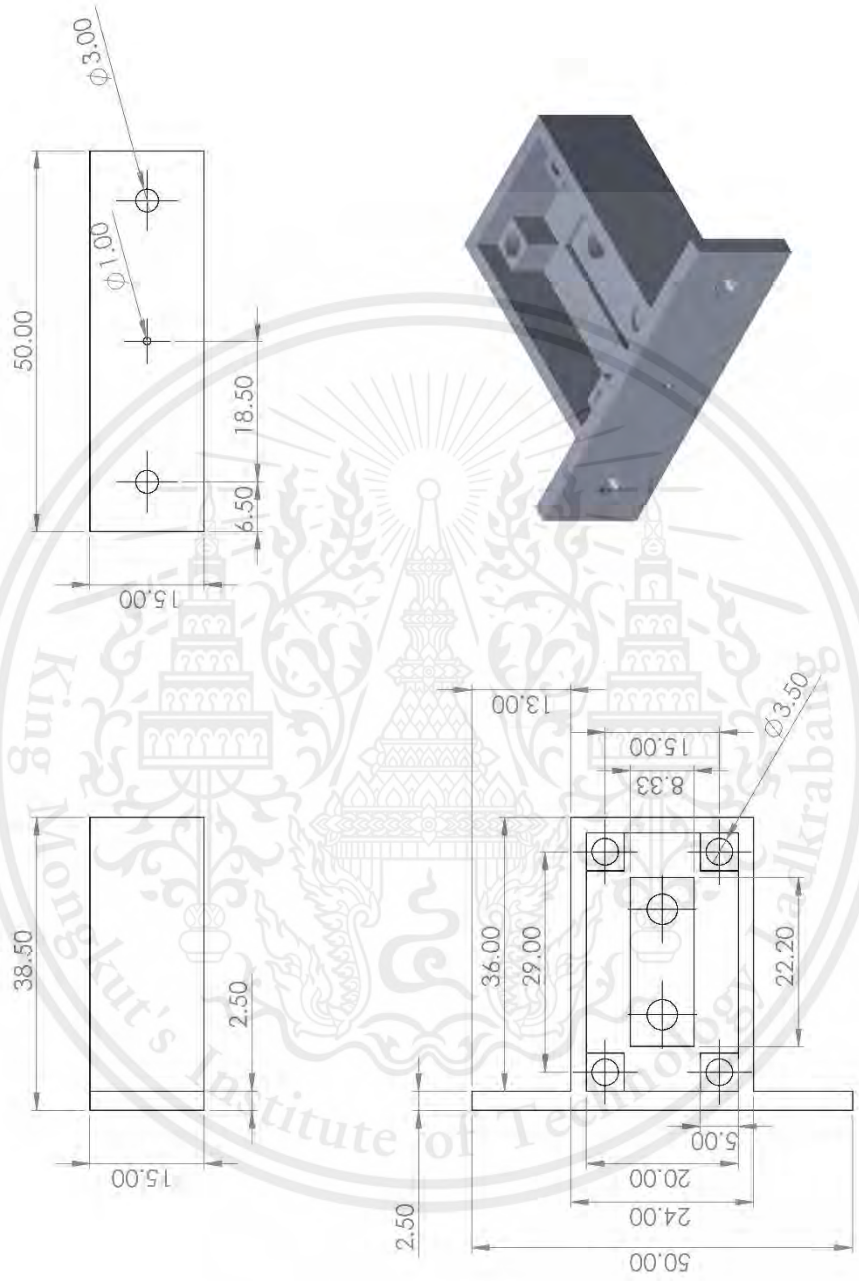

TITLE :	PART NUMBER :	DESIGNED BY:	DATE :	UNIT : mm
Ground CHG plate	**4B**	**Panod Nilphai**	**18 April 2024**	

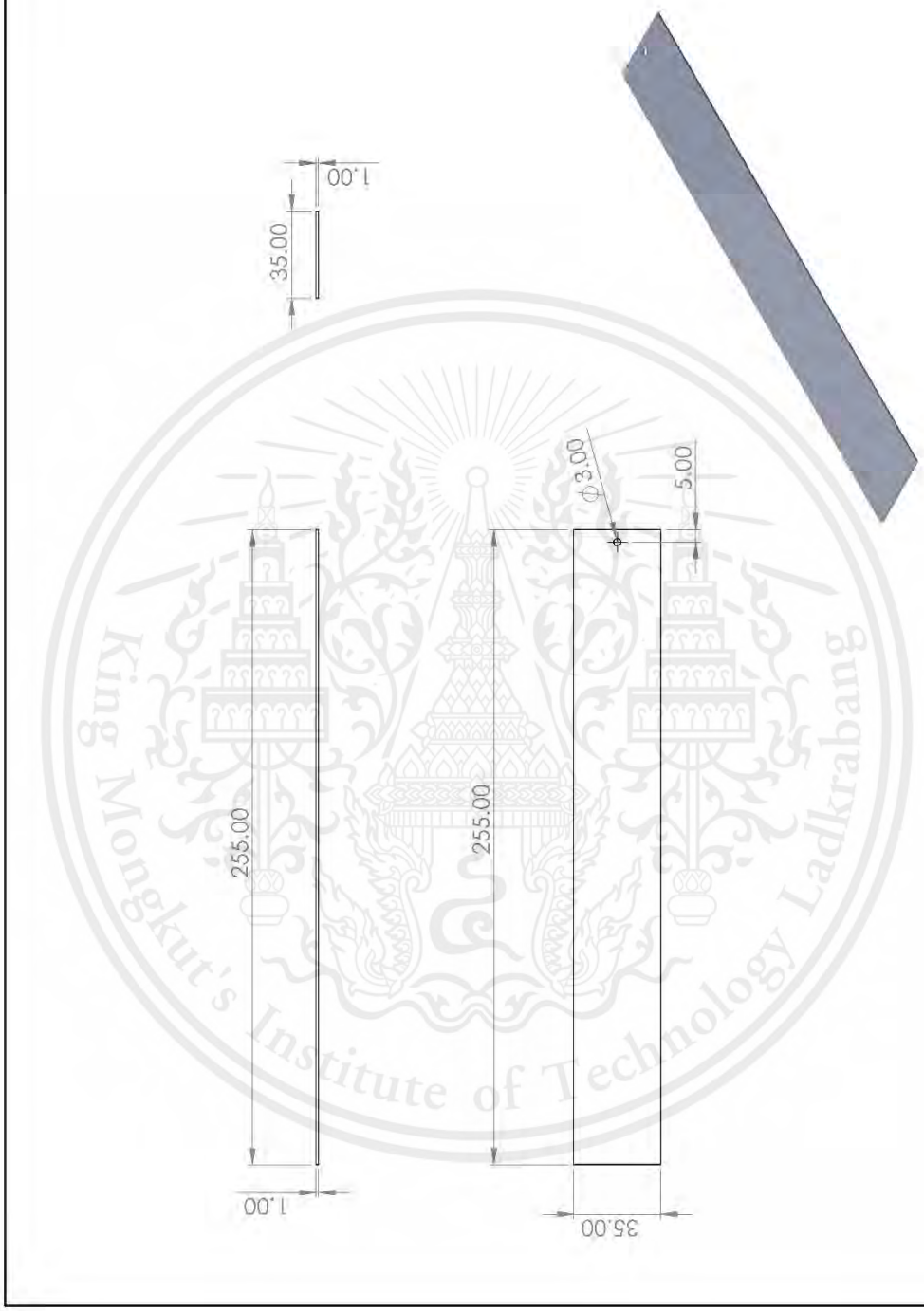

TITLE :	PART NUMBER :	DESIGNED BY:	DATE :	UNIT : mm
Collector plate	**5B**	**Panod Nilphai**	**18 April 2024**	

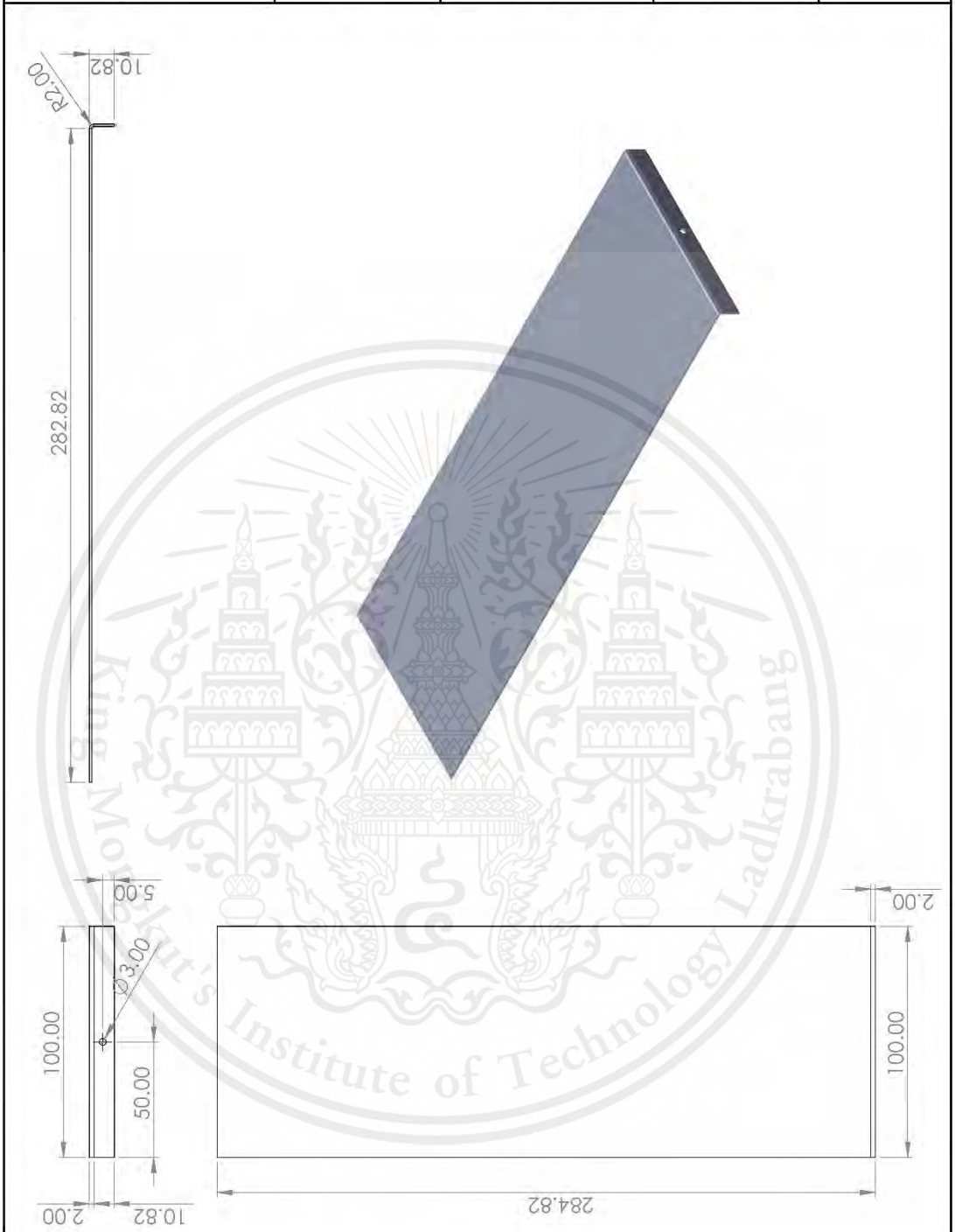

TITLE :	PART NUMBER :	DESIGNED BY:	DATE :	UNIT : mm
Plate Locker	**6B**	**Panod Nilphai**	**18 April 2024**	

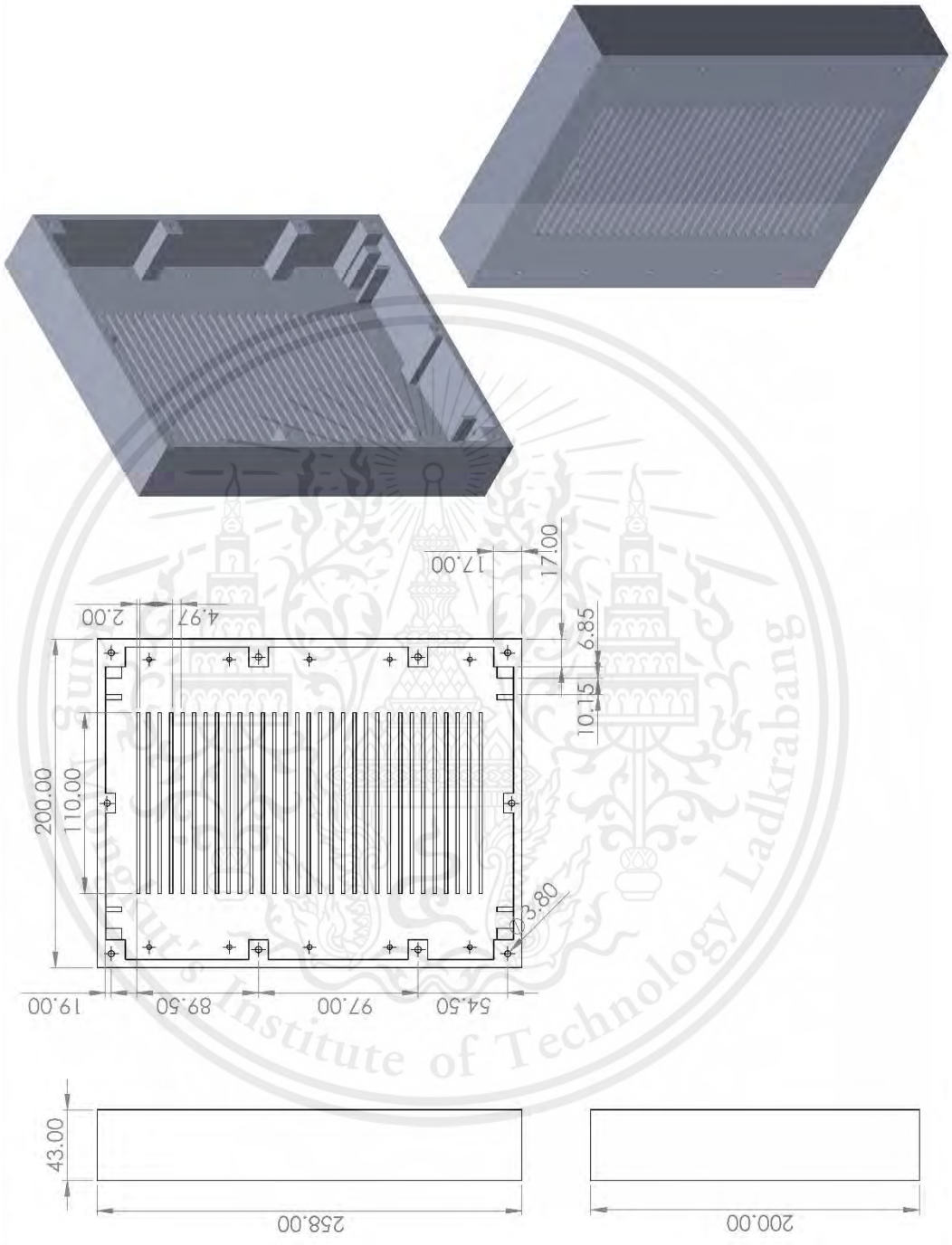

TITLE :	PART NUMBER :	DESIGNED BY:	DATE :	UNIT : mm
Ground plate locker	**7B**	**Panod Nilphai**	**18 April 2024**	

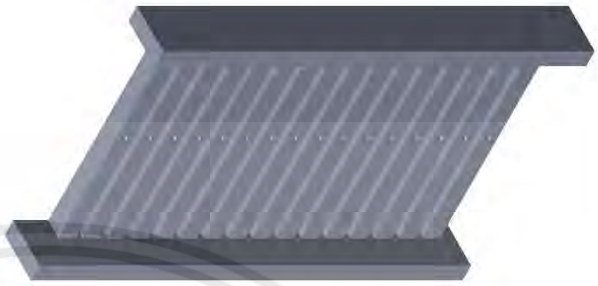

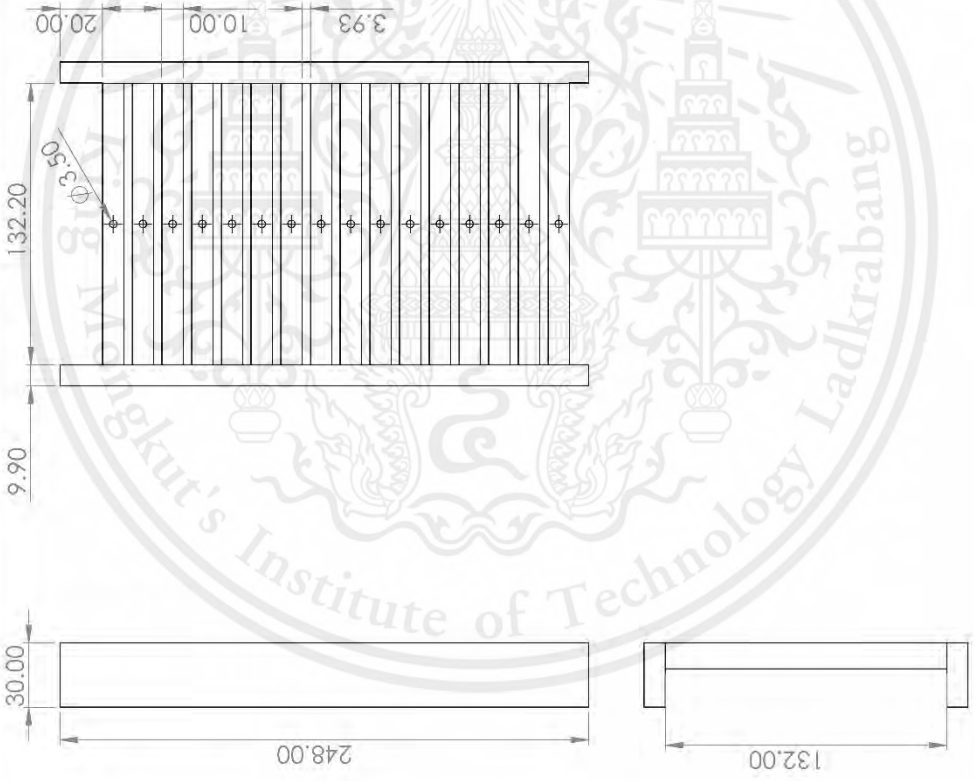

TITLE :	PART NUMBER :	DESIGNED BY:	DATE :	UNIT : mm
Positive plate locker	**8B**	**Panod Nilphai**	**18 April 2024**	

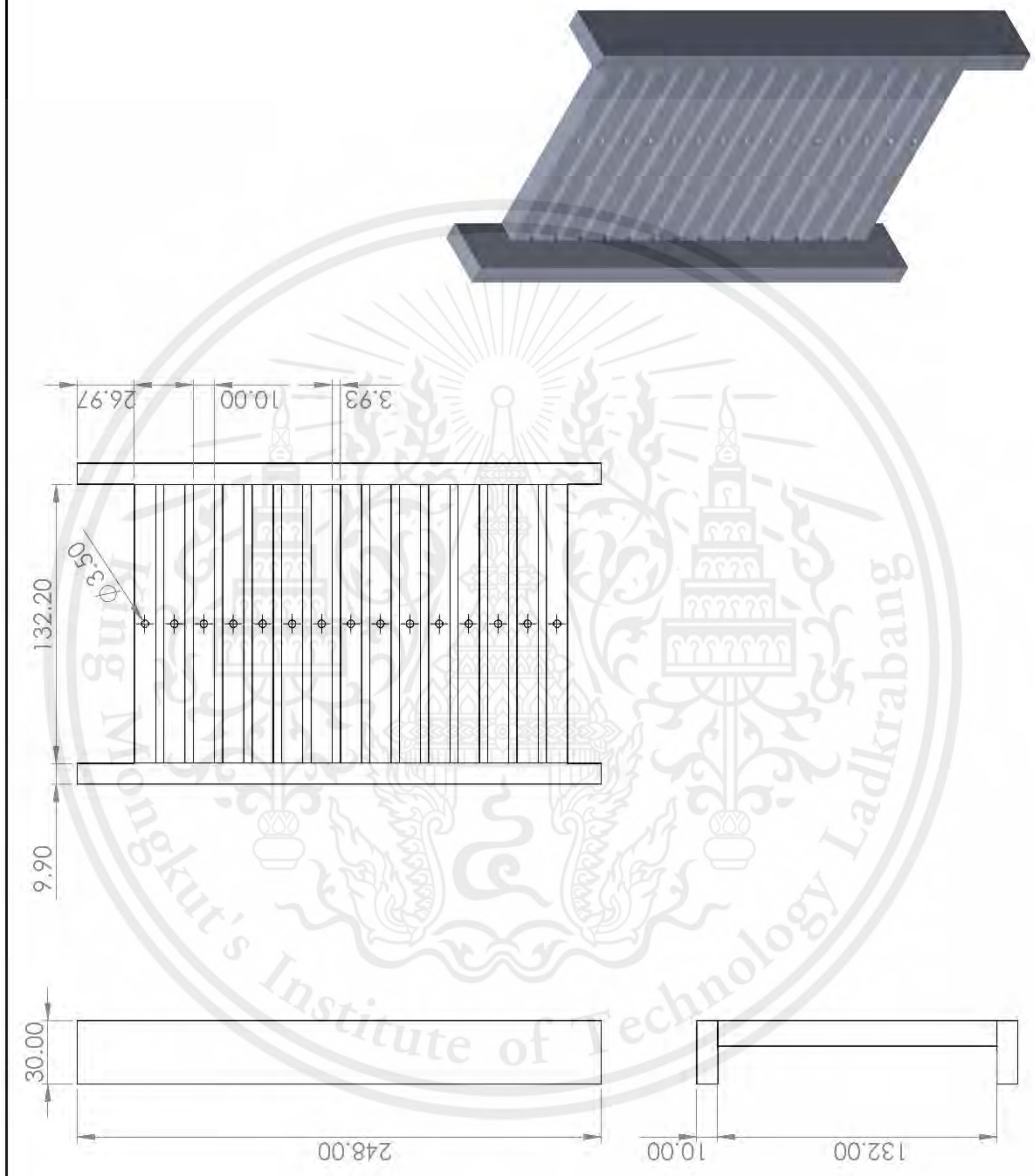

TITLE :	PART NUMBER :	DESIGNED BY:	DATE :	UNIT : mm
Ground bar	**9B**	**Panod Nilphai**	**18 April 2024**	

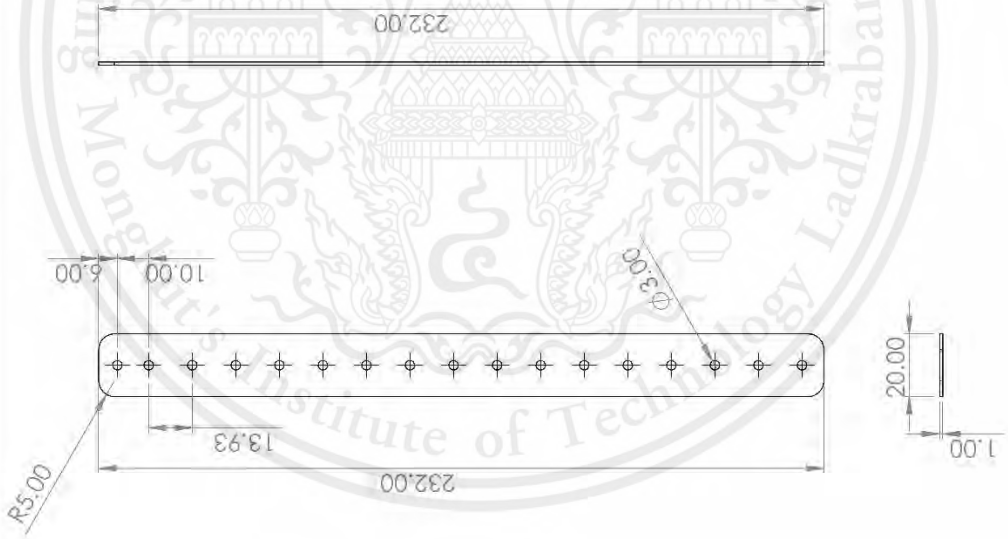

TITLE :	PART NUMBER :	DESIGNED BY:	DATE :	UNIT : mm
Positive bar	**10B**	**Panod Nilphai**	**18 April 2024**	

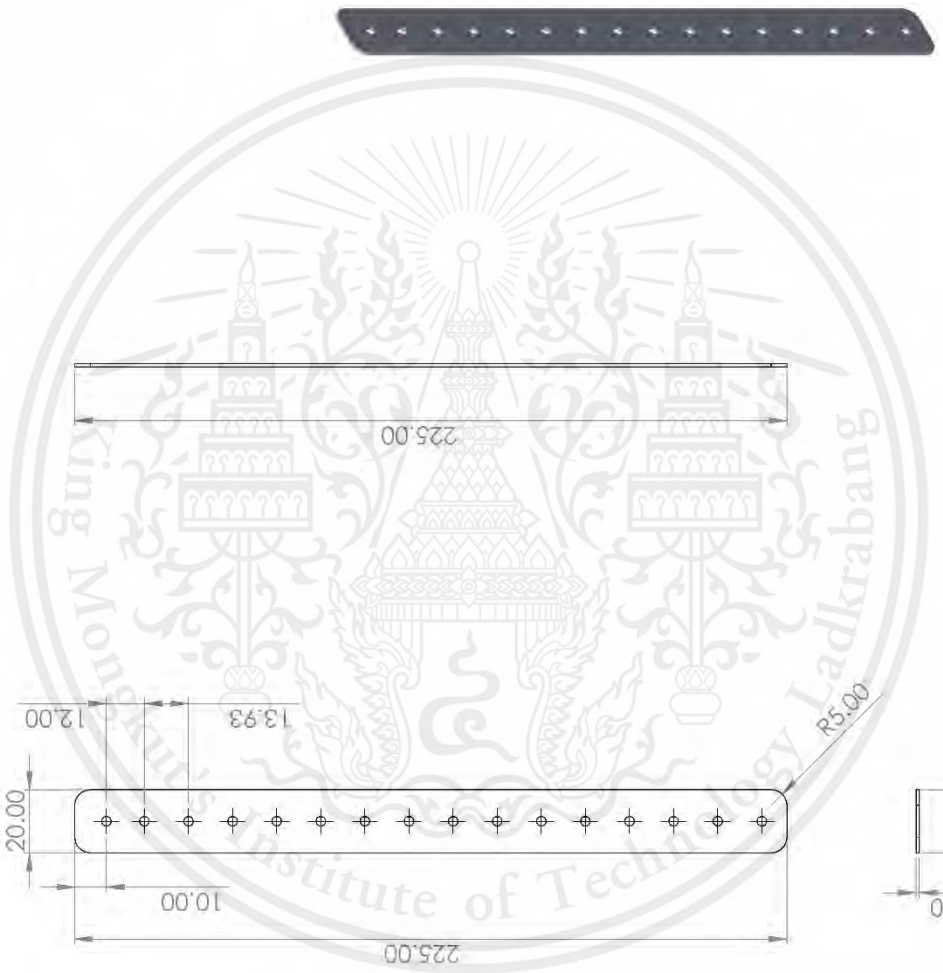

TITLE :	PART NUMBER :	DESIGNED BY:	DATE :	UNIT : mm
Collector plate cover	**11B**	**Panod Nilphai**	**18 April 2024**	

TITLE :	PART NUMBER :	DESIGNED BY:	DATE :	UNIT : mm
Front Plan	**12B**	**Panod Nilphai**	**18 April 2024**	

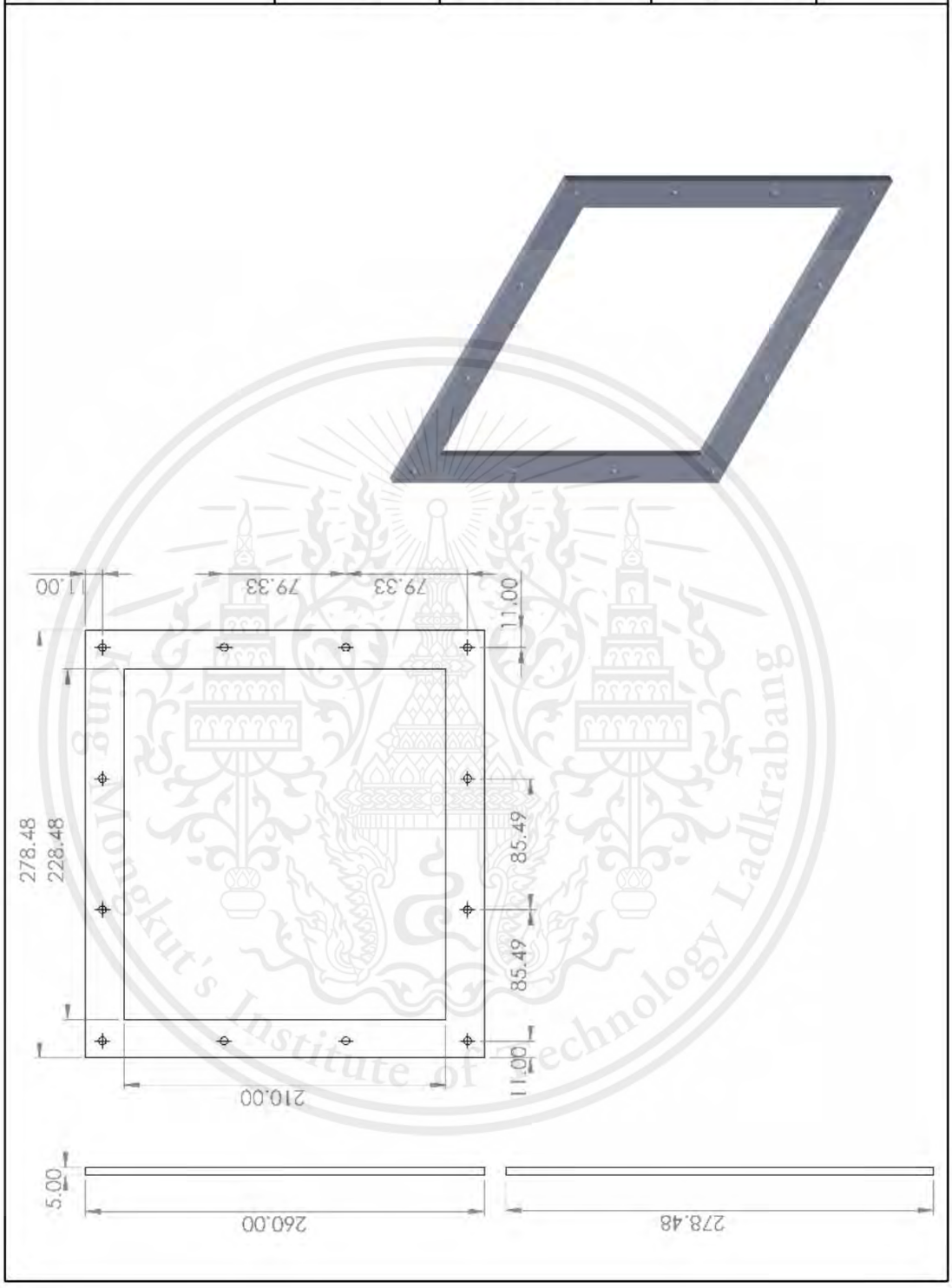

TITLE :	PART NUMBER :	DESIGNED BY:	DATE :	UNIT : mm
Collector plate holder	**13B**	**Panod Nilphai**	**18 April 2024**	

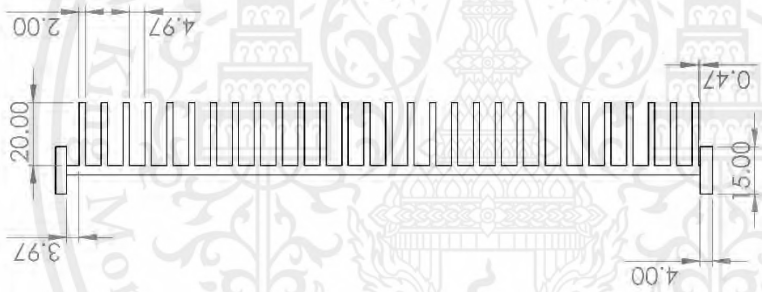

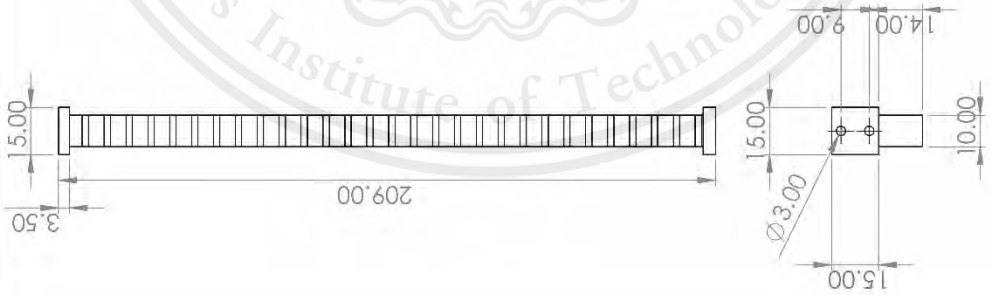

TITLE :	PART NUMBER :	DESIGNED BY:	DATE :	UNIT : mm
ESP Unit aseembly	-	Panod Nilphai	18 April 2024	

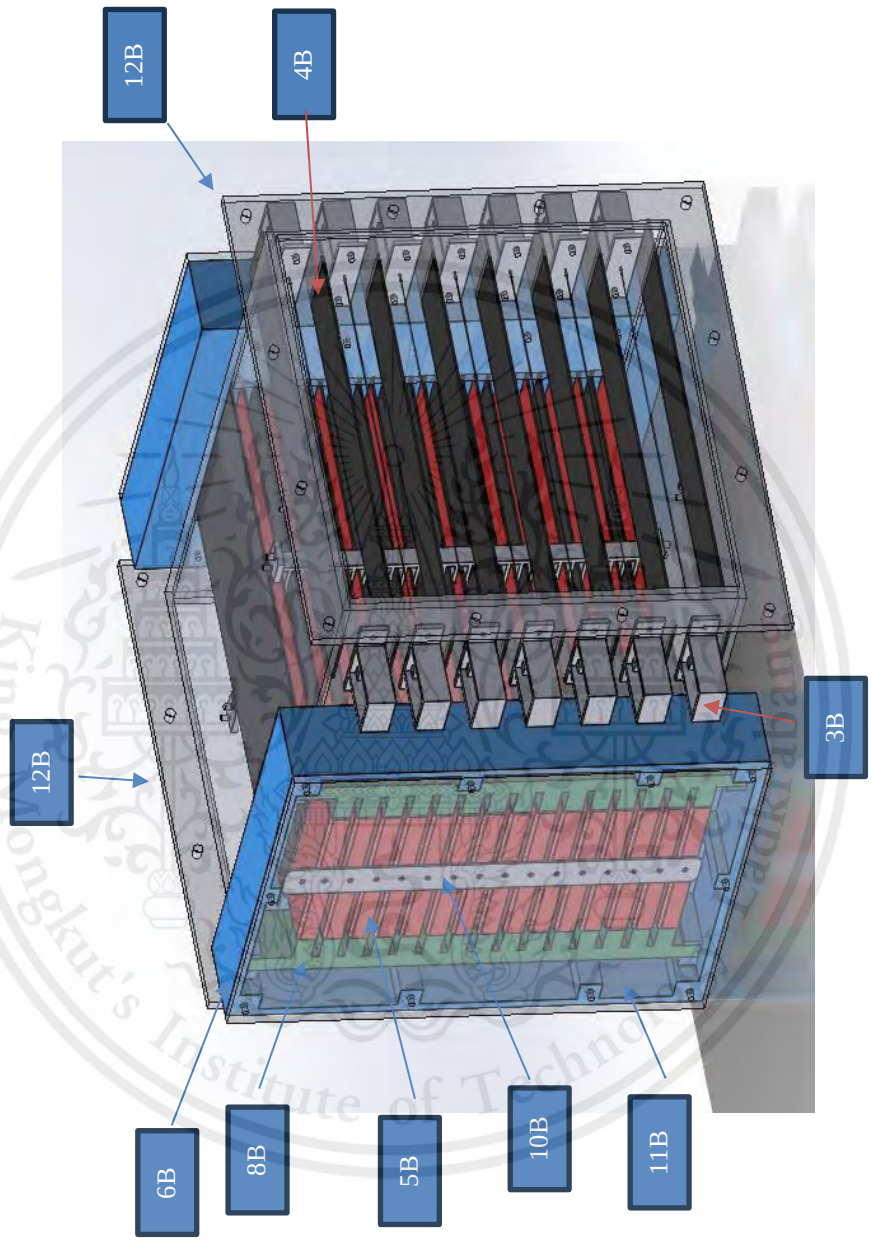

TITLE :	PART NUMBER :	DESIGNED BY:	DATE :	UNIT : mm
ESP Unit aseembly	-	Panod Nilphai	18 April 2024